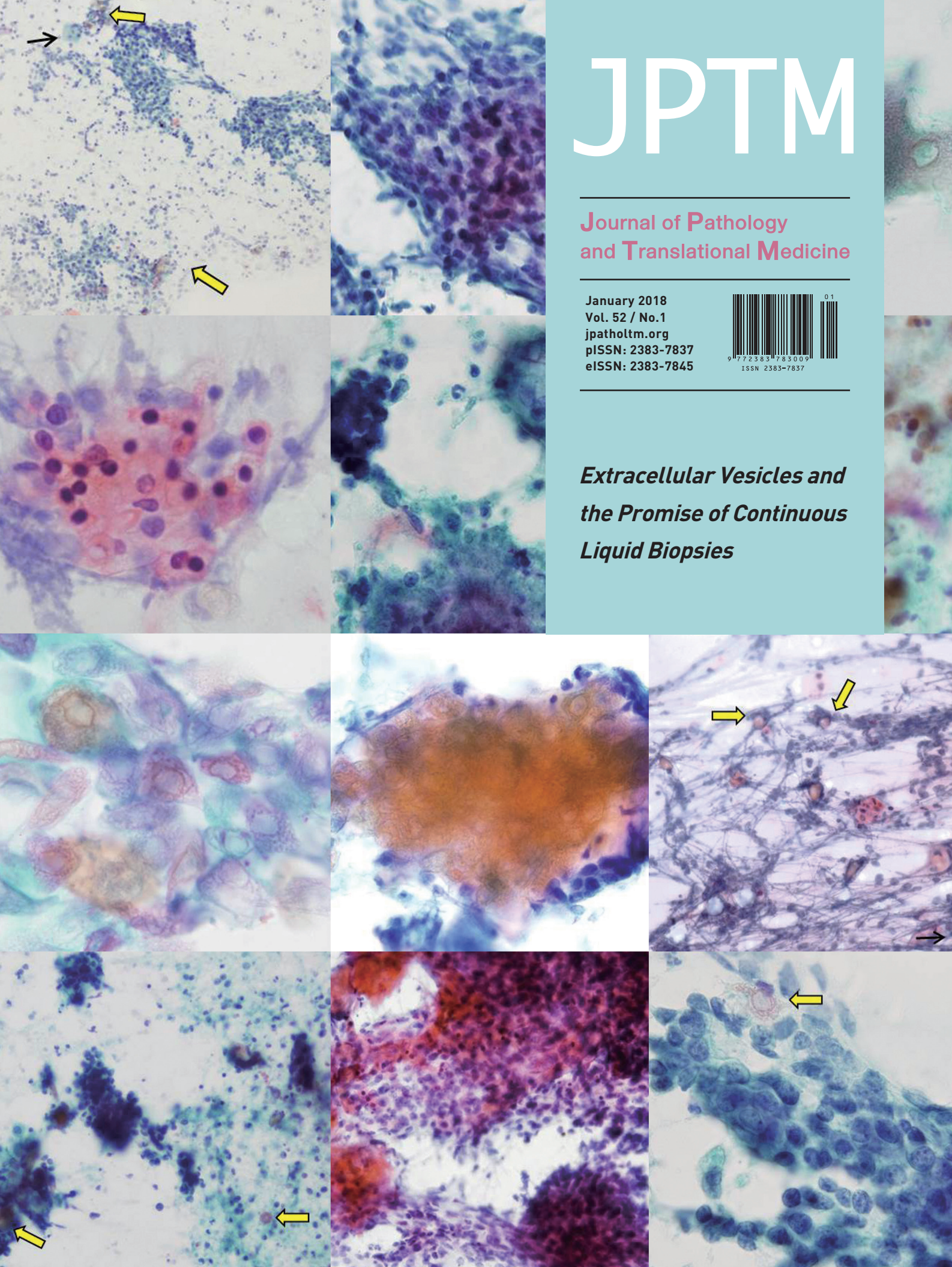

JPTM

Journal of Pathology and Translational Medicine

January 2018
Vol. 52 / No.1
jpatholtm.org
pISSN: 2383-7837
eISSN: 2383-7845

Extracellular Vesicles and the Promise of Continuous Liquid Biopsies

Journal of Pathology and Translational Medicine

Volume 52 • Number 1 • January 2018 (bimonthly)
Published since 1967
Printed on 11 January 2018 Published on 15 January 2018

J Pathol Transl Med
pISSN: 2383-7837
eISSN: 2383-7845

Aims & Scope

The Journal of Pathology and Translational Medicine is an open venue for the rapid publication of major achievements in various fields of pathology, cytopathology, and biomedical and translational research. The Journal aims to share new insights into the molecular and cellular mechanisms of human diseases and to report major advances in both experimental and clinical medicine, with a particular emphasis on translational research. The investigations of human cells and tissues using high-dimensional biology techniques such as genomics and proteomics will be given a high priority. Articles on stem cell biology are also welcome. The categories of manuscript include original articles, review and perspective articles, case studies, brief case reports, and letters to the editor.

Subscription Information

To subscribe to this journal, please contact the Korean Society of Pathologists/the Korean Society for Cytopathology. Full text PDF files are also available at the official website (http://jpatholtm.org). *Journal of Pathology and Translational Medicine* is indexed by Emerging Sources Citation Index (ESCI), PubMed, PubMed Central, Scopus, KoreaMed, KoMCI, WPRIM, Directory of Open Access Journals (DOAJ), and CrossRef. Circulation number per issue is 700.

Contact the Korean Society of Pathologists/the Korean Society for Cytopathology

Publishers: Jae Bok Park, MD, Hye Kyoung Yoon, MD
Editors-in-Chief: Soon Won Hong, MD, Chong Jai Kim, MD
Published by the Korean Society of Pathologists/the Korean Society for Cytopathology

Editorial Office
Room 1209 Gwanghwamun Officia, 92 Saemunan-ro, Jongno-gu, Seoul 03186, Korea
Tel: +82-2-795-3094 Fax: +82-2-790-6635 E-mail: office@jpatholtm.org

#1508 Renaissancetower, 14 Mallijae-ro, Mapo-gu, Seoul 04195, Korea
Tel: +82-2-593-6943 Fax: +82-2-593-6944 E-mail: office@jpatholtm.org

Printed by iMiS Company Co., Ltd. (JMC)
Jungang Bldg. 18-8 Wonhyo-ro 89-gil, Yongsan-gu, Seoul 04314, Korea
Tel: +82-2-717-5511 Fax: +82-2-717-5515 E-mail: ml@smileml.com

Manuscript Editing by InfoLumi Co.
210-202, 421 Pangyo-ro, Bundang-gu, Seongnam 13522, Korea
Tel: +82-70-8839-8800 E-mail: infolumi.chang@gmail.com

Front cover image: Importance of individual ghost cells in fine-needle aspiration cytology diagnosis of Pilomatricoma (Figs. 1, 2). p47, p48.

This journal was supported by the Korean Federation of Science and Technology Societies Grant funded by the Korean Government.

Journal of Pathology and Translational Medicine

J Pathol Transl Med
pISSN: 2383-7837
eISSN: 2383-7845

Volume 52, Number 1, January 2018

CONTENTS

CONTENTS CONTINUED

Instructions for Authors for *Journal of Pathology and Translational Medicine* are available at http://jpatholtm.org/authors/authors.php

Journal of Pathology and Translational Medicine 2018; 52: 1-8
https://doi.org/10.4132/jptm.2017.05.21

REVIEW

Extracellular Vesicles and the Promise of Continuous Liquid Biopsies

Don Armstrong[1]
Derek E. Wildman[1,2]

[1]Carl R. Woese Institute for Genomic Biology, University of Illinois at Urbana-Champaign, Urbana, IL; [2]Department of Molecular and Integrative Physiology, University of Illinois at Urbana-Champaign, Urbana, IL, USA

Received: April 1, 2017
Revised: May 13, 2017
Accepted: May 21, 2017

Corresponding Author
Derek E. Wildman, MD
Department of Molecular and Integrative Physiology, University of Illinois at Urbana-Champaign, 1206 W Gregory Drive MC-195, Urbana, IL 61801, USA
Tel: +1-217-300-0939
E-mail: wildmand@illinois.edu

The rapid and accurate diagnosis of patients with minimally invasive procedures was once only found in science fiction. However, the discovery of extracellular vesicles (EVs) and their near ubiquity in body fluids, coupled with the advent of inexpensive next generation sequencing techniques and EV purification protocols, promises to make science fiction a reality. Purifying and sequencing the RNA content of EV from routine blood draws and urine samples are likely to enable pathologists and physicians to diagnose and track the progress of diseases in many inaccessible tissues in the near future. Here we present the evolutionary background of EV, summarize the biology of EV formation and cargo selection, and discuss the current barriers to making continuous liquid biopsies through the use of EV a science reality.

Key Words: Exosomes; Microvesicles; Extracellular vesicles; Cell-free RNA; Liquid biopsy

The production and release of membrane-bound vesicles by cells (which we will refer to generally as extracellular vesicles [EVs] in this review) is a process found in members of all three domains, including Archaea,[1,2] Bacteria,[3-5] and Eukaryotes (Fig. 1).[3-15] EVs contain a diverse complement of proteins, nucleotides, and lipids,[16,17] perform a large variety of functions, including antigen processing,[18] host-parasite communication[19] and competition with other species,[1] and are hypothesized to be formed by multiple mechanisms.[8] The observation of EVs in fluids such as saliva,[20] urine,[21] and blood[22] as well as the visualization and selection of EVs released from many human cells and cell lines including placenta (syncytiotrophoblasts,[23] HTR-8, and JEG-3[24]), kidneys,[25] and blood cells (including lymphocytes,[14] platelets,[26] and reticulocytes[27]) argues for the continued function of EV in humans when coupled with the history of convergent evolution and conservation of function of EVs. In this review, we will first present some of the current hypotheses for the functions of human-derived EV, and second suggest how the phenomenon of EV production can be utilized for the remote sensing of inaccessible tissues and discuss the roadblocks to immediate utilization.

PRODUCTION AND FUNCTION OF EXTRACELLULAR VESICLES

EVs have been found in almost every human body fluid,[28] including urine,[21,29] blood,[22,30] saliva,[20,31] cerebrospinal fluid (CSF),[32] synovial fluid,[33] semen,[34] breast milk,[35] amniotic fluid,[36] aqueous humor (from cadavers),[37] lymph,[38] and bronchoalveolar lavage fluid.[39] Because of the ubiquity of EVs, the mechanism of production and the likely functions of EVs have been the subject of intense study.

Production of extracellular vesicles

Eukaryotes generate multiple kinds of EVs. The major classes include exosomes, which are generated from multi-vesicular endosomes (MVEs), shedding microvesicles, which originate from the plasma membrane, apoptotic blebs, which result from programmed cell death, and gesicles, which are produced by vesicular stomatitis virus and potentially incorporate specific cargo proteins.[40] Exosomes are generated by the inward budding of MVEs and early endosomes which is mediated by the actions of endosomal sorting complexes required for transport (ESCRTs), ceramides, and tetraspanins.[41] The inward budding results in the potentially selective incorporation of cytoplasmic components

pISSN 2383-7837
eISSN 2383-7845

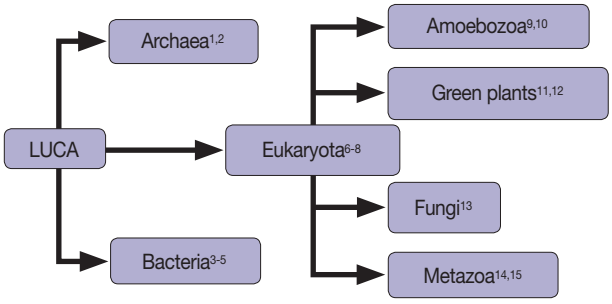

Fig. 1. Extracellular vesicles are found in all domains of life, including Archaea,[1,2] Bacteria,[3-5] and Eukaryotes.[3-15]

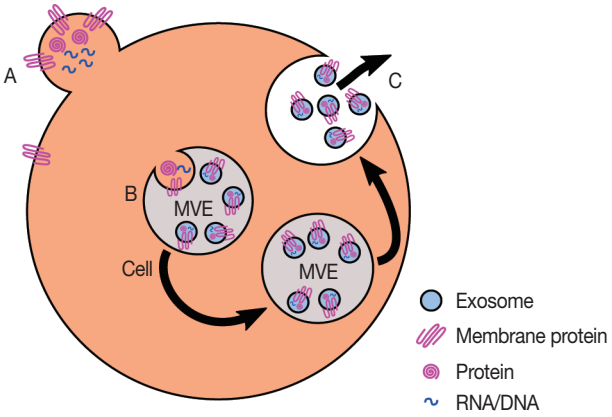

Fig. 2. Production of exosomes and microvesicles in cells. Microvesicles are generated from the budding of the plasma membrane (A). Exosomes are generated from the inward budding of multi-vesicular endosomes (MVEs) by the action of multiple proteins (B) and result in the release of exosomes (C) if the MVE is targeted to the plasma membrane instead of the late endosome.

including RNA, DNA, and proteins into the lumen of the exosome, as well as membrane lipids and transmembrane proteins. If the resultant MVEs are targeted to the plasma membrane instead of the lysosome, the fusion of MVEs with the plasma membrane leads to the release of exosomes. The fusion event is mediated by the action of multiple Rab proteins, including RAB27A (RAB27A, member RAS oncogene family), RAB35 (RAB35, member RAS oncogene family), and RAB11A (RAB11A, member RAS oncogene family)[42] in addition to the action of the cytoskeleton and fusion machinery (soluble NSF attachment protein receptors [SNAREs], etc.).[41] The proteins involved in the processing of MVEs into EVs, including the ESCRTs, Rabs, and SNAREs, are present across the eukaryotes, which argues for EV production in at least the last common eukaryotic ancestor. The presence of orthologs of ESCRTs in archaea suggests that the last universal common ancestor may also have produced EVs.[43] However, since these proteins are also essential to ubiquitination pathways, it is possible that the conservation of EV production is a by-product of the conservation of the targeting of proteins to the lysosome for degradation.

The budding of microvesicles from the plasma membrane requires the actin-myosin machinery and small GTPases such as ADP ribosylation factor 6 (ARF6), but does not appear to require ESCRTs, although there is evidence that ESCRT-I is associated with some microvesicles. Further advances in microscopy, including autofluorescence contrast microscopy, are likely to enable the visualization of EV production.[44]

Cargo selection in extracellular vesicles

The content of EVs often differs significantly from the cellular compartments from which the EVs are generated, both in terms of membrane composition and surface markers, as well as the contents of the lumen (RNA, DNA, and proteins) (Fig. 2).[16,17] While some of the differences in membrane composition may be due purely to free energy considerations within the membrane such as curvature and charge, the enrichment of specific RNA motifs (ACCAGCCU, CAGUGAGC, and UAAUCCCA)[45] and protein surface markers (epithelial cell adhesion molecule [EPCAM], Erb-b2 receptor tyrosine kinase 2 [ERBB2], protein tyrosine phosphatase, receptor type C [PTPRC], or CD63 molecule [CD63])[46] argues for the selective packaging of EV contents. Proteins that may fulfill the role of RNA sorting include members of the ESCRT-II complex as well as the RNA-induced silencing complex (RISC) (including trinucleotide repeat containing 6A [TNRC6A] and argonaute 2 [AGO2, RISC catalytic component][41,47]), but the complete picture of the RNA sorting is still unclear. For example, it is not yet clear whether the sorting of RNA into exosomes is for the primary purpose of export in EV or if it is a side effect of targeting RNA to the lysosome which is sometimes exploited to provide export in EV. Pulse-chase experiments with labelled RNA may help elucidate the kinetics of this transport, and thereby determine whether specific RNAs are targeted for secretion, or if the process is RNA agnostic.

Function of extracellular vesicles

There are multiple hypotheses for the ancestral function of EVs. The first set of hypotheses deal with the function of the content of EVs; the second with the need to enclose the content of EVs within vesicles, and the degree of importance of the vesicle membrane surface markers. EVs from gram-negative bacteria have been shown to contain Quorum sensing molecules,[48] toxins (Shiga toxin,[49] ClyA[50]), and immune system modulators.[5,8] Enteroparasites such as nematodes have also been shown to modulate innate immunity by transferring small RNAs (miR-100 and Y RNA)

https://doi.org/10.4132/jptm.2017.05.21

to mammalian cells.[19,51]

In humans, EVs can modulate the immune system by presenting antigens to antigen presenting cells (APCs) through internalization or fusion, being released by APCs to activate natural killer (NK), $CD8^+$ T, and $CD4^+$ T cells, directly activating neutrophils, macrophages and NK cells, repressing immune responses through $CD8^+$ T cells, NK cells, or myeloid derived suppressor cells, and finally by conveying opsonins and complement components to modulate phagocytosis and apoptotic cell phagocytosis.[52] These mechanisms are even exploited by some cancer cells by releasing EVs which induce apoptosis of activated T cells.[52] During human pregnancy, EVs with a distinct population of mRNA and miRNA are released from villous trophoblasts in the placenta; these EVs also contain FasL and TRAIL which promote apoptosis and subsequent immunosuppression of T cells.[53,54] These EVs are likely utilized by the placenta to help maintain allograft tolerance during pregnancy.[24]

Using vesicles for packaging EVs can reduce the exposure of the contents to host proteases and antibodies,[48] as well as coupling cargo with targeting receptors/agonists without requiring direct targeting molecule to cargo interactions. This mechanism of packaging hints at the vast potential of therapeutic cargo inside of EVs with specific surface markers for the treatment of many diseases, such as cancer, where a cargo needs to be delivered to a precise tissue or cell type which is otherwise difficult to access (Table 1).[28]

Table 1. Tissues, cells, and fluids in which EVs have been identified as listed in Vesiclepedia[76]

Tissue	Study
Amniotic fluid	Keller *et al*.[36]
Aqueous humor	Stamer *et al*.[37]
Ascites	Andre *et al*.[55]
Atherosclerotic plaques	Mallat *et al*.[56]
B cells	Miguet *et al*.[57]
Breast milk	Admyre *et al*.[35]
Bronchoalveolar lavage fluid	Admyre *et al*.[39]
Dendritic cells	Admyre *et al*.[39]
Embryonic stem cells	Yuan *et al*.[58]
Endothelial cells	Deregibus *et al*.[59]
Epididymal fluid	Thimon *et al*.[60]
Glioblastoma cells	Skog *et al*.[61]
Inflammatory fluids	Fourcade *et al*.[62]
Keratinocytes	Chavez-Muñoz *et al*.[63]
Liver stem cells	Collino *et al*.[64]
Lung cancer cells	Del Tatto *et al*.[65]
Macrophages	Yang *et al*.[66]
Malignant pleural effusions	Andre *et al*.,[55] Bard *et al*.[67]
Mesenchymal stem cells	Collino *et al*.[64]
Monocytes	Del Conde *et al*.[68]
Mononuclear cells	Mack *et al*.[69]
Placenta	Gardiner *et al*.[70]
Plasma	Del Conde *et al*.,[68] Sabapatha *et al*.[71]
Platelets	Heijnen *et al*.[72]
Red blood cells	Fourcade *et al*.[62]
Saliva	Ogawa *et al*.,[20] Michael *et al*.[31]
Seminal fluid	Utleg *et al*.[73]
Serum	Skog *et al*.[61]
T cells	Martínez-Lorenzo *et al*.[74]
Trabecular meshwork cells	Stamer *et al*.[37]
Tracheobronchial cells	Kesimer *et al*.[75]
Urine	Cheng *et al*.,[21] Keller *et al*.,[36] Stamer *et al*.[37]

For the most up-to-date list, see Vesiclepedia,[76] EVpedia,[17] and Exocarta.[37]

EXTRACELLULAR VESICLES FOR DIAGNOSIS AND THERAPEUTICS

EVs in diagnosis

Diagnosing cancer using EVs

The contents of EVs have been found to be modified in multiple different cancers, including colorectal cancer,[77] prostate cancer,[78,79] glioblastomas,[61,80] and breast cancer,[81] as well as many others (see Maas *et al*.[82] for review). Multiple patents have already been filed to use the contents of EVs for diagnosis (see Urbanelli *et al*.[28] for review) so it is likely only a matter of time before EVs are used in the clinic for diagnosis.

Remote sensor of inaccessible organs

The most promising use of EVs is as a remote sensor of organs which are inaccessible to routine monitoring. In patients with breast cancer, EVs isolated from the serum contain higher levels of glypican 1 (GPC1); in patients with early pancreatic cancer, in addition to elevated GPC1, EVs contained mutant transcripts of *KRAS* (KRAS proto-oncogene, GTPase).[83] EVs released by the placenta during pregnancies and identified in maternal blood (and potentially other body fluids, such as urine) will enable clinicians to routinely monitor the health of placentation and pregnancy throughout gestation without invasive tests.[24,53,54,84] There is also mounting evidence that EVs package and may spread misfolded proteins associated with neurodegenerative diseases, which can be detected in CSF and blood, including the scrapie isoform of cellular prion protein (PrPsc) that is involved in Creutzfeldt-Jakob disease.[85] EVs may potentially be useful in the diagnosis and progression tracking of similar neurodegenerative diseases.

Typing of infections which are otherwise inaccessible

Because the releasing of EVs is widely conserved in all three

domains of life, it is possible that EVs which are present in accessible fluids, such as urine, saliva, or blood, may be of bacterial or fungal origins. Sequencing RNA present in EVs may identify the infectious agent responsible even though the source tissue is diffcult to access, enabling more effective treatment.

Additional potential uses of EVs

EVs which are introduced from an exogenous source have the potential to be used as the therapeutic agent, in much the same way as liposomes have been utilized.[28,86] Because EVs can be generated using simple bioreactors using appropriate engineered cell lines coupled with immunoaffnity or other purification,[87] EVs based therapeutics may prove to be more specific, uniform, and cheaper to produce than current liposome based technology. In theory, any transmembrane receptor or receptor agonist can be coupled with any other cargo which is small enough to fit into an EV and injected, potentially targeting widespread metastases or locations which are otherwise inaccessible to targeted therapeutics.[28,86]

ROADBLOCKS TO FURTHER USE OF EXTRACELLULAR VESICLES IN DIAGNOSIS

There are three distinct ways in which isolated EVs can be used in diagnosis. The first is a *marker-only approach*, where the concentration of the marker(s) in EV in the fluid of interest predicts disease or phenotype, and no other disease or healthy condition is likely to result in elevated concentrations of the marker(s). The second is a *decomposition-based multi-marker approach*, where the relative contribution of each tissue to the sub-sample of EVs is estimated using tissue-specific markers, and is correlated with differences in disease- or phenotype-relevant markers in that subsample. The third is a *single-EV multi-marker approach*, where single EV are interrogated to identify their tissue of origin and disease- or phenotype-relevant marker concentrations.

EV isolation

The methods of isolation currently used include ultracentrifugation, density gradient centrifugation, size exclusion through membranes, polymeric precipitation, immunoaffinity capture, and microfluidics.[46,88,89] Ultracentrifugation is an easily executed protocol, but also results in the enrichment of proteins with high sedimentation rates which are not bound to exosomes, including major vault protein, heparan sulfate proteoglycan 2 (HSPG2), fatty acid synthase (FASN), and the 26S proteasome.[88] Density gradient centrifugation reduces the contamination with high sedimentation rate protein complexes, but requires additional western blotting steps to verify that the density fraction isolated contains exosomes and has lower effciency than immunoaffinity capture.

Immunoaffinity capture using bead-conjugated antibodies to EPCAM or another exosome marker (such as ERBB2, PTPRC, or CD63) is simpler than density gradient centrifugation, and produces exosomes of high purity, but is limited to exosomal populations which express specific surface markers and may potentially miss novel exosome populations. Therefore, discovery experiments looking for novel populations of exosomes should use density gradient centrifugation, whereas established assays looking at known exosome populations can use appropriate immunoaffinity capture methods. Witwer *et al.*[89] and future recommendations of the International Society for Extracellular Vesicles provide valuable recommendations for investigators examining EVs in humans.

Normalization of EV content across tissues/samples

For circulating miRNA, Fesler *et al.*[90] suggests uniform volumes of plasma or exogenous sequences and points out that endogenous control genes may vary between subjects (as well as in the control population).

Identification of tissue of origin

Because EVs located in body fluids can potentially originate from any source tissue for which there is a path to that fluid, accurate diagnostics of remote tissues also require identification of the tissue of origin of a particular EV or set of EVs. As the miRNA and mRNA contents of EVs came from cells in the originating tissue, miRNA and mRNA which are specific to those originating tissue but found within EVs in body fluid indicate that at least some of the EVs came from the original tissue. For example, the presence of high abundance placenta-specific transcripts such as *LGALS14* in a sample of EVs would indicate that at least some of the EVs came from the placenta. Determining the fraction of EVs which are from a particular tissue of origin would allow for changes in miRNA and mRNA abundance over time to be assigned to a particular source tissue when multiple samples of different per-tissue abundances are obtained at a single timepoint. Marker-free (such as CellCODE[91]) and/or marker-dependent methods will likely be necessary to determine the proportion of exosomes which come from different source tissues in a mixed population.

Quantification of a single EV

In cases where the source tissue has not been assayed, an alterna-

https://doi.org/10.4132/jptm.2017.05.21

tive is the (much more diffcult) process of sequencing individual EV separately. Presumably, the advances in single-cell and single nucleus sequencing will provide the tools for single EV sequencing as a side benefit. Previous work by Smith *et al*.[92] using laser tweezers Raman spectroscopy that identified the lipid content of EVs on a per-EV basis identified multiple exosome subtypes which do not correlate strongly with the originating cell type, and therefore may represent different exosome subclasses which may be present in a single bulk exosome preparation. However, Raman spectroscopy is very slow and does not easily enable identification of the contents of exosomes. In an alternative approach, Kibria *et al*.[93] used micro flow cytometry after differential centrifugation to analyze CD44 (CD44 molecule) surface marker intensity on individual exosomes. This overcomes the limitations of typical flow cytometers, which can only detect minimum particle sizes of 200–500 nm, which is much larger than typical EVs. We suspect that the combination of micro flow cytometry with droplet based barcoding and sequencing techniques can enable the sequencing of the RNA contents of individual EVs in the not-too-distant future.

CONCLUSION

EVs are poised to fulfill the promise of routine liquid biopsies in healthcare, whether used for diagnosing disease, tracking the effectiveness of therapy, or providing insight into multiple diseases as well as potentially tracking the progress of pregnancies in a non-invasive fashion.

Conflicts of Interest

No potential conflict of interest relevant to this article was reported.

Acknowledgments

We would like to thank the insightful comments of Priyadarshini Pantham and Monica Uddin on drafts of this manuscript. This work was funded in part by the National Institutes of Health 1R21ES027878-01 grant to DEW.

REFERENCES

1. Ellen AF, Rohulya OV, Fusetti F, Wagner M, Albers SV, Driessen AJ. The sulfolobicin genes of *Sulfolobus acidocaldarius* encode novel antimicrobial proteins. J Bacteriol 2011; 193: 4380-7.
2. Ellen AF, Zolghadr B, Driessen AM, Albers SV. Shaping the archaeal cell envelope. Archaea 2010; 2010: 608243.
3. Avila-Calderon ED, Araiza-Villanueva MG, Cancino-Diaz JC, *et al*. Roles of bacterial membrane vesicles. Arch Microbiol 2015; 197: 1-10.
4. Haurat MF, Elhenawy W, Feldman MF. Prokaryotic membrane vesicles: new insights on biogenesis and biological roles. Biol Chem 2015; 396: 95-109.
5. Lai FW, Lichty BD, Bowdish DM. Microvesicles: ubiquitous contributors to infection and immunity. J Leukoc Biol 2015; 97: 237-45.
6. Lopez-Verrilli MA, Court FA. Exosomes: mediators of communication in eukaryotes. Biol Res 2013; 46: 5-11.
7. Lykke-Andersen S, Brodersen DE, Jensen TH. Origins and activities of the eukaryotic exosome. J Cell Sci 2009; 122(Pt 10): 1487-94.
8. Deatherage BL, Cookson BT. Membrane vesicle release in bacteria, eukaryotes, and archaea: a conserved yet underappreciated aspect of microbial life. Infect Immun 2012; 80: 1948-57.
9. Kriebel PW, Barr VA, Rericha EC, Zhang G, Parent CA. Collective cell migration requires vesicular trafficking for chemoattractant delivery at the trailing edge. J Cell Biol 2008; 183: 949-61.
10. Lavialle F, Deshayes S, Gonnet F, *et al*. Nanovesicles released by *Dictyostelium* cells: a potential carrier for drug delivery. Int J Pharm 2009; 380: 206-15.
11. Regente M, Corti-Monzón G, Maldonado AM, Pinedo M, Jorrín J, de la Canal L. Vesicular fractions of sunflower apoplastic fluids are associated with potential exosome marker proteins. FEBS Lett 2009; 583: 3363-6.
12. An Q, van Bel AJ, Huckelhoven R. Do plant cells secrete exosomes derived from multivesicular bodies? Plant Signal Behav 2007; 2: 4-7.
13. Albuquerque PC, Nakayasu ES, Rodrigues ML, *et al*. Vesicular transport in *Histoplasma capsulatum*: an effective mechanism for trans-cell wall transfer of proteins and lipids in ascomycetes. Cell Microbiol 2008; 10: 1695-710.
14. Raposo G, Nijman HW, Stoorvogel W, *et al*. B lymphocytes secrete antigen-presenting vesicles. J Exp Med 1996; 183: 1161-72.
15. Lo Cicero A, Stahl PD, Raposo G. Extracellular vesicles shuffling intercellular messages: for good or for bad. Curr Opin Cell Biol 2015; 35: 69-77.
16. Choi DS, Kim DK, Kim YK, Gho YS. Proteomics of extracellular vesicles: exosomes and ectosomes. Mass Spectrom Rev 2015; 34: 474-90.
17. Kim DK, Kang B, Kim OY, *et al*. EVpedia: an integrated database of high-throughput data for systemic analyses of extracellular vesicles. J Extracell Vesicles 2013; 2: 20384.
18. Morelli AE, Larregina AT, Shufesky WJ, *et al*. Endocytosis, intracellular sorting, and processing of exosomes by dendritic cells. Blood

2004; 104: 3257-66.
19. Coakley G, Maizels RM, Buck AH. Exosomes and other extracellular vesicles: the new communicators in parasite infections. Trends Parasitol 2015; 31: 477-89.
20. Ogawa Y, Kanai-Azuma M, Akimoto Y, Kawakami H, Yanoshita R. Exosome-like vesicles with dipeptidyl peptidase IV in human saliva. Biol Pharm Bull 2008; 31: 1059-62.
21. Cheng L, Sun X, Scicluna BJ, Coleman BM, Hill AF. Characterization and deep sequencing analysis of exosomal and non-exosomal miRNA in human urine. Kidney Int 2014; 86: 433-44.
22. Huang X, Yuan T, Tschannen M, *et al*. Characterization of human plasma-derived exosomal RNAs by deep sequencing. BMC Genomics 2013; 14: 319.
23. Knight M, Redman CW, Linton EA, Sargent IL. Shedding of syncytiotrophoblast microvilli into the maternal circulation in pre-eclamptic pregnancies. Br J Obstet Gynaecol 1998; 105: 632-40.
24. Mitchell MD, Peiris HN, Kobayashi M, *et al*. Placental exosomes in normal and complicated pregnancy. Am J Obstet Gynecol 2015; 213(4 Suppl): S173-81.
25. Gerlach JQ, Kruger A, Gallogly S, *et al*. Surface glycosylation profiles of urine extracellular vesicles. PLoS One 2013; 8: e74801.
26. Wolf P. The nature and significance of platelet products in human plasma. Br J Haematol 1967; 13: 269-88.
27. Harding C, Heuser J, Stahl P. Receptor-mediated endocytosis of transferrin and recycling of the transferrin receptor in rat reticulocytes. J Cell Biol 1983; 97: 329-39.
28. Urbanelli L, Buratta S, Sagini K, Ferrara G, Lanni M, Emiliani C. Exosome-based strategies for diagnosis and therapy. Recent Pat CNS Drug Discov 2015; 10: 10-27.
29. Li M, Zeringer E, Barta T, Schageman J, Cheng A, Vlassov AV. Analysis of the RNA content of the exosomes derived from blood serum and urine and its potential as biomarkers. Philos Trans R Soc Lond B Biol Sci 2014; 369: 20130502.
30. Johnstone RM, Adam M, Hammond JR, Orr L, Turbide C. Vesicle formation during reticulocyte maturation: association of plasma membrane activities with released vesicles (exosomes). J Biol Chem 1987; 262: 9412-20.
31. Michael A, Bajracharya SD, Yuen PS, *et al*. Exosomes from human saliva as a source of microRNA biomarkers. Oral Dis 2010; 16: 34-8.
32. Vella LJ, Greenwood DL, Cappai R, Scheerlinck JP, Hill AF. Enrichment of prion protein in exosomes derived from ovine cerebral spinal fluid. Vet Immunol Immunopathol 2008; 124: 385-93.
33. Skriner K, Adolph K, Jungblut PR, Burmester GR. Association of citrullinated proteins with synovial exosomes. Arthritis Rheum 2006; 54: 3809-14.
34. Sullivan R, Saez F, Girouard J, Frenette G. Role of exosomes in sperm maturation during the transit along the male reproductive tract. Blood Cells Mol Dis 2005; 35: 1-10.
35. Admyre C, Johansson SM, Qazi KR, *et al*. Exosomes with immune modulatory features are present in human breast milk. J Immunol 2007; 179: 1969-78.
36. Keller S, Rupp C, Stoeck A, *et al*. CD24 is a marker of exosomes secreted into urine and amniotic fluid. Kidney Int 2007; 72: 1095-102.
37. Stamer WD, Hoffman EA, Luther JM, Hachey DL, Schey KL. Protein profile of exosomes from trabecular meshwork cells. J Proteomics 2011; 74: 796-804.
38. Hood JL. The association of exosomes with lymph nodes. Semin Cell Dev Biol 2017; 67: 29-38.
39. Admyre C, Grunewald J, Thyberg J, *et al*. Exosomes with major histocompatibility complex class II and co-stimulatory molecules are present in human BAL fluid. Eur Respir J 2003; 22: 578-83.
40. Mangeot PE, Dollet S, Girard M, *et al*. Protein transfer into human cells by VSV-G-induced nanovesicles. Mol Ther 2011; 19: 1656-66.
41. Raposo G, Stoorvogel W. Extracellular vesicles: exosomes, microvesicles, and friends. J Cell Biol 2013; 200: 373-83.
42. Ostrowski EA, Shen Y, Tian X, *et al*. Genomic signatures of cooperation and conflict in the social amoeba. Curr Biol 2015; 25: 1661-5.
43. Leung KF, Dacks JB, Field MC. Evolution of the multivesicular body ESCRT machinery: retention across the eukaryotic lineage. Traffic 2008; 9: 1698-716.
44. Tu H, Liu Y, Marjanovic M, *et al*. Concurrence of extracellular vesicle enrichment and metabolic switch visualized label-free in the tumor microenvironment. Sci Adv 2017; 3: e1600675.
45. Batagov AO, Kurochkin IV. Exosomes secreted by human cells transport largely mRNA fragments that are enriched in the 3'-untranslated regions. Biol Direct 2013; 8: 12.
46. Greening DW, Xu R, Ji H, Tauro BJ, Simpson RJ. A protocol for exosome isolation and characterization: evaluation of ultracentrifugation, density-gradient separation, and immunoaffinity capture methods. Methods Mol Biol 2015; 1295: 179-209.
47. Gibbings DJ, Ciaudo C, Erhardt M, Voinnet O. Multivesicular bodies associate with components of miRNA effector complexes and modulate miRNA activity. Nat Cell Biol 2009; 11: 1143-9.
48. Aldick T, Bielaszewska M, Uhlin BE, Humpf HU, Wai SN, Karch H. Vesicular stabilization and activity augmentation of enterohaemorrhagic *Escherichia coli* haemolysin. Mol Microbiol 2009; 71: 1496-508.
49. Dutta S, Iida K, Takade A, Meno Y, Nair GB, Yoshida S. Release of Shiga toxin by membrane vesicles in *Shigella dysenteria*e serotype 1 strains and *in vitro* effects of antimicrobials on toxin production and release. Microbiol Immunol 2004; 48: 965-9.

50. Wai SN, Lindmark B, Söderblom T, *et al*. Vesicle-mediated export and assembly of pore-forming oligomers of the enterobacterial ClyA cytotoxin. Cell 2003; 115: 25-35.
51. Buck AH, Coakley G, Simbari F, *et al*. Exosomes secreted by nematode parasites transfer small RNAs to mammalian cells and modulate innate immunity. Nat Commun 2014; 5: 5488.
52. Greening DW, Gopal SK, Xu R, Simpson RJ, Chen W. Exosomes and their roles in immune regulation and cancer. Semin Cell Dev Biol 2015; 40: 72-81.
53. Mincheva-Nilsson L, Baranov V. Placenta-derived exosomes and syncytiotrophoblast microparticles and their role in human reproduction: immune modulation for pregnancy success. Am J Reprod Immunol 2014; 72: 440-57.
54. Stenqvist AC, Nagaeva O, Baranov V, Mincheva-Nilsson L. Exosomes secreted by human placenta carry functional Fas ligand and TRAIL molecules and convey apoptosis in activated immune cells, suggesting exosome-mediated immune privilege of the fetus. J Immunol 2013; 191: 5515-23.
55. Andre F, Schartz NE, Movassagh M, *et al*. Malignant effusions and immunogenic tumour-derived exosomes. Lancet 2002; 360: 295-305.
56. Mallat Z, Hugel B, Ohan J, Lesèche G, Freyssinet JM, Tedgui A. Shed membrane microparticles with procoagulant potential in human atherosclerotic plaques: a role for apoptosis in plaque thrombogenicity. Circulation 1999; 99: 348-53.
57. Miguet L, Pacaud K, Felden C, *et al*. Proteomic analysis of malignant lymphocyte membrane microparticles using double ionization coverage optimization. Proteomics 2006; 6: 153-71.
58. Yuan A, Farber EL, Rapoport AL, *et al*. Transfer of microRNAs by embryonic stem cell microvesicles. PLoS One 2009; 4: e4722.
59. Deregibus MC, Cantaluppi V, Calogero R, *et al*. Endothelial progenitor cell derived microvesicles activate an angiogenic program in endothelial cells by a horizontal transfer of mRNA. Blood 2007; 110: 2440-8.
60. Thimon V, Frenette G, Saez F, Thabet M, Sullivan R. Protein composition of human epididymosomes collected during surgical vasectomy reversal: a proteomic and genomic approach. Hum Reprod 2008; 23: 1698-707.
61. Skog J, Wurdinger T, van Rijn S, *et al*. Glioblastoma microvesicles transport RNA and proteins that promote tumour growth and provide diagnostic biomarkers. Nat Cell Biol 2008; 10: 1470-6.
62. Fourcade O, Simon MF, Viodé C, *et al*. Secretory phospholipase A2 generates the novel lipid mediator lysophosphatidic acid in membrane microvesicles shed from activated cells. Cell 1995; 80: 919-27.
63. Chavez-Muñoz C, Morse J, Kilani R, Ghahary A. Primary human keratinocytes externalize stratifin protein via exosomes. J Cell Biochem 2008; 104: 2165-73.
64. Collino F, Deregibus MC, Bruno S, *et al*. Microvesicles derived from adult human bone marrow and tissue specific mesenchymal stem cells shuttle selected pattern of miRNAs. PLoS One 2010; 5: e11803.
65. Del Tatto M, Ng T, Aliotta JM, *et al*. Marrow cell genetic phenotype change induced by human lung cancer cells. Exp Hematol 2011; 39: 1072-80.
66. Yang M, Chen J, Su F, *et al*. Microvesicles secreted by macrophages shuttle invasion-potentiating microRNAs into breast cancer cells. Mol Cancer 2011; 10: 117.
67. Bard MP, Hegmans JP, Hemmes A, *et al*. Proteomic analysis of exosomes isolated from human malignant pleural effusions. Am J Respir Cell Mol Biol 2004; 31: 114-21.
68. Del Conde I, Shrimpton CN, Thiagarajan P, López JA. Tissue-factor-bearing microvesicles arise from lipid rafts and fuse with activated platelets to initiate coagulation. Blood 2005; 106: 1604-11.
69. Mack M, Kleinschmidt A, Brühl H, *et al*. Transfer of the chemokine receptor CCR5 between cells by membrane-derived microparticles: a mechanism for cellular human immunodeficiency virus 1 infection. Nat Med 2000; 6: 769-75.
70. Gardiner C, Tannetta DS, Simms CA, Harrison P, Redman CW, Sargent IL. Syncytiotrophoblast microvesicles released from pre-eclampsia placentae exhibit increased tissue factor activity. PLoS One 2011; 6: e26313.
71. Sabapatha A, Gercel-Taylor C, Taylor DD. Specific isolation of placenta-derived exosomes from the circulation of pregnant women and their immunoregulatory consequences. Am J Reprod Immunol 2006; 56: 345-55.
72. Heijnen HF, Schiel AE, Fijnheer R, Geuze HJ, Sixma JJ. Activated platelets release two types of membrane vesicles: microvesicles by surface shedding and exosomes derived from exocytosis of multivesicular bodies and alpha-granules. Blood 1999; 94: 3791-9.
73. Utleg AG, Yi EC, Xie T, *et al*. Proteomic analysis of human prostasomes. Prostate 2003; 56: 150-61.
74. Martínez-Lorenzo MJ, Anel A, Gamen S, *et al*. Activated human T cells release bioactive Fas ligand and APO2 ligand in microvesicles. J Immunol 1999; 163: 1274-81.
75. Kesimer M, Scull M, Brighton B, *et al*. Characterization of exosome-like vesicles released from human tracheobronchial ciliated epithelium: a possible role in innate defense. FASEB J 2009; 23: 1858-68.
76. Kalra H, Simpson RJ, Ji H, *et al*. Vesiclepedia: a compendium for extracellular vesicles with continuous community annotation. PLoS Biol 2012; 10: e1001450.
77. Matsumura T, Sugimachi K, Iinuma H, *et al*. Exosomal microRNA in serum is a novel biomarker of recurrence in human colorectal cancer. Br J Cancer 2015; 113: 275-81.

78. Hessvik NP, Phuyal S, Brech A, Sandvig K, Llorente A. Profiling of microRNAs in exosomes released from PC-3 prostate cancer cells. Biochim Biophys Acta 2012; 1819: 1154-63.
79. Bryant RJ, Pawlowski T, Catto JW, *et al*. Changes in circulating microRNA levels associated with prostate cancer. Br J Cancer 2012; 106: 768-74.
80. Saadatpour L, Fadaee E, Fadaei S, *et al*. Glioblastoma: exosome and microRNA as novel diagnosis biomarkers. Cancer Gene Ther 2016; 23: 415-8.
81. Asaga S, Kuo C, Nguyen T, Terpenning M, Giuliano AE, Hoon DS. Direct serum assay for microRNA-21 concentrations in early and advanced breast cancer. Clin Chem 2011; 57: 84-91.
82. Maas SL, Breakefield XO, Weaver AM. Extracellular vesicles: unique intercellular delivery vehicles. Trends Cell Biol 2017; 27: 172-88.
83. Melo SA, Luecke LB, Kahlert C, *et al*. Glypican-1 identifies cancer exosomes and detects early pancreatic cancer. Nature 2015; 523: 177-82.
84. Salomon C, Yee S, Scholz-Romero K, *et al*. Extravillous trophoblast cells-derived exosomes promote vascular smooth muscle cell migration. Front Pharmacol 2014; 5: 175.
85. Coleman BM, Hill AF. Extracellular vesicles: their role in the packaging and spread of misfolded proteins associated with neurodegenerative diseases. Semin Cell Dev Biol 2015; 40: 89-96.
86. Lener T, Gimona M, Aigner L, *et al*. Applying extracellular vesicles based therapeutics in clinical trials: an ISEV position paper. J Extracell Vesicles 2015; 4: 30087.
87. Whitford W, Ludlow JW, Cadwell JJ. Continuous production of exosomes: utilizing the technical advantages of hollow-fiber bioreactor technology. Gen Eng Biotechnol News 2015; 35: 34.
88. Tauro BJ, Greening DW, Mathias RA, *et al*. Comparison of ultracentrifugation, density gradient separation, and immunoaffinity capture methods for isolating human colon cancer cell line LIM1863-derived exosomes. Methods 2012; 56: 293-304.
89. Witwer KW, Buzás EI, Bemis LT, *et al*. Standardization of sample collection, isolation and analysis methods in extracellular vesicle research. J Extracell Vesicles 2013; 2: 20360.
90. Fesler A, Jiang J, Zhai H, Ju J. Circulating microRNA testing for the early diagnosis and follow-up of colorectal cancer patients. Mol Diagn Ther 2014; 18: 303-8.
91. Chikina M, Zaslavsky E, Sealfon SC. CellCODE: a robust latent variable approach to differential expression analysis for heterogeneous cell populations. Bioinformatics 2015; 31: 1584-91.
92. Smith ZJ, Lee C, Rojalin T, *et al*. Single exosome study reveals subpopulations distributed among cell lines with variability related to membrane content. J Extracell Vesicles 2015; 4: 28533.
93. Kibria G, Ramos EK, Lee KE, *et al*. A rapid, automated surface protein profiling of single circulating exosomes in human blood. Sci Rep 2016; 6: 36502.

 https://doi.org/10.4132/jptm.2017.05.21

Journal of Pathology and Translational Medicine 2018; 52: 9-13
https://doi.org/10.4132/jptm.2017.07.26

■ ORIGINAL ARTICLE ■

Programmed Death-Ligand 1 Expression and Its Correlation with Lymph Node Metastasis in Papillary Thyroid Carcinoma

Hyo Jung An[1] · Gyung Hyuck Ko[2,3,4]
Jeong-Hee Lee[2,3,4] · Jong Sil Lee[2,3,4]
Dong Chul Kim[2,3,4] · Jung Wook Yang[4]
Min Hye Kim[4] · Jin Pyeong Kim[2,3,5]
Eun Jung Jung[2,3,6] · Dae Hyun Song[1,2,3]

[1]Department of Pathology, Gyeongsang National University Changwon Hospital, Changwon; [2]Gyeongsang National University School of Medicine, Jinju; [3]Gyeongsang Institute of Health Science, Jinju; [4]Department of Pathology, Gyeongsang National University Hospital, Jinju; Deparments of [5]Otorhinolaryngology and [6]Surgery, Gyeongsang National University Changwon Hospital, Changwon, Korea

Received: June 14, 2017
Revised: July 24, 2017
Accepted: July 25, 2017

Corresponding Author
Dae Hyun Song, MD
Department of Pathology, Gyeongsang National University School of Medicine, 15 Jinju-daero 816beon-gil, Jinju 52727, Korea
Tel: +82-55-214-3150
Fax: +82-55-214-3174
E-mail: golgy@hanmail.net

Background: The immunotherapeutic role of programmed death-ligand 1 (PD-L1) in life expectancy in many cancers has been highlighted. However, data regarding PD-L1 expression in papillary thyroid carcinoma (PTC) are limited. In this study, we describe the PD-L1 and programmed cell death protein 1 (PD-1) expressions in PTC and analyze their correlation with lymph node (LN) metastasis. **Methods:** Clinicopathological data were obtained from 116 patients with PTC who were treated in Gyeongsang National University Hospital, Jinju, Korea in 2009. Tissue microarray blocks were made using representative paraffin blocks of classical PTCs excluding follicular variants. Two pathologists graded the proportion and intensity of PD-L1 and PD-1 expression in both tumor and inflammatory cells. According to their proportions, positive PTC cells were scored as negative (0%), grade 1 (1%–50%), and grade 2 (51%–100%). Similarly, positive inflammatory cells were graded as negative (0%), grade 1 (1%–10%), and grade 2 (11%–20%). The intensity of each protein expression was simplified as positive or negative. **Results:** A statistically significant correlation exists between the proportions of PD-1 and PD-L1 expression both in papillary carcinoma ($p = .001$) and peritumoral lymphoid cells in the thyroid ($p < .001$). In addition, the proportion of PD-L1 expression in PTC cells was closely related to metastatic LNs ($p = .036$). **Conclusions:** PD-L1 is a valuable predictive marker for LN metastasis in PTC. Immunomodulating therapies that inhibit PD-L1 might be an option for patients with LN metastasis.

Key Words: Programmed death-ligand 1; Carcinoma, papillary; Thyroid; Lymph nodes; Neoplasm metastasis

The immunotherapeutic role of programmed death-ligand 1 (PD-L1) in life expectancy in many cancers has been highlighted. In particular, pembrolizumab, which is an immune checkpoint inhibitor of PD-L1, showed significantly prolonged overall survivals in non-small-cell lung cancer patients.[1] PD-L1 expression has been described in other cancers, such as lymphoma, papillary renal cell carcinoma, intrahepatic cholangiocarcinoma, esophageal squamous cell carcinoma, prostatic adenocarcinoma, breast carcinoma, gastric signet ring cell carcinoma, nasopharyngeal carcinoma, lung adenocarcinoma, testicular germ cell tumor, and glioblastoma.[2-14] However, data regarding PD-L1 expression in papillary thyroid carcinoma (PTC) is scarce. In this study, we describe the expressions of PD-L1 and programmed cell death protein 1 (PD-1) and analyze their correlation with the clinical features of PTC.

MATERIALS AND METHODS

Case selection

By reviewing electronic clinical charts, we obtained clinicopathologic data of PTC patients treated at Gyeongsang National University Hospital, Jinju, Korea in 2009. A total of 116 patients with classical PTCs, excluding follicular or encapsulated follicular variants, were enrolled.[15] Total thyroidectomy or lobectomy with lymph node (LN) dissection was performed. The tumor stage of each patient was assessed via the American Joint Committee on Cancer (AJCC) 7th ed. Cancer Staging system.[16]

Two pathologists reviewed the hematoxylin and eosin–stained glass slides. This study was approved by the Institutional Review Board of Gyeongsang National University Hospital with a waiver of informed consent (GNUH-10-026).

pISSN 2383-7837
eISSN 2383-7845

Tissue microarray

Surgically resected specimens were fixed overnight in buffered neutral formalin (20%). The samples were embedded in paraffin blocks and examined. One or two representative glass slides and matched blocks were selected via microscopic review. One core of 2-mm representative tissue was collected from each paraffin block and transplanted onto new recipient tissue microarray (TMA) blocks.

Immunohistochemical analysis

Primary antibody for PD-L1 (1:200, E1L3N, Cell Signaling Technology, Danvers, MA, USA) and PD-1 (1:100, ab52587, Abcam, Cambridge, UK) was used to investigate protein expression. The immunohistochemical (IHC) method was described in our previous report.[17] Fibrotic stromal area was used as negative internal control. IHC results were scored in both tumor and inflammatory cells by two pathologists. Delicate membranous or distinct cytoplasmic staining without nonspecific stromal staining was considered positive. The number of positive cells was analyzed in two categories, PTC cells and inflammatory cells. According to their proportion, PTC cells stained positive in each core of TMA block were scored as negative, grade 1 (1%–50%), and grade 2 (51%–100%). Similarly, positive inflammatory cells were graded as negative, grade 1 (1%–10%), and grade 2 (11%–20%). The intensity of each protein expression was simplified as negative or positive to increase reproducibility.

Statistical analysis

The correlation of each factor was analyzed using chi-square tests. The results were considered statistically significant with p-value less than .05. SPSS ver. 18.0 (SPSS Inc., Chicago, IL, USA) was used for all statistical analysis.

RESULTS

Clinicopathological features of 116 PTC patients

The clinicopathological features of the 116 PTC patients are summarized in Table 1. The mean age of the PTC patients was 49.5 years (range, 25 to 88 years). A total of 54 (46.6%), three (2.6%), and 59 (50.9%) patients were evaluated as T stage 1, 2, and 3, respectively. LN metastasis was diagnosed in 24 patients (20.7%).

Correlation of PD-L1 and PD-1 expression in PTC cells and inflammatory cells

The proportion of positive cells is summarized in Table 2. For PTC cells, 39 (33.6%) patients exhibited PD-L1 expression, and five (8.3%) were positive for PD-1 protein (Fig. 1). Meanwhile, for inflammatory cells, seven (6%) and six (5.2%) patients were positive for PD-L1 and PD-1 expressions, respectively.

Correlation among PD-L1 and PD-1 expressions and clinicopathological data

The correlation between PD-L1 and PD-1 expressions is shown in Table 3. The increased proportion of PD-L1–positive PTC cells (PDL1-PTC) was significantly correlated with increased proportion of PD-1–positive PTC cells ($p = .001$) and PD-1–positive inflammatory cells (PD1-IC) ($p < .001$). The increased proportion of PD-L1–positive inflammatory cells was closely related with the

Table 1. Clinicopathological features

Variable	No. (%)
Clinical information	
Age, mean (range)	49.5 (25–88)
Sex (male:female)	20:96
Patients number with LND	51 (44.0)
Pathologic information	
T stage	
1	54 (46.6)
2	3 (2.6)
3	59 (50.9)
N stage	
0	92 (79.3)
1	24 (20.7)
PD-L1	
Positive in PTC	39 (33.6)
Positive in IC	7 (6.0)
PD-1	
Positive in PTC	5 (8.3)
Positive in IC	6 (5.2)
Total	116

LND, lymph node dissection; PD-L1, programmed death-ligand 1; PTC, papillary thyroid carcinoma; IC, inflammatory cells; PD-1, programmed cell death protein 1.

Table 2. Number of patients who showed PD-L1– and PD-1–positive cells

	PD-L1	PD-1
PTC (n = 116)		
Negative	77	111
1%–50% positive	34	3
51%–100% positive	5	2
IC (n = 116)		
Negative	109	110
1%–10% positive	7	5
11%–20% positive	0	1

PD-L1, programmed death-ligand 1; PD-1, programmed cell death protein 1; PTC, papillary thyroid carcinoma; IC, inflammatory cells.

https://doi.org/10.4132/jptm.2017.07.26

increased proportion of PD1-IC ($p < .001$).

The relationship between the collected clinicopathological data (age, sex, T stage, and N stage) and the expressions of PD-L1 and PD-1 in PTC cells and inflammatory cells was analyzed. The results indicated no significant correlation, except for the proportion of PDL1-PTC and LN metastasis ($p = .036$) (Table 4).

DISCUSSION

In the control of T-cell immunity, positive and negative signals regulated within the T cells make balance between immune cell responses.[18] The receptor and ligand interactions of T cells can support not only positive signals to improve T-cell activation but also negative signals to eliminate T cells.[19] Among the negative signals, immune checkpoint proteins, PD-1 or PD-L1 are crucial to keep self-tolerance to avoid autoimmunity, through the interaction between T cells and antigen-presenting cells.[20] Ligation of PD-1 by PD-L1 inhibits proliferation of lymphocytes and cytokine production by activated cytotoxic T cells.[21] The PD-1/PD-L1 checkpoint pathway regulates not only virally infected T cells in the peripheral tissue[21] but also transformed cells within the tumor microenvironment.[22,23] Tumor cells co-work with immune checkpoints to avoid being destructed by host immune system.

Activated T lymphocytes normally induce PD-L1 expression on macrophages or host cells. Besides, there are some tumor cells that erratically express PD-L1.[19] PD-L1, which is called B7-H1 or CD27, is one of the B7 gene family members expressed on the surface of the tumor cells. When effector T cells are activated, PD-1 is highly expressed on the regulatory T cells (Treg cells). The immune responses of Treg cells remain to be discovered completely. By producing inhibitory cytokines, they have an essential role for immune resistance in many tumors.[20] Meanwhile, T cell exhaustion was first reported with chronic lymphocytic choriomeningitis virus infection of mice during which activated virus-specific T cells without effector function persist.[24] Exhausted T cells overexpress multiple cell-surface inhibitory receptors, including PD-1, LAG-3, and 2B4.[25] These cells are not able to reduce PD-L1 expression, which is normally suppressed when T cells are activated.[25]

Tumors with PD-1 positive exhausted T cells and Treg cells may show high proportion of PD-L1–positive tumor cells. In this study, a statistically significant association existed between the expression of PD-1 and PD-L1 markers both in papillary carcinoma ($p = .001$) and lymphoid cells ($p < .001$). Moreover, the proportion of PD-L1 expression in papillary carcinoma cells was closely associated with metastatic LNs ($p = .036$). Similarly, PD-L1 was high ($p = .0443$) in patients with nodal metastases in a previous study.[26] In summary, our clinical data of PTC with LN metastasis was significantly associated with PD-1/PD-L1 pathway. Although 12 out of 24 cases were negative for PD-L1 expression in PTC with metastatic LNs, the proportion of its expression and the predictive value are still meaningful. Exhausted T cells change the expression of molecules related to cell adhesion, migration, and chemotaxis during chronic viral infection.[25] We assumed that PD-1–positive exhausted T cells must have altered the expression of molecules, probably modifying migratory characters in the tumor microenvironment along the metastatic cascade.

In previous studies regarding regionally metastatic differentiated thyroid carcinomas, PD-1–positive T cells and Treg cells were higher in tumor-involved LNs compared with those not involved and were related to recurrent disease.[26] The association between elevated Treg cell levels and recurrent disease supports the hypothesis that Treg cells are induced by the residual metastatic tumor to avoid immune responses.[23] Because tumors with high levels of infiltrating Treg cells may suppress immune responses, inhibition of the PD-1/PD-L1 pathway may improve antitumor immune responses by reducing the number of or suppressing Treg cells.[20]

Our data support the existence of PD-L1 blockades in patients with thyroid carcinoma with metastatic LNs and its predictive

Table 3. The p-values of chi-square tests between positive proportion of PD-L1 and PD-1 at each TMA cores

	PTC		IC	
	PD-L1	PD-1	PD-L1	PD-1
PTC				
PD-L1	-	.001	.071	<.001
PD-1	.001	-	.126	.172
IC				
PD-L1	.071	.126	-	<.001
PD-1	<.001	.172	<.001	-

PD-L1, programmed death-ligand 1; PD-1, programmed cell death protein 1; TMA, tissue microarray; PTC, papillary thyroid carcinoma; IC, inflammatory cells.

Table 4. Correlation between PD-L1–positive PTC cells and metastasis to lymph nodes

Proportion of PD-L1 expression in PTC cells (%)	LN metastasis		
	No	Yes	Total
0	65	12	77
1–50	25	9	34
51–100	2	3	5
Total	92	24	p=.036

PD-L1, programmed death-ligand 1; PTC, papillary thyroid carcinoma; LN, lymph node.

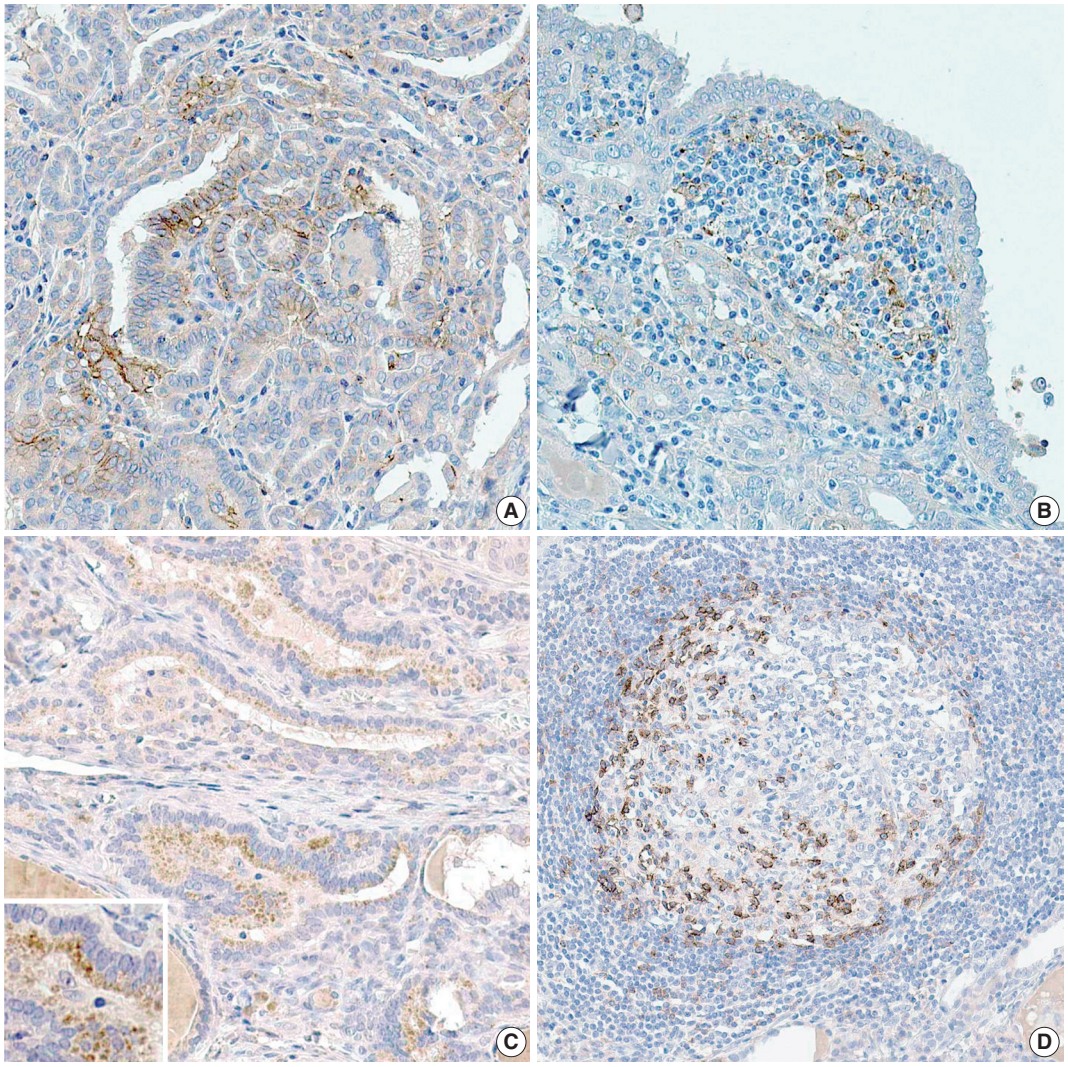

Fig. 1. (A) More than one-half of papillary carcinoma cells (PTCs) show mild programmed death-ligand 1 (PD-L1) expression in the cytoplasm. There are many PTCs with strong PD-L1 expression in cellular membrane in the center of the figure. (B) Inflammatory cells that surround PTCs exhibit PD-L1 expression. (C) Most of the PTCs reveal programmed cell death protein 1 (PD-1) expression in the perinuclear cytoplasmic area. (D) Inflammatory cells in the germinal center have reactivity to PD-1.

value as a biomarker for metastatic LNs. Immunomodulating therapies that suppress PD-L1 might be used for patients with persistent disease because regionally metastatic thyroid carcinomas are not eliminated by the host immune system. The prognostic role of PD-L1 expression associated with LN metastasis was elucidated in this study.

Conflicts of Interest

No potential conflict of interest relevant to this article was reported.

Acknowledgments

This work was funded by the research promotion program of Gyeongsang National University, 2016.

REFERENCES

1. Herbst RS, Baas P, Kim DW, *et al*. Pembrolizumab versus docetaxel for previously treated, PD-L1-positive, advanced non-small-cell lung cancer (KEYNOTE-010): a randomised controlled trial. Lancet 2016; 387: 1540-50.
2. Juárez-Salcedo LM, Sandoval-Sus J, Sokol L, Chavez JC, Dalia S. The role of anti-PD-1 and anti-PD-L1 agents in the treatment of diffuse large B-cell lymphoma: The future is now. Crit Rev Oncol Hematol

2017; 113: 52-62.
3. Motoshima T, Komohara Y, Ma C, *et al*. PD-L1 expression in papillary renal cell carcinoma. BMC Urol 2017; 17: 8.
4. Fontugne J, Augustin J, Pujals A, *et al*. PD-L1 expression in perihilar and intrahepatic cholangiocarcinoma. Oncotarget 2017; 8: 24644-51.
5. Jiang Y, Lo AW, Wong A, *et al*. Prognostic significance of tumor-infiltrating immune cells and PD-L1 expression in esophageal squamous cell carcinoma. Oncotarget 2017; 8: 30175-89.
6. Ness N, Andersen S, Khanehkenari MR, *et al*. The prognostic role of immune checkpoint markers programmed cell death protein 1 (PD-1) and programmed death ligand 1 (PD-L1) in a large, multicenter prostate cancer cohort. Oncotarget 2017; 8: 26789-801.
7. Park IH, Yang HN, Lee KJ, *et al*. Tumor-derived IL-18 induces PD-1 expression on immunosuppressive NK cells in triple-negative breast cancer. Oncotarget 2017; 8: 32722-30.
8. Jin S, Xu B, Yu L, *et al*. The PD-1, PD-L1 expression and CD3+ T cell infiltration in relation to outcome in advanced gastric signet-ring cell carcinoma, representing a potential biomarker for immunotherapy. Oncotarget 2017; 8: 38850-62.
9. Gravelle P, Burroni B, Péricart S, *et al*. Mechanisms of PD-1/PD-L1 expression and prognostic relevance in non-Hodgkin lymphoma: a summary of immunohistochemical studies. Oncotarget 2017; 8: 44960-75.
10. Zhou Y, Miao J, Wu H, *et al*. PD-1 and PD-L1 expression in 132 recurrent nasopharyngeal carcinoma: the correlation with anemia and outcomes. Oncotarget 2017; 8: 51210-23.
11. Chen N, Fang W, Lin Z, *et al*. KRAS mutation-induced upregulation of PD-L1 mediates immune escape in human lung adenocarcinoma. Cancer Immunol Immunother 2017; 66: 1175-87.
12. Chovanec M, Cierna Z, Miskovska V, *et al*. Prognostic role of programmed-death ligand 1 (PD-L1) expressing tumor infiltrating lymphocytes in testicular germ cell tumors. Oncotarget 2017; 8: 21794-805.
13. Botti G, Collina F, Scognamiglio G, *et al*. Programmed death ligand 1 (PD-L1) tumor expression is associated with a better prognosis and diabetic disease in triple negative breast cancer patients. Int J Mol Sci 2017; 18: E459.
14. Han J, Hong Y, Lee YS. PD-L1 expression and combined status of PD-L1/PD-1-positive tumor infiltrating mononuclear cell density predict prognosis in glioblastoma patients. J Pathol Transl Med 2017; 51: 40-8.
15. Nikiforov YE, Seethala RR, Tallini G, *et al*. Nomenclature revision for encapsulated follicular variant of papillary thyroid carcinoma: a paradigm shift to reduce overtreatment of indolent tumors. JAMA Oncol 2016; 2: 1023-9.
16. Nixon IJ, Wang LY, Migliacci JC, *et al*. An international multi-institutional validation of age 55 years as a cutoff for risk stratification in the AJCC/UICC staging system for well-differentiated thyroid cancer. Thyroid 2016; 26: 373-80.
17. Song DH, Ko GH, Lee JH, *et al*. Myoferlin expression in non-small cell lung cancer: Prognostic role and correlation with VEGFR-2 expression. Oncol Lett 2016; 11: 998-1006.
18. Chen L. Co-inhibitory molecules of the B7-CD28 family in the control of T-cell immunity. Nat Rev Immunol 2004; 4: 336-47.
19. Thompson RH, Dong H, Kwon ED. Implications of B7-H1 expression in clear cell carcinoma of the kidney for prognostication and therapy. Clin Cancer Res 2007; 13(2 Pt 2): 709s-15s.
20. Pardoll DM. The blockade of immune checkpoints in cancer immunotherapy. Nat Rev Cancer 2012; 12: 252-64.
21. Freeman GJ, Long AJ, Iwai Y, *et al*. Engagement of the PD-1 immunoinhibitory receptor by a novel B7 family member leads to negative regulation of lymphocyte activation. J Exp Med 2000; 192: 1027-34.
22. Dong H, Strome SE, Salomao DR, *et al*. Tumor-associated B7-H1 promotes T-cell apoptosis: a potential mechanism of immune evasion. Nat Med 2002; 8: 793-800.
23. French JD, Kotnis GR, Said S, *et al*. Programmed death-1+ T cells and regulatory T cells are enriched in tumor-involved lymph nodes and associated with aggressive features in papillary thyroid cancer. J Clin Endocrinol Metab 2012; 97: E934-43.
24. Zajac AJ, Blattman JN, Murali-Krishna K, *et al*. Viral immune evasion due to persistence of activated T cells without effector function. J Exp Med 1998; 188: 2205-13.
25. Wherry EJ, Ha SJ, Kaech SM, *et al*. Molecular signature of CD8+ T cell exhaustion during chronic viral infection. Immunity 2007; 27: 670-84.
26. Bastman JJ, Serracino HS, Zhu Y, *et al*. Tumor-infiltrating T cells and the PD-1 checkpoint pathway in advanced differentiated and anaplastic thyroid cancer. J Clin Endocrinol Metab 2016; 101: 2863-73.

Journal of Pathology and Translational Medicine 2018; 52: 14-20
https://doi.org/10.4132/jptm.2017.10.17

■ ORIGINAL ARTICLE ■

The Significance of TROP2 Expression in Predicting *BRAF* Mutations in Papillary Thyroid Carcinoma

Joon Seog Kong[1] · Hyeon Jin Kim[2]
Min-Jung Kim[2] · Areumnuri Kim[2]
Dalnim Lee[2] · Kanghee Han[1]
Sunhoo Park[1,2] · Jae Soo Koh[1]
Jae Kyung Myung[1,2]

[1]Department of Pathology, Korea Cancer Center Hospital, Seoul; [2]Laboratory of Radiation Exposure and Therapeutics, National Radiation Emergency Medical Center, Korea Institute of Radiological and Medical Sciences, Seoul, Korea

Received: August 4, 2017
Revised: October 8, 2017
Accepted: October 16, 2017

Corresponding Author
Jae Kyung Myung, MD, PhD
Department of Pathology, Korea Cancer Center Hospital, 75 Nowon-ro, Nowon-gu, Seoul 01812, Korea
Tel: +82-2-970-1257
Fax: +82-2-970-2430
E-mail: tontos016@naver.com

Background: Trophoblast antigen 2 (TROP2) is a human trophoblast cell-surface glycoprotein that is overexpressed in several types of epithelial cancers, and is suggested to be associated with an unfavorable prognosis. *BRAF* mutations are the most common genetic alteration in papillary thyroid carcinoma (PTC). We evaluated the correlation between TROP2 expression and *BRAF* mutation in PTC. **Methods:** First, we carried out pyrosequencing for *BRAF* mutations and immunohistochemistry for TROP2 expression with a tissue microarray consisting of 52 PTC cases. Membranous staining in at least 5% of tumor cells was designated as positive staining and we analyzed the relationship between TROP2 expression and diverse clinicopathological factors, including *BRAF* mutation. Second, we tested TROP2 mRNA expression in three thyroid cancer cell lines with *BRAF* mutations (BCPAP, SNU790, and 8505C) and a normal thyroid cell line. Additionally, we checked TROP2 protein levels in a normal thyroid cell line after introduction of the *BRAF* V600E mutation. **Results:** In this study, 21 of 26 cases with *BRAF* mutation showed TROP2 immunoreactivity, whereas all 26 cases without *BRAF* mutation showed no immunoreactivity for TROP2 with a statistically significant difference ($p < .001$). Upregulation of TROP2 mRNA was observed in all three thyroid cancer cell lines, but not in the normal thyroid cell line. Interestingly, however, the TROP2 expression was increased in the normal thyroid cell line after introduction of the *BRAF* V600E mutation. **Conclusions:** Based on these results, we concluded that TROP2 expression is significantly associated with *BRAF* mutation and that TROP2 immunohistochemistry could be used for predicting *BRAF* mutations or diagnosing papillary thyroid carcinoma.

Key Words: TROP2; *BRAF* mutation; Papillary thyroid carcinoma

Thyroid cancer, the most prevalent endocrine malignancy, is histologically classified into papillary thyroid carcinoma (PTC), follicular thyroid carcinoma, poorly differentiated thyroid carcinoma, anaplastic thyroid carcinoma, and medullary thyroid carcinoma. PTC is the most frequently encountered subtype, accounting for 80 to 85% of all thyroid cancers.[1] Trophoblast antigen 2 (TROP2) is a transmembrane receptor glycoprotein encoded by the tumor-associated calcium signal transducer 2 (*Tacstd2*) gene, which is located on chromosome 1p32.[2] TROP2 is also known as membrane component 1 surface marker 1, epithelial glycoprotein 1, gastrointestinal antigen 733-1, and gelatinous drop-like corneal dystrophy (GDLD). TROP2 consists of an extracellular domain, a transmembrane domain, and an intracellular cytoplasmic tail.[2,3] TROP2 was first discovered on the surface of trophoblast cells, where it enables the trophoblasts to invade into the decidualized tissue during placental implantation.[4] TROP2 overexpression has been observed in various types of epithelial cancers, including pancreatic, gastric, colorectal, oral, endometrial, and ovarian cancers, and its overexpression correlates with diverse clinicopathological factors and poor clinical outcome.[5-11] Recently, several studies have evaluated the role of TROP2 protein expression using formalin-fixed paraffin-embedded (FFPE) samples of diverse thyroid tumors, and TROP2 protein expression was detected in PTCs with high sensitivity and specificity.[12-14] Based on these results, immunohistochemical (IHC) staining for TROP2 was determined to be a good diagnostic marker for PTC, not only for surgical specimens, but also for fine needle aspirates. Although these results clearly reveal the usefulness of TROP2 expression for diagnosing PTCs in clinical settings, no mechanism was explored regarding why TROP2 expression was elevated especially in PTC and not in other thyroid cancers. Therefore, to answer this question, we focused on *BRAF* mutations, a major genetic alteration in PTC,[15] as having a crucial effect on TROP2 expression with high sensitivity and specificity in PTC.

pISSN 2383-7837
eISSN 2383-7845

MATERIALS AND METHODS

Overview

In this study, we used immunohistochemistry to investigate TROP2 protein expression on a tissue microarray (TMA) that included 52 PTC cases with or without *BRAF* mutation. We analyzed the relationship between TROP2 expression and diverse clinicopathological factors including age, sex, extrathyroidal extension, and *BRAF* mutation status. In addition, we measured TROP2 mRNA expression in three thyroid cell lines with *BRAF* mutations and a normal thyroid cell line without *BRAF* mutation. We also investigated TROP2 protein levels in a normal thyroid cell line after introduction of the *BRAF* V600E mutation.

Patient characteristics

We retrospectively searched the pathology database of Korea Cancer Center Hospital, Seoul, South Korea, for cases of PTC between January 2012 and June 2013. This study was approved by the Institutional Review Board of Korea Cancer Center Hospital with a waiver of informed consent (K-1707-002-048). Histopathological slides were reviewed by two observers (J.S. Kong and J.K. Myung) and *BRAF* mutation status of these cases was subsequently determined. After dividing the cases into two groups according to *BRAF* mutation, we analyzed diverse clinicopathological factors in each group. Finally, we selected 26 cases with *BRAF* mutation and 26 cases without *BRAF* mutation, with each group having similar clinicopathological factors. The clinicopathological features of the two groups are described in Table 1.

Table 1. Clinicopathological features of papillary thyroid carcinoma (52 cases)

Characteristic	*BRAF* V600E mutation		p-value
	Negative (26 cases)	Positive (26 cases)	
Sex (male:female)	1:12 (2:24)	1:1.8 (10:18)	.035
Age (yr)	47.3 (29–66)	48.1 (25–66)	.806[a]
Histological subtype			.005
Classical	17 (65.4)	25 (96.2)	
Follicular variant	9 (34.6)	1 (3.8)	
Tumor size (cm)	0.91 (0.2–2.8)	1.07 (0.4–2.5)	.560
≤1	18 (69.2)	16 (61.5)	
>1	8 (30.8)	10 (38.5)	
Lymph node metastasis			.266
Absent	15 (57.7)	12 (46.2)	
Present	11 (42.3)	14 (53.8)	
Extrathyroidal extension			.092
Absent	14 (53.8)	8 (30.8)	
Present	12 (46.2)	18 (69.2)	
Recurrence or distant metastasis			NA
Absent	26 (100)	26 (100)	
Present	0	0	
Survival			NA
Alive	26 (100)	26 (100)	
Death	0	0	

Values are presented as mean (range) or number (%).
NA, not appilicable.
[a]t test.

Tissue microarrays

TMAs were constructed from thyroid resection specimens. Cores (2-mm diameter) from each block were obtained from the donor and put into a recipient block using a trephine apparatus (SuperBioChips Laboratories, Seoul, Korea). The TMAs contained 26 cases of PTC with *BRAF* mutation and 26 cases of PTC without *BRAF* mutation.

Immunohistochemistry

Tissue sections (4 μm thick) were obtained from TMA blocks. The slides were stained using automatic IHC staining equipment (Lab Vision Autostainer 480S, Thermo Scientific, Fremont, CA, USA). After deparaffinization and epitope retrieval using PT module buffer 1 (Thermo Scientific) at 98°C for 20 minutes, we utilized the UltraVision LP Detection System (Thermo Scientific) according to the manufacturer's protocol. Monoclonal antibody against TROP2 (1:200, Santa Cruz Biotechnology, Santa Cruz, CA, USA) was applied to sections and incubated for 60 minutes at room temperature. After incubation with a primary antibody enhancer (Thermo Scientific) for 20 minutes, we carried out a horseradish peroxidase (HRP) polymer (Thermo Scientific) and DAB chromogen-substrate for reaction. Slides were counterstained with Gill2-hematoxylin for 1 second and mounted. Appropriate positive and negative controls were included. Interpretation of TROP2 expression was performed by two independent pathologists (J.S. Kong and J.K. Myung). The cases showing membranous staining in more than 5% of cells was designated as TROP2-positive, similar to guidelines utilized by other studies.[6,13]

Detection of *BRAF* mutation

Genomic DNA was extracted from FFPE blocks with the highest percentage of tumors using a QIA amp Mini Kit (Qiagen, Hilden, Germany). DNA was amplified with polymerase chain reaction (PCR) primer sets, and one strand of each set was bound to biotin at the 5' end (primer forward, 5'-biotin-CTTCATAATGCTTGCTCTGATAGG-3'; reverse, 5'-GGCCAAAAATTTAATCAGTGGAA-3'). The PCR procedure was carried out

in a total volume of 50 μL containing 5 μL of the DNA (2 ng/μL), 1 μL of each primer (10 pM), 4 μL of $MgCl_2$, 5 μL of 10×PCR buffer, 2.5 μL of dNTP (2.5 mM), 0.3 μL of Taq Gold DNA polymerase, and 31.2 μL of H_2O. The PCR conditions consisted of initial denaturing at 95°C for 5 minutes, 45 cycles at 95°C for 15 seconds, 54°C for 30 seconds, and 72°C for 15 seconds, and a final extension at 72°C for 5 minutes. The PCR products were analyzed by electrophoresis in a 2% agarose gel to confirm successful amplification. The other 20 μL of PCR product was bound to streptavidin beads (GE Healthcare, Buckinghamshire, UK), purified, washed, and denatured with 0.2 mol/L NaOH solution. Then, 0.3 μmol/L pyrosequencing primer (5'-CCACTCCATCGAGATT-3') was annealed to the purified single-stranded PCR product, and sequencing was performed using a PyroMark ID system (Qiagen, Valencia, CA, USA), according to the manufacturer's instructions.

Cell culture

Three human thyroid cancer cell lines with *BRAF* V600E mutations, BCPAP, SNU790, and 8505C, were obtained from Dr. M.J. Kim (Seoul National University Hospital, Seoul, Korea) and the human normal thyroid Nthy-ori 3-1 (Nthy) cell line was purchased from Sigma-Aldrich Biotechnology (St. Louis, MO, USA). All cells were cultured in RPMI-1640 medium (Lonza, Walkersville, MD, USA) supplemented with 10% fetal bovine serum (JR Scientific Inc., Woodland, CA, USA) and 0.1% gentamicin (Lonza). Cells were maintained in a humidified incubator at 37°C with 5% CO_2.

Reverse transcription polymerase chain reaction

Total RNA was isolated from cultured cells using Trizol reagent (Molecular Research Center Inc., Cincinnati, OH, USA). Reverse transcription was carried out with a cDNA reverse transcription kit (AccuPower RT, Bioneer, Seoul, Korea) following the manufacturer's protocol. The PCR conditions were as follows: initial denaturation at 95°C for 5 minutes; followed by 35 cycles of 95°C for 1 minute, 56°C for 1 minute, and 72°C for 1 minute; and a final extension step of 72°C for 10 minutes. The amplified products were resolved on a 1.5% agarose-ethidium bromide gel and quantified by a Chemi XRS Gel Documentation System (Bio-Rad, Hercules, CA, USA). The following primers were used: the housekeeping gene glyceraldehyde-3-phosphate dehydrogenase, forward 5'-CGAGA TCCCTCCAAAATCAA-3' and reverse 5'-TGTGGTCATGAGTCCTTCCA-3'; *TROP2* #1, forward 5'-CCTCATCGCCGTCATCGT-3' and reverse 5'-CGGTT CCTTTCTCAACTCCC-3'; and *TROP2* #2, forward 5'-TATTACCTGGACGAGATTCCCC-3' and reverse 5'-CCCCGACTTTCTCCGGTTG-3'.

Vector construction and cell infection

The human oncogenic *BRAF* construct, pBABEbleo-Flag-*BRAF* V600E, was obtained from Addgene (Cambridge, MA, USA). Retroviral particles were produced by H29D packaging cells using a TransIT-X2 Dynamic Delivery System (Mirus Bio, LLC, Madison, WI, USA) according to the manufacturer's protocols. Nthy cells were infected with viral supernatant containing 8 μg/mL polybrene. Zeocin (100 μg/mL, Invitrogen, San Diego, CA, USA) was used for selecting Zeocin-resistant transfectants.

Western blot analysis

Cells were harvested in NP-40 lysis buffer (Invitrogen) according to the manufacturer's instructions. Following incubation at 4°C for 30 minutes, lysate was centrifuged at 13,000×g for 20 minutes at 4°C. Protein concentration was determined using a BCA assay (Bio-Rad). Whole cell lysates were separated by 10% sodium dodecyl sulfate-polyacrylamide gel electrophoresis. The separated proteins were electrophoretically transferred onto PVDF membranes (Millipore, Bedford, MA, USA) overnight at 4°C. Immunoreactive bands were developed using a HRP-conjugated secondary antibody, and the proteins were visualized by enhanced chemiluminescence (Amersham Biosciences, Piscataway, NJ, USA). The following primary antibodies were used: TROP2 (1:1,000, Santa Cruz Biotechnology), *BRAF* (1:1000, Santa Cruz Biotechnology), β-actin (1:1,000, Santa Cruz Biotechnology), phosphorylated-extracellular signal-regulated kinase (p-ERK; 1:1,000, Cell Signaling Technology, Beverly, MA, USA), and ERK (1:1,000, Cell Signaling Technology).

Statistical analysis

All statistical analyses were performed using the SPSS ver. 23.0 (IBM Corp., Armonk, NY, USA). Pearson's chi-square test and t tests were used to compare the different clinicopathological factors in each group according to *BRAF* mutation. Pearson's chi-square test and Fisher exact test were used to evaluate the association of *BRAF* mutation and TROP2 expression in PTC. For all analyses, a p-value of $<.05$ was considered statistically significant.

RESULTS

Patient characteristics

A total of 52 patients were included in this study. Most pa-

https://doi.org/10.4132/jptm.2017.10.17

tients were female (n = 42, 80.8%), with a male to female ratio of 1:4.2. The median age of the 52 PTC patients was 47.7 years. All cases were divided into two groups according to *BRAF* V600E mutation. The median ages of the *BRAF* wildtype group and mutant group were 47.3 years and 48.1 years, respectively. The average tumor diameters of the two groups were 0.91 cm (*BRAF* wildtype group) and 1.07 cm (*BRAF* mutant group). The *BRAF* wildtype group showed 17 cases of classical PTC and nine cases of follicular variant of PTC. Twenty-five cases of classical PTC and one case of follicular variant of PTC were included in the *BRAF* mutant group. Lymph node metastasis was observed in 11 cases of *BRAF* wildtype group (42.3%) and in 14 cases of *BRAF* mutant group (53.8%). Extrathyroidal extension was identified in 12 cases (46.2%, *BRAF* wildtype group) and in 18 cases (69.2%, *BRAF* mutant group). There was no case of recurrence or distant metastasis in the two groups. At the time of analysis, all 52 patients were still alive. Sex and histological subtype were significantly different between the two groups (p = .035 and p = .005, respectively). Age, tumor size, lymph node metastasis, and extrathyroidal extension revealed no statistically significant difference between the two groups. These results are summarized in Table 1.

Expression of TROP2 and its correlation with clinicopathological factors

Positive TROP2 immunoreactivity was designated as homogeneously strong membranous staining in at least 5% of tumor cells (Fig. 1). Positive TROP2 immunoreactivity was found in 21 cases (40.4%). Twenty of 21 cases with positive immunostaining for TROP2 were classical PTC and one case was follicular variant of PTC. Of the 42 classical PTC cases, 20 (47.6%) cases revealed positive immunostaining for TROP2, whereas one of 10 follicular variants of PTC showed TROP2 immunoreactivity. TROP2 expression was significantly correlated with histological subtype (p = .036). Of the 26 patients with a *BRAF* V600E mutation, 21 (80.8%) were positive for TROP2. In contrast, all 26 patients lacking *BRAF* V600E mutation showed no TROP2 immunoreactivity. TROP2 expression was significantly correlated with *BRAF* V600E mutation (p < .001). We also analyzed the association between TROP2 expression and diverse clinicopathological factors. Neither sex nor age, which was divided into two groups (above and below 47 years old), was correlated with TROP2 expression. Lymph node metastasis and extrathyroidal extension, which reflect poor clinical outcomes in PTC patients, were also not related to TROP2 expression. These results are summarized in Table 2.

mRNA expression of TROP2 in normal and PTC cell lines

We identified a strong association between TROP2 protein expression and *BRAF* V600E mutation in PTC tissue samples. Therefore, we also performed reverse transcription polymerase chain reaction (RT-PCR) to evaluate the correlation of TROP2 mRNA expression and *BRAF* V600E mutation. We analyzed the mRNA level of TROP2 in a normal thyroid cell line (Nthy) and thyroid cancer cell lines (BCPAP, SUN790, and 8505C). We identified the *BRAF* V600E mutation in these three thyroid cancer cell lines in previous studies.[16,17] TROP2 mRNA expression was not detected in Nthy cells. In contrast, PTC cell lines (BCPAP and SUN790) and the anaplastic thyroid cancer cell line (8505C) showed TROP2 mRNA expression (Fig. 2A).

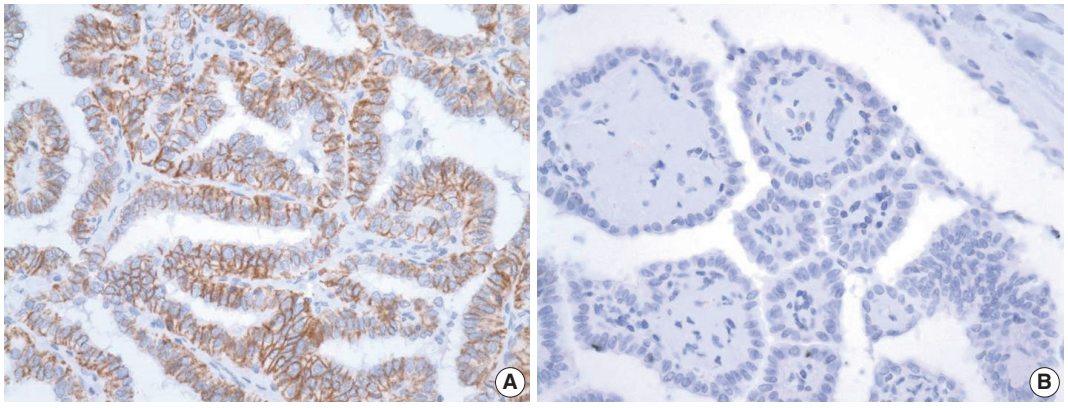

Fig. 1. Representative image of trophoblast antigen 2 (TROP2) immunohistochemistry. Membranous staining of TROP2 in more than 5% area of entire field was considered positive (A) and no immunoreactivity for TROP2 expression or case showing the area of staining in less than 5% were negative (B).

TROP2 protein expression after *BRAF* V600E mutation introduction in normal thyroid cells

We examined TROP2 mRNA expression in a normal thyroid cell line and three thyroid cancer cell lines and found that all cancer lines had the *BRAF* V600E mutation and showed TROP2 mRNA expression, while the normal cell line had neither. Therefore, we infected the normal thyroid cell line with the human oncogenic *BRAF* construct pBABEbleo-Flag-*BRAF*V600E, and evaluated changes in TROP2 protein level by Western blotting. TROP2 protein was detected in the normal thyroid cell line after introducing the *BRAF* V600E mutation via viral infection (Fig. 2B). As expected, we also observed that p-ERK and ERK levels were elevated in the presence of *BRAF* V600E mutation.[18,19]

Table 2. Correlation between TROP2 expression and clinicopathological features

Characteristic	TROP2 expression		Total	p-value
	–	+		
Sex				.282[a]
Male	4 (40.0)	6 (60.0)	10	
Female	27 (64.3)	15 (35.7)	42	
Histological subtype				.036[a]
Classical	22 (52.4)	20 (47.6)	42	
Follicular variant	9 (90.0)	1 (10.0)	10	
Age (yr)				.782
<45	13 (61.9)	8 (38.1)	21	
≥45	18 (58.1)	13 (41.9)	31	
Tumor size (cm)				.873
≤1	20 (58.8)	14 (41.2)	34	
>1	11 (61.1)	7 (38.9)	18	
Lymph node metastasis				.191
Absent	19 (67.9)	9 (32.1)	28	
Present	12 (50.0)	12 (50.0)	24	
Extrathyroidal extension				.099
Absent	16 (72.7)	6 (27.3)	22	
Present	15 (50.0)	15 (50.0)	30	
BRAF V600E mutation				<.001
Wild	26 (100)	0	26	
Mutant	5 (19.2)	21 (80.8)	26	

Values are presented as number (%).
TROP2, trophoblast antigen 2.
[a]Fisher exact test.

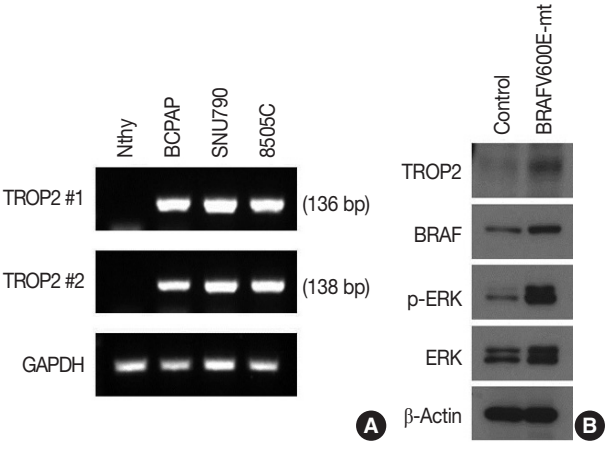

Fig. 2. Expression of trophoblast antigen 2 (TROP2) *in vitro*. (A) Reverse transcription polymerase chain reaction. High levels of TROP2 expression were observed in all three thyroid cancer cell lines (BCPAP, SNU790, and 8505C) compared to normal thyroid cell line (Nthy). Expression of glyceraldehyde 3-phosphate dehydrogenase was used as an internal control. (B) Western blot analysis. TROP2 protein levels were increased in the normal thyroid cell line after expression of *BRAF* V600E mutant. The levels of p-ERK and ERK were also elevated with increasing *BRAF* mutational status.

DISCUSSION

In this study, we aimed to evaluate the role of TROP2 expression in PTC based on the fact that TROP2 expression affects the prognosis in diverse epithelial cancers. Knowledge of the role of TROP2 expression, especially in thyroid tumors, has been limited until now. Only three previous studies have evaluated the role of TROP2 expression in thyroid tumors.[12-14] These studies mainly focused on the clinical utility of TROP2 expression for differential diagnosis of thyroid tumors, especially in fine-needle aspiration (FNA) specimens. According to these studies, TROP2 expression had a higher sensitivity and specificity for diagnosing PTC than other established markers such as cytokeratin 19, HBME1, and galectin 3, which were commonly used in practice. Therefore, IHC for TROP2 expression was a good diagnostic tool in pathological practices for differential diagnosis of thyroid tumors. In this regard, we wanted to investigate why TROP2 was overexpressed in PTC, but not in other thyroid tumors, and evaluate if the *BRAF* mutation was related. To answer this question, we performed IHC to detect TROP2 expression and pyrosequencing to detect *BRAF* mutation, and then evaluated the association between TROP2 expression and *BRAF* mutation. Consequentially, TROP2 expression was significantly related with *BRAF* mutation. We concluded that the diagnostic utility of TROP2 expression came from the *BRAF* mutation, which contributes to PTC tumorigenesis. Although there was no mention of an association between *BRAF* mutation and TROP2 expression in the abovementioned studies, *BRAF* mutation was an important factor influencing TROP2 expression. Therefore, when diagnosing the cases with no TROP2 expression, PTC cannot be ruled out because PTC without *BRAF* mutation does occur. In other words, before interpreting TROP2 expression for differential diagnosis of PTC especially with FNA, *BRAF* mutation status should be considered. We also divided PTC into the two histo-

https://doi.org/10.4132/jptm.2017.10.17

logical subtypes, classical and follicular variant of PTC. Most cases of follicular variant of PTC showed no TROP2 immunoreactivity, however, 20 classical PTC cases (47.6%) showed TROP2 immunoreactivity. TROP2 expression had a significant correlation with histological subtype. Therefore, in clinical practice, applying TROP2 IHC may help in the diagnosis of classical PTC cases having *BRAF* mutation. We also carried out further *in vitro* studies to clarify the association between *BRAF* mutation and TROP2 expression. We observed TROP2 mRNA expression in three thyroid cancer cell lines with *BRAF* mutation, but no such expression in a normal thyroid cell line. Interestingly, Western blot analysis revealed that TROP2 protein expression was detected in a normal thyroid cell line after introduction of the *BRAF* V600E mutation via viral infection. These results support our IHC study of the association between TROP2 expression and the *BRAF* V600E mutation in PTC. Expressions of ERK and p-ERK were also increased after introduction of the *BRAF* V600E mutation compared to controls. The fact that *BRAF* mutations contribute to PTC tumorigenesis by activating the mitogen-activated protein kinase (MAPK) pathway has been well-established.[19,20] TROP2 expression also promotes tumorigenesis by activating the MAPK/ERK pathway, which has important implications for various cellular pathways, leading to cancer cell proliferation, migration, invasion, and survival.[21] Activation of the MAPK/ERK pathway also contributes to tumor invasion and metastasis as well as tumor growth by interacting with other molecules and signaling pathways.[22,23] In view of this, we hypothesized that TROP2 expression may be correlated with *BRAF* mutation status to directly or indirectly induce ERK pathway activation. ERK pathway activation affects the tumor progression or clinical outcomes. However, our present study did not explain exactly what molecules are involved in activating ERK. Therefore, we will determine the details of signaling between TROP2 and *BRAF* mutation in a future study. As previously mentioned, TROP2 overexpression is associated with aggressive biological behavior and poor prognosis in pancreatic, gastric, colorectal, oral, endometrial, and ovarian cancers. However, the relationship between TROP2 expression and PTC outcome remained unclear until now; we assume that TROP2 expression may confer poor PTC prognosis like other epithelial tumors. However, our results did not show a correlation between TROP2 expression and aggressive clinicopathological features including extrathyroidal extension ($p = .099$) and lymph node metastasis ($p = .191$). We believe these limitations arose from the relatively small sample size and lack of long-term follow-up. Also, data analysis of the cases divided into two groups according to *BRAF* mutation and analysis after combining them into one group should be interpreted with caution. Therefore, further studies with a larger number of cases are required to determine whether TROP2 is an indicator of poor PTC prognosis. In conclusion, we found a significant association between TROP2 expression and *BRAF* mutation in PTC. This correlation was confirmed by IHC staining, RT-PCR, and Western blot analysis. Although the molecular players in thyroid cancer progression have not yet been entirely elucidated, TROP2 may be a key molecule to better understand PTC pathogenesis.

Conflicts of Interest

No potential conflict of interest relevant to this article was reported.

Acknowledgments

This study was supported by a grant from the Korea Institute of Radiological and Medical Sciences (KIRAMS), funded by the Ministry of Science, ICT and Future Planning, Republic of Korea (1711045543;1711045540/50476-2017).

REFERENCES

1. Jemal A, Bray F, Center MM, Ferlay J, Ward E, Forman D. Global cancer statistics. CA Cancer J Clin 2011; 61: 69-90.
2. Shvartsur A, Bonavida B. Trop2 and its overexpression in cancers: regulation and clinical/therapeutic implications. Genes Cancer 2015; 6: 84-105.
3. McDougall AR, Tolcos M, Hooper SB, Cole TJ, Wallace MJ. Trop2: from development to disease. Dev Dyn 2015; 244: 99-109.
4. Lipinski M, Parks DR, Rouse RV, Herzenberg LA. Human trophoblast cell-surface antigens defined by monoclonal antibodies. Proc Natl Acad Sci U S A 1981; 78: 5147-50.
5. Fang YJ, Lu ZH, Wang GQ, *et al*. Elevated expressions of MMP7, TROP2, and survivin are associated with survival, disease recurrence, and liver metastasis of colon cancer. Int J Colorectal Dis 2009; 24: 875-84.
6. Fong D, Moser P, Krammel C, *et al*. High expression of TROP2 correlates with poor prognosis in pancreatic cancer. Br J Cancer 2008; 99: 1290-5.
7. Fong D, Spizzo G, Gostner JM, *et al*. TROP2: a novel prognostic marker in squamous cell carcinoma of the oral cavity. Mod Pathol 2008; 21: 186-91.
8. Mühlmann G, Spizzo G, Gostner J, *et al*. TROP2 expression as prognostic marker for gastric carcinoma. J Clin Pathol 2009; 62:

152-8.
9. Guan GF, Zhang DJ, Wen LJ, *et al*. Prognostic value of TROP2 in human nasopharyngeal carcinoma. Int J Clin Exp Pathol 2015; 8: 10995-1004.
10. Bignotti E, Todeschini P, Calza S, *et al*. Trop-2 overexpression as an independent marker for poor overall survival in ovarian carcinoma patients. Eur J Cancer 2010; 46: 944-53.
11. Bignotti E, Zanotti L, Calza S, *et al*. Trop-2 protein overexpression is an independent marker for predicting disease recurrence in endometrioid endometrial carcinoma. BMC Clin Pathol 2012; 12: 22.
12. Addati T, Achille G, Centrone M, *et al*. TROP-2 expression in papillary thyroid cancer: a preliminary cyto-histological study. Cytopathology 2015; 26: 303-11.
13. Simms A, Jacob RP, Cohen C, Siddiqui MT. TROP-2 expression in papillary thyroid carcinoma: potential diagnostic utility. Diagn Cytopathol 2016; 44: 26-31.
14. Liu H, Shi J, Lin F. The potential diagnostic utility of TROP-2 in thyroid neoplasms. Appl Immunohistochem Mol Morphol 2017; 25: 525-33.
15. Xing M. *BRAF* mutation in thyroid cancer. Endocr Relat Cancer 2005; 12: 245-62.
16. Schweppe RE, Klopper JP, Korch C, *et al*. Deoxyribonucleic acid profiling analysis of 40 human thyroid cancer cell lines reveals cross-contamination resulting in cell line redundancy and misidentification. J Clin Endocrinol Metab 2008; 93: 4331-41.
17. Koh CS, Ku JL, Park SY, *et al*. Establishment and characterization of cell lines from three human thyroid carcinomas: responses to all-trans-retinoic acid and mutations in the BRAF gene. Mol Cell Endocrinol 2007; 264: 118-27.
18. Busca R, Abbe P, Mantoux F, *et al*. Ras mediates the cAMP-dependent activation of extracellular signal-regulated kinases (ERKs) in melanocytes. EMBO J 2000; 19: 2900-10.
19. Davies H, Bignell GR, Cox C, *et al*. Mutations of the *BRAF* gene in human cancer. Nature 2002; 417: 949-54.
20. Peyssonnaux C, Eychène A. The Raf/MEK/ERK pathway: new concepts of activation. Biol Cell 2001; 93: 53-62.
21. Cubas R, Zhang S, Li M, Chen C, Yao Q. Trop2 expression contributes to tumor pathogenesis by activating the ERK MAPK pathway. Mol Cancer 2010; 9: 253.
22. Ahmed N, Oliva K, Wang Y, Quinn M, Rice G. Downregulation of urokinase plasminogen activator receptor expression inhibits Erk signalling with concomitant suppression of invasiveness due to loss of uPAR-beta1 integrin complex in colon cancer cells. Br J Cancer 2003; 89: 374-84.
23. Fang JY, Richardson BC. The MAPK signalling pathways and colorectal cancer. Lancet Oncol 2005; 6: 322-7.

 https://doi.org/10.4132/jptm.2017.10.17

Journal of Pathology and Translational Medicine 2018; 52: 21-27
https://doi.org/10.4132/jptm.2016.06.17

■ ORIGINAL ARTICLE ■

Comparison of the Classical Method and SEE-FIM Protocol in Detecting Microscopic Lesions in Fallopian Tubes with Gynecological Lesions

Nermin Koc · Selçuk Ayas[1]
Sevcan Arzu Arinkan[1]

Departments of Pathology and [1]Obstetrics and Gynecology, Zeynep Kamil Maternity and Pediatric Research and Training Hospital, Istanbul, Turkey

Received: March 13, 2016
Revised: June 11, 2016
Accepted: June 16, 2016

Corresponding Author
Sevcan Arzu Arinkan, MD
Department of Obstetrics and Gynecology, Zeynep Kamil Maternity and Pediatric Research and Training Hospital, Istanbul 34660, Turkey
Tel: +90-505-683-7557
E-mail: pataraa96@gmail.com

Background: The objective of this study was to compare the classical method and Sectioning and Extensively Examining the Fimbriated End Protocol (SEE-FIM) in detecting microscopic lesions in fallopian tubes with gynecological lesions. **Methods:** From a total of 1,118 cases, 582 with various parts of both fallopian tubes sampled in three-ring-shape sections and 536 sampled with the SEE-FIM protocol were included in this study. Pathological findings of cases with endometrial carcinoma, non-uterine pelvic malignant tumor, ovarian borderline tumors, premalignancy, and benign lesions were compared. **Results:** We detected two tubal infiltrative carcinomas among 40 uterine endometrioid adenocarcinomas, 15 serous tubal intraepithelial carcinomas in 39 non-uterine pelvic serous high-grade carcinoma cases, seven papillary tubal hyperplasias in 13 serous borderline tumor cases, and 11 endometriotic foci and four adenomatoid tumors among all cases sampled with the SEE-FIM protocol. Using the classical method, we detected only one serous tubal intraepithelial carcinoma in 113 non-uterine pelvic serous high-grade carcinoma cases and two papillary tubal hyperplasia cases in 31 serous borderline tumors. We did not identify additional findings in 185 uterine endometrioid carcinoma cases, and neither endometriotic focus nor adenomatoid tumor was shown in other lesions by the classical method. **Conclusions:** Benign, premalignant, and malignant lesions can possibly be missed using the classical method. The SEE-FIM protocol should be considered especially in cases of endometrial carcinoma, non-uterine pelvic serous cancers, or serous borderline ovarian tumors. For other lesions, at least a detailed examination of the fimbrial end should be undertaken.

Key Words: SEE-FIM method; Classical method; Fallopian tube lesions

Clinical interest in the fallopian tube continues to increase. Recent studies on the carcinogenesis and origin of ovarian carcinoma have suggested tubal epithelium as a source of high-grade serous carcinoma (HGSC).[1-4] Tubal carcinoma has been demonstrated in pathological specimens of *BRCA1* and *BRCA2* mutation carrier women who chose to have prophylactic salpingo-oophorectomy to reduce their risk of ovarian carcinoma.[4] In addition to HGSC, low-grade serous carcinomas are thought to originate from the tubal epithelium, and papillary tubal hyperplasia (PTH) is considered a precursor to serous borderline tumors (SBT), non-invasive implants, and endosalpingiosis.[4] In addition, a significant association of salpingoliths with SBT has been demonstrated.[5]

The fallopian tube has an indirect role in the pathogenesis of endometrioid and clear cell carcinomas of the endometrium and ovary.[3] The presence of simultaneous or incidental lesions in fallopian tubes, the need for determination of their pathogenesis or their precursors, and the effects of fallopian tube metastasis on treatment modalities and on disease stage indicate the importance of fallopian tube sampling techniques.[6]

There are different approaches for sampling fallopian tubes. The pathology textbook Ackerman-Rosai Surgical Pathology recommends the classical sampling technique including collection of three "ring-shaped" sections from various parts of each tube.[7] In *Blaustein's Pathology of the Female Genital Tract*,[8] sampling of entire bilateral fallopian tubes with fimbrial ends is recommended for pelvic serous tumors and prophylactic salphingo-oophorectomies. However, for benign diseases and other malignant conditions, collection of at least one sample from each tube is recommended.[8] The Association of Directors of Anatomic and Surgical Pathology recommends three sections for tubal carcinomas and at least three sections including isthmus, ampulla, and infundibulum/fimbria for routine cases.[9]

In this study, we aimed to compare the clasical method and Sectioning and Extensively Examining the Fimbriated End Protocol (SEE-FIM) in detecting microscopic lesions in fallopian tubes with gynecological lesions.

pISSN 2383-7837
eISSN 2383-7845

MATERIALS AND METHODS

In the pathology department of our hospital, the SEE-FIM protocol has been used since 2012. Before that, fallopian tubes were sampled using the classical method involving collection of three "ring-shaped" sections from various parts of each tube. The SEE-FIM protocol includes amputation of each fimbria at the infundibulum, longitudinal sectioning of the fimbria, and extensive cross sectioning of the remaining tube at 2-mm intervals.[10]

This study was conducted on 1,118 patients who underwent total abdominal hysterectomy and bilateral salpingo-oophorectomy at our hospital from January 2006 to May 2014. The fallopian tubes were sampled by the classical method in 582 cases between 2006 and 2011, and 536 cases performed after 2011 underwent the SEE-FIM protocol. All sample slides were reexamined with light microscopy by two pathologists. Data on the macroscopic evaluations and other clinicopathological examinations were collected by chart review.

Cases were grouped according to the final diagnosis as endometrial carcinoma, non-uterine pelvic malignant tumors (ovarian, peritoneal, and tubal), ovarian borderline tumor and premalignant-benign lesions, and other tumors. Pathological findings of the classical and SEE-FIM protocols were compared between subgroups. Pelvic serous carcinomas (PSCs) were classified as "primary ovarian," "fallopian tube," and "primary peritoneal" according to Gynecologic Oncology Group criteria.[11] In fallopian tube cancer cases, intact tubal parts were also examined.

Serous tubal intraepithelial carcinoma (STIC) was diagnosed as noninvasive tubal epithelium displaying marked nuclear atypia characterized by loss of polarity, increased nuclear/cytoplasmic ratios, increased nuclear size, hyperchromasia, irregular nuclear membranes, and chromatin distribution. In addition, absence of cilia and mitotic figures was also characterized as STICs.[6] Immunostainings for p53 and Ki-67 were performed to diagnose STIC.[12,13] p53 signatures are defined as benign-appearing tubal epithelium with strong staining for p53 by immunohistochemistry and a low Ki-67 index.[6] Immunohistochemistry was performed on formalin-fixed, paraffin-embedded tissue sections using a manual polymer detection system with citrate buffer heat-induced epitope retrieval. Pre-diluted ready-to-use primary antibodies were used including p53 (clone DO-7 + BP53-12v, Thermo Scientific, Waltham, MA, USA) and Ki-67 (clone SP-6, Thermo Scientific).

Salpingoliths were described as mucosal and luminal calcifications that were frequently surrounded by bland epithelium in the fallopian tube. PTH was described as small rounded clusters of tubal epithelial cells and small papillae floating within the tubal lumen, with or without associated psammoma bodies, and demonstration of these findings with at least three papillae. The statistical difference between the two groups was examined by Fisher exact test.

The study was approved by the Institutional Review Board of Zeynep Kamil Women and Children Diseases Research and Training Hospital (IRB No. 143) and performed in accordance with the principles of the Declaration of Helsinki. Written informed consents were obtained.

RESULTS

This study included a total of 1,096 abdominal hysterectomy and salpingo-oophorectomy cases. Table 1 illustrates the number of cases in each group. Benign lesions, malignant neoplasms,

Table 1. Pathological diagnoses and number of cases in each group

Pathology	Classical method (n=582)	SEE-FIM protocol (n=536)
Endometrial carcinoma	210	48
Non-uterine pelvic malignant tumor		
Ovarian malignant tumors	150	49
Tubal malignant tumor	11	9
Peritoneal carcinoma	5	3
Ovarian borderline tumor	44	17
Premalignant and benign lesions, other tumors[a]	162	410

SEE-FIM, Sectioning and Extensively Examining the Fimbriated End Protocol.
[a]Premalignant lesions (endometrial hyperplasia, cervical intraepithelial lesions), benign lesions (endometrial polyp, myoma), carcinomas of the cervix, vagina, and vulva.

Table 2. Clinical and pathological features of endometrioid adenocarcinoma cases

Variable	Classical method (n=185)	SEE-FIM protocol (n=40)
Age, mean (yr)	60	61
Tumor grade		
1	58	14
2	70	18
3	57	8
Myometrial invasion		
None	34	8
<1/2	78	20
>1/2	73	12
Lymph node metastasis	14	4
Extrauterine extension	9	5
No. of cases with tubal infiltrative carcinoma[a]	2	0

SEE-FIM, Sectioning and Extensively Examining the Fimbriated End Protocol.
[a]p=.031.

https://doi.org/10.4132/jptm.2016.06.17

and premalignant lesions of the fallopian tubes in each group were evaluated in detail.

Endometrial carcinoma

Endometrioid adenocarcinoma was detected in 185 of 210 endometrial carcinomas using the classical method and was detected in 40 of 48 endometrioid malignant tumors using the SEE-FIM protocol. Other cases were clear cell carcinoma, undifferentiated tumor, malignant mixed müllerian tumor, and serous carcinoma. The clinical and pathological characteristics of the endometrioid adenocarcinoma cases are shown in Table 2.

Among the endometrioid adenocarcinomas sampled by the SEE-FIM protocol, tubal infiltrative carcinoma was identified in two cases (Fig. 1). The clinical and pathological features of these cases are shown in Table 3. Polypoid lesions were detected in these two tubal infiltrative carcinoma cases, and these lesions showed similar microscopic features with lesions in the endometrium. Neither *in situ* nor invasive lesions were identified in fallopian tubes sampled by the classical method. This difference was statistically significant (p = .031). Tubal endometriotic foci were shown in four endometrioid carcinoma cases using the new technique, while two endometriotic foci were seen in fallopian tubes sampled by the classical method.

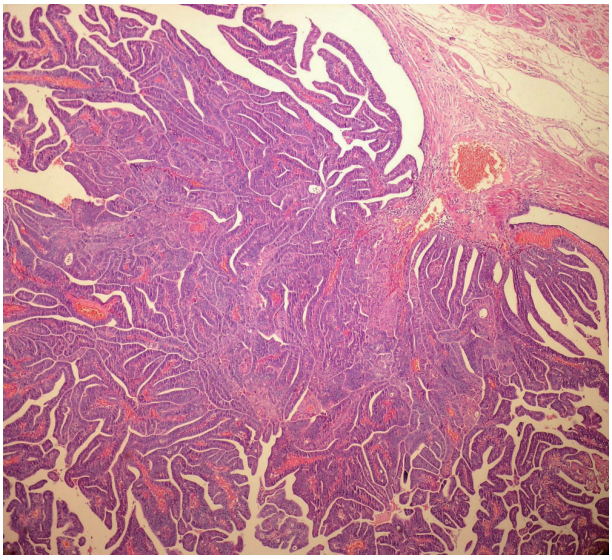

Fig. 1. Polypoid infiltrative endometrioid carcinoma extending to the tubal lumen.

Non-uterine pelvic malignant tumors

Of non-uterine pelvic malignant tumor cases sampled by the new technique, 42 were serous carcinoma. Among these, there were eight tubal, three peritoneal, and 28 ovarian HGSCs. Serous carcinoma was detected in 113 of 166 non-uterine pelvic carcinoma cases sampled by the classical method. Among these cases, there were 85 ovarian, 11 tubal, and five peritoneal HGSCs (Table 4). Of all cases, p53 positivity was detected in 22 tubal epithelium samples. Among these, six tubal epithelium samples were identified as macroscopically benign with a low Ki-67 index. These samples were identified as "p53 signature" (Fig. 2). In cases sampled by the new technique, STIC was detected in 10 of 28 ovarian HGSCs and four tubal carcinomas. All lesions except one were located in fimbrial ends (93%).

In peritoneal serous carcinomas, invasive serous carcinoma with a diameter of 0.2 cm was detected, and STIC was shown in the same case in the fimbrial end. STIC was identified in 15 of 39 HGSCs (40%). Among the tubal carcinoma cases, STIC was

Table 3. Clinical and pathological characteristics of the tubal infiltrative carcinoma cases

Case No.	Age (yr)	Primary tumor type	Myometrial involvement	Primary tumor grade	Localization of tubal involvement	Size of tubal involvement (cm)	Other metastatic sites
1	38	Endometrioid	< 1/2	1	Fimbrial	0.2	Ovary, cervix
2	56	Endometrioid	> 1/2	2	Ampullary	0.3	None

Table 4. Non-uterine pelvic carsinoma cases and STIC ratios identified by the classical method and SEE-FIM method

Histopathology	Classical method	STIC cases	SEE-FIM	STIC cases
Ovary high-grade serous carcinoma	85	0	28	10 (35)
Ovary low-grade serous carcinoma	12	0	3	0
Ovary nonserous carcinoma[a]	53	0	18	0
Tubal serous carcinoma	11	1 (9)	8	4 (50)
Tubal nonserous carcinoma[b]	0	0	1	0
Peritoneum	5	0	3	1 (33)
Total No. of cases[c]	156	1	4	15

Values are presented as number (%).
STIC, serous tubal intraepithelial carcinoma; SEE-FIM, Sectioning and Extensively Examining the Fimbriated End Protocol.
[a]Endometrioid, clear cell, mucinous, Krukenberg, malignant mixed mullerian tumor, granulosa; [b]Endometrioid; [c]p < .001.

Fig. 2. Serous tubal intraepithelial carcinoma (A), positive immunostaining for p53 (B), and for Ki-67 (C).

Table 5. Clinical and pathological features of serous borderline tumors

Variable	Classical method (n=31)	SEE-FIM protocol (n=13)
Age, mean (yr)	44	40
Bilateral	24	9
Microinvasion	8	5
Implant[a]	3	2
Endosalpingiosis	2	1
No. of cases with papillary tubal hyperplasia	2	7

SEE-FIM, Sectioning and Extensively Examining the Fimbriated End Protocol.
[a]Implants are noninvasive and nondesmoplastic.

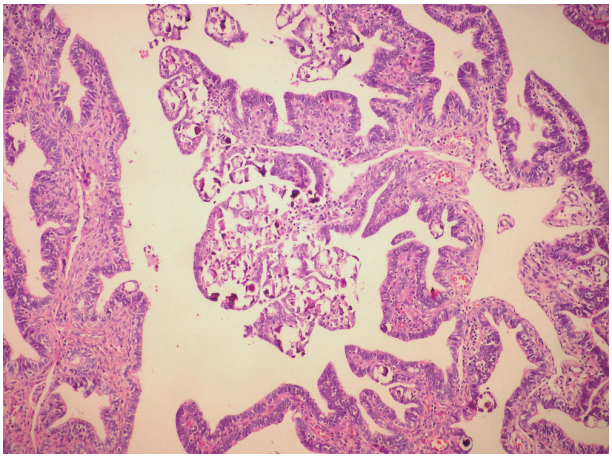

Fig. 3. Papillary tubal hyperplasia. Small rounded clusters of tubal epithelial cells and small papillae associated with psammoma bodies.

shown in only one case (0.5%) by the classical method. This difference was statistically significant (p = .001). We did not detect any p53 signature with the classical method, but six new cases were detected with the new method.

Ovarian borderline tumors

While serous borderline tumor was identified in 31 of 44 ovarian borderline tumors using the classical method, it was detected in 13 of 17 cases in the SEE-FIM group. Other cases were mucinous, seromucinous, and endometrioid. The clinical and pathological features of the SBT in each group are shown in Table 5.

PTH was shown in seven of 13 cases (55%) sampled by the SEE-FIM protocol (Fig. 3). One case was bilateral, four were diffuse, and four were focal lesions. Three of the focal lesions were located in the ampulla and infundibulum. PTH was detected in two of the cases with implants. In the classical method group, PTH was shown in two cases (6%). There was a statistically significant difference (p = .001). Moreover, although salpingoliths were detected in two cases sampled by the new technique, it was not identified in the classical method group. Except for serous borderline tumor cases, PTH was not detected by either the classical method or the SEE-FIM protocol.

Premalignant and benign lesions and other tumors

Of 410 cases sampled by the new technique, tubal endometriosis and adenomatoid tumor were detected in seven and four cases, respectively. While five endometriotic foci were located in the infundibulum, two were in the ampulla. Adenomatoid tumors were located in the ampulla and infundibulum, with a mean diameter of 1.2 cm both at the serosa and subserosa. Neither tubal endometriotic focus nor adenomatoid tumor was identified in any of the 162 cases sampled by the classical method. There was a statistically significant difference between the two techniques regarding the diagnosis of adenomatoid tumor and endometriotic focus (p = .039).

DISCUSSION

Endometrial carcinomas

Detection of tubal lesions synchronous with endometrial cancer is important in management. Appropriate sampling of the tubes, ovaries, and lymph nodes is crucial in staging and treatment. The correct prognosis estimation is related to detection of tubal

https://doi.org/10.4132/jptm.2016.06.17

lesions in endometrial cancer. In our study, we detected two new tubal infiltrative carcinomas that were not seen by the classical method. As a result, the stage of one of these two cases was changed after the detection of the lesion. Since the other case demonstrated metastasis, detection of the lesion did not change the stage. Culton *et al*.[14] reported synchronous endometrial and fallopian tube tumors in 13 cases. The sizes of the tumors ranged from 0.2 cm to 17.5 cm.[15] Kulac and Usubutun[15] compared 100 fallopian tubes sampled by the classical method with 100 fallopian tubes with fimbrial end sampling and reported two invasive and two proliferative lesions that were not seen macroscopically. In our study, the sizes of the tubal lesions were 0.2 cm and 0.3 cm, and they were not detected macroscopically. Culton *et al*.[14] reported seven of 13 lesions using fimbrial end sampling, and Kulac and Usubutun[15] identified three of four lesions using fimbrial end sampling. In our study, one of the two lesions was in the fimbrial end. Since tubal lesions can originate from lesions in the endometrium or endometrioid epithelium transformed from the tubal epithelium, studies on tubal lesions are important for determination of origin and pathogenesis of these tumors. Kulac *et al*.[15] reported an association of endometriotic foci with tubal lesions in two of four cases. We did not identify any endometriotic focus in our cases.

Non-uterine pelvic malignant tumors

The majority of the non-uterine pelvic carcinomas are serous carcinomas that originate from the ovaries, fallopian tubes, or peritoneum. As non-uterine pelvic carcinomas have poor prognosis, the pathogenesis and origin should be well understood in order to develop new screening methods, new treatment modalities, and improved diagnosis at an early stage. STIC located in fimbria has been demonstrated as the origin of HGSC in recent studies.[1-3] In addition to serous carcinoma, clear cell and endometrioid carcinomas have been thought to originate from endometriotic foci that are assumed to occur through retrograde menstruation.[1-3]

In our study, we sampled the entire fallopian tubes, and STIC was shown in 15 of 39 cases with HGSCs. The rate was reported as 59%, 52%, and 20% in studies by Przybycin *et al*.,[16] Kindelberg *et al*.,[17] and Tang *et al*.,[18] respectively. In our study, the percentages of ovarian, tubal, and peritoneal serous carcinomas in all non-uterine PSCs were changed from 72%, 20%, and 8% to 45%, 50%, and 5%, respectively. Most lesions were located at the fimbrial end, and this finding is consistent with the other studies. No additional lesions in the fallopian tubes were detected in three endometrioid and one clear cell carcinoma cases sampled by the new technique. In non-uterine serous pelvic carcinomas sampled by the conventional method, STIC was identified in one case with HGSC. There were no additional lesions in the tubes in the endometrioid or clear cell carcinoma cases.

Ovarian borderline tumors

Regarding the origin of SBT, Kurman *et al*.[4] reported that all ovarian and extraovarian low-grade serous proliferations originate from spilling and implantation of tubal epithelium in the form of PTH generated due to chronic inflammation. In their study, 20 of 22 cases (91%) with noninvasive and invasive implants were associated with PTH.[4] Similarly, Robey and Silva[19] reported that 68% of SBT cases were associated with PTH.

Kurman *et al*.[4] reported that PTH is mostly located in the ampulla; while the majority of lesions show a diffuse pattern, they can also be focal. Our study showed a lower percentage (55%) of cases demonstrating an association of PTH with SBT sampled by the new technique. This difference may be due to the smaller number of cases with an implant in our study. The majority of focal lesions were located in the ampulla and infundibulum.

Yanai-Inbar *et al*.[20] reported that there was no statistically significant difference in detection of tubal pathology between sampling tubes from one section, two sections, or sampling the entire tube. Yanai-Inbar *et al*.[20] analyzed the fallopian tubes of 48 SBT cases and found no difference between the study and control groups. In our study, we detected an association between PTH and ovarian borderline tumors in 6% of the cases sampled by the classical method. While diffuse lesions and random proliferations specific to this section were detected by the classical method, all PTH lesions were detected by the new technique.

Salpingoliths can be found in normal fallopian tubes. Kurman *et al*.[4] and Seidman *et al*.[5] have pointed out the association of salpingoliths with SBT. In our study, salpingoliths were found in 10% of SBT cases sampled by the new technique and were not demonstrated in SBT cases sampled by the classical method.

Premalignant and benign cases and other tumors

The pathogenesis of endometriosis and its association with malignancies remain interesting topics of gynecopathology.[21,22] Endometrial tissue can be physiologically seen in the isthmus, but there is not enough data on the involvement of other areas.

In 410 fallopian tubes sampled by the new technique, we identified seven endometriotic foci (2%). However, it was not shown in any of the fallopian tubes sampled by the classical method. Adenomatoid tumors are the most common benign

neoplasm of the fallopian tubes. Their neoplastic potential and the fact that they can be misdiagnosed as other malignant or benign neoplasms should be considered during the management of these tumors.[23] In our study, although we did not detect adenomatoid tumor by the classical method, four adenomatoid tumors were identified by the new technique.

It is possible to misdiagnose benign lesions, premalignant lesions, and malignant lesions using the classical method in pathological examination of the fallopian tubes. For this reason, the SEE-FIM protocol should be considered in cases of endometrial cancers, non-uterine pelvic serous cancers, or serous borderline ovarian tumors. The SEE-FIM protocol seems to have advantages for sampling of the entire fallopian tube. However, it may increase the surgical workload if it is used for all routine salpingectomy specimens. For cases with other benign, premalignant, and malignant lesions, at least a detailed examination of the fimbrial end of the fallopian tubes should be undertaken.

Conflicts of Interest

No potential conflict of interest relevant to this article was reported.

REFERENCES

1. Carcangiu ML, Peissel B, Pasini B, Spatti G, Radice P, Manoukian S. Incidental carcinomas in prophylactic specimens in *BRCA1* and *BRCA2* germ-line mutation carriers, with emphasis on fallopian tube lesions: report of 6 cases and review of the literature. Am J Surg Pathol 2006; 30: 1222-30.
2. Yates MS, Meyer LA, Deavers MT, *et al*. Microscopic and early-stage ovarian cancers in *BRCA1/2* mutation carriers: building a model for early BRCA-associated tumorigenesis. Cancer Prev Res (Phila) 2011; 4: 463-70.
3. Kurman RJ, Shih IM. Molecular pathogenesis and extraovarian origin of epithelial ovarian cancer: shifting the paradigm. Hum Pathol 2011; 42: 918-31.
4. Kurman RJ, Vang R, Junge J, Hannibal CG, Kjaer SK, Shih IM. Papillary tubal hyperplasia: the putative precursor of ovarian atypical proliferative (borderline) serous tumors, noninvasive implants, and endosalpingiosis. Am J Surg Pathol 2011; 35: 1605-14.
5. Seidman JD, Sherman ME, Bell KA, Katabuchi H, O'Leary TJ, Kurman RJ. Salpingitis, salpingoliths, and serous tumors of the ovaries: is there a connection? Int J Gynecol Pathol 2002; 21: 101-7.
6. Mehrad M, Ning G, Chen EY, Mehra KK, Crum CP. A pathologist's road map to benign, precancerous, and malignant intraepithelial proliferations in the fallopian tube. Adv Anat Pathol 2010; 17: 293-302.
7. Rosai J. Rosai and Ackerman's surgical pathology. St. Louis: Mosby Elsevier, 2011.
8. Kurman RJ, Hedrick Ellenson L, Ronnett BM. Blaustein's pathology of the female genital tract. New York: Springer-Verlag, 2011.
9. Longacre TA, Oliva E, Soslow RA; Association of Directors of Anatomic and Surgical Pathology. Recommendations for the reporting of fallopian tube neoplasms. Hum Pathol 2007; 38: 1160-3.
10. Medeiros F, Muto MG, Lee Y, *et al*. The tubal fimbria is a preferred site for early adenocarcinoma in women with familial ovarian cancer syndrome. Am J Surg Pathol 2006; 30: 230-6.
11. Bloss JD, Liao SY, Buller RE, *et al*. Extraovarian peritoneal serous papillary carcinoma: a case-control retrospective comparison to papillary adenocarcinoma of the ovary. Gynecol Oncol 1993; 50: 347-51.
12. Kuhn E, Kurman RJ, Sehdev AS, Shih IM. Ki-67 labeling index as an adjunct in the diagnosis of serous tubal intraepithelial carcinoma. Int J Gynecol Pathol 2012; 31: 416-22.
13. Yemelyanova A, Vang R, Kshirsagar M, *et al*. Immunohistochemical staining patterns of p53 can serve as a surrogate marker for *TP53* mutations in ovarian carcinoma: an immunohistochemical and nucleotide sequencing analysis. Mod Pathol 2011; 24: 1248-53.
14. Culton LK, Deavers MT, Silva EG, Liu J, Malpica A. Endometrioid carcinoma simultaneously involving the uterus and the fallopian tube: a clinicopathologic study of 13 cases. Am J Surg Pathol 2006; 30: 844-9.
15. Kulac I, Usubutun A. Microscopic lesions of fallopian tubes in endometrioid carcinoma of the endometrium: How effective are the macroscopic tubal sampling techniques? J Gynecol Oncol 2013; 24: 114-9.
16. Przybycin CG, Kurman RJ, Ronnett BM, Shih IM, Vang R. Are all pelvic (nonuterine) serous carcinomas of tubal origin? Am J Surg Pathol 2010; 34: 1407-16.
17. Kindelberger DW, Lee Y, Miron A, *et al*. Intraepithelial carcinoma of the fimbria and pelvic serous carcinoma: evidence for a causal relationship. Am J Surg Pathol 2007; 31: 161-9.
18. Tang S, Onuma K, Deb P, *et al*. Frequency of serous tubal intraepithelial carcinoma in various gynecologic malignancies: a study of 300 consecutive cases. Int J Gynecol Pathol 2012; 31: 103-10.
19. Robey SS, Silva EG. Epithelial hyperplasia of the fallopian tube: its association with serous borderline tumors of the ovary. Int J Gynecol Pathol 1989; 8: 214-20.
20. Yanai-Inbar I, Siriaunkgul S, Silverberg SG. Mucosal epithelial proliferation of the fallopian tube: a particular association with ovarian serous tumor of low malignant potential? Int J Gynecol Pathol

1995; 14: 107-13.
21. Clement PB. The pathology of endometriosis: a survey of the many faces of a common disease emphasizing diagnostic pitfalls and unusual and newly appreciated aspects. Adv Anat Pathol 2007; 14: 241-60.
22. Modesitt SC, Tortolero-Luna G, Robinson JB, Gershenson DM, Wolf JK. Ovarian and extraovarian endometriosis-associated cancer. Obstet Gynecol 2002; 100: 788-95.
23. Quigley JC, Hart WR. Adenomatoid tumors of the uterus. Am J Clin Pathol 1981; 76: 627-35.

Journal of Pathology and Translational Medicine 2018; 52: 28-36
https://doi.org/10.4132/jptm.2017.09.25

■ ORIGINAL ARTICLE ■

Reclassification of Mixed Oligoastrocytic Tumors Using a Genetically Integrated Diagnostic Approach

Seong-Ik Kim[1] · Yujin Lee[1,2]
Jae-Kyung Won[1] · Chul-Kee Park[2]
Seung Hong Choi[3] · Sung-Hye Park[1,4]

Departments of [1]Pathology, [2]Neurosurgery, and [3]Radiology, [4]Neurosicence Institute, Seoul National University College of Medicine, Seoul, Korea

Received: June 17, 2017
Revised: September 18, 2017
Accepted: September 25, 2017

Corresponding Author
Sung-Hye Park, MD
Departments of Pathology, Neurosicence Institute, Seoul National University College of Medicine, 103 Daehak-ro, Jongno-gu, Seoul 03080, Korea
Tel: +82-2-2072-3090
Fax: +82-2-765-5600
E-mail: shparknp@snu.ac.kr

Background: Mixed gliomas, such as oligoastrocytomas (OA), anaplastic oligoastrocytomas, and glioblastomas (GBMs) with an oligodendroglial component (GBMO) are defined as tumors composed of a mixture of two distinct neoplastic cell types, astrocytic and oligodendroglial. Recently, mutations *ATRX* and *TP53*, and codeletion of 1p/19q are shown to be genetic hallmarks of astrocytic and oligodendroglial tumors, respectively. Subsequent molecular analyses of mixed gliomas preferred the reclassification to either oligodendroglioma or astrocytoma. This study was designed to apply genetically integrated diagnostic criteria to mixed gliomas and determine usefulness and prognostic value of new classification in Korean patients. **Methods:** Fifty-eight cases of mixed OAs and GBMOs were retrieved from the pathology archives of Seoul National University Hospital from 2004 to 2015. Reclassification was performed according to genetic and immunohistochemical properties. Clinicopathological characteristics of each subgroup were evaluated. Overall survival was assessed and compared between subgroups. **Results:** We could reclassify all mixed OAs and GBMOs into either astrocytic or oligodendroglial tumors. Notably, 29 GBMOs could be reclassified into 11 cases of GBM, IDH-mutant, 16 cases of GBM, IDH-wildtype, and two cases of anaplastic oligodendroglioma, IDH mutant. Overall survival was significantly different among these new groups ($p < .001$). Overall survival and progression-free survival were statistically better in gliomas with *IDH* mutation, *ATRX* mutation, no microscopic necrosis, and young patient age (cut off, 45 years old). **Conclusions:** Our results strongly suggest that a genetically integrated diagnosis of glioma better reflects prognosis than former morphology-based methods.

Key Words: Oligoastrocytoma; Glioblastoma with oligodendroglioma component; WHO classification; Genetics; Integrated diagnosis

Mixed gliomas, such as oligoastrocytomas (OA), anaplastic oligoastrocytomas (AOA), and glioblastomas (GBMs) with oligodendroglial component (GBMO), are defined as tumors composed of a mixture of two distinct neoplastic cell types; astrocytic and oligodendroglial. However, there have been controversies as to whether these mixed tumors are really distinct entities. First, research has found no significant difference in survival between mixed gliomas versus either astrocytic or oligodendroglial tumors, such as GBMO versus GBM,[1] anaplastic astrocytoma (AA) versus AOA,[2] anaplastic oligodendroglioma (AO) versus AOA,[3] diffuse astrocytoma (DA) versus OA,[4] and oligodendroglioma versus OA.[4] Second, results of genetic studies suggest that morphologically mixed OA or ambiguous glioma is genetically monoclonal and similar to either DA or oligodendroglioma, rather than a mixture of them.[5] In addition, it is well known that the diagnosis of mixed glioma shows a high interobserver variability.[6]

The accumulation of research on gliomas has led to a growth in understanding of its molecular aspects. Previous molecular study of astrocytic tumors revealed frequent mutations in *IDH*, *ATRX*, and *TP53*, suggesting that these mutations might be genetic features of astrocytic tumors.[7,8] On the other hand, concurrent deletion of chromosomal arms 1p and 19q constitute a hallmark alteration in oligodendroglial tumors.[9] Because 1p/19q codeleted gliomas are strongly associated with *IDH* mutation,[10] *IDH* mutation is considered as a genetic feature of oligodendroglioma. The disclosure of these molecular aberrations of glioma led to the discussion on whether to include these molecular markers in the 2016 revised World Health Organization (WHO) classification of central nervous system tumors. As such, neuropathologists with expertise in molecular diagnosis met in a meeting held in Haarlem.[11] This "International Society of Neuropathology (ISN)-Haarlem Consensus Meeting" decided to include the ambiguous category of "DA, 1p/19q-codeleted"; however, this class turned out to be oligodendroglioma with an astrocytic

pISSN 2383-7837
eISSN 2383-7845

phenotype. In August 2014, Sahm *et al*.[12] suggested no longer using the term "OA" because *in situ* molecular genetics showed that previously diagnosed OAs were largely divided into oligodendroglioma with reactive astrogliosis or astrocytoma with partial oligodendroglial morphology with no genetic basis of the oligodendroglial component. Rather, the latter showed genetic aberration compatible with DA in the whole tumor area.[12] Subsequently, a genetically integrated diagnostic approach was proposed.[13] With respect to both overall survival (OS) and time until treatment failure, the integrated approach separated the diagnostic groups more stringently, and it also proved to be more successful in the outcome prediction.[13] Not only in terms of prognosis, but also for predictive information, the previous studies suggest that *IDH*, *ATRX*, and 1p/19q status can offer useful criteria and aid in selection of proper therapy for the patients.[14,15]

With this background, we reclassified the archives of mixed gliomas at Seoul National University Hospital, including GBMO, by the new genetically integrated diagnostic criteria. This study was designed to determine the usefulness of a genetically integrated diagnostic approach and the prognostic power of a new classification system in Korean patients.

MATERIALS AND METHODS

Study population

Formalin-fixed paraffin-embedded (FFPE) tissues from a total of 58 patients were obtained from the archives of the Department of Pathology, Seoul National University Hospital. All patients were Korean (Table 1). Age at first diagnosis was between 14 and 73 years old (median: previously OA, 36 years; previously GBMO, 56 years). All cases were diagnosed between 2004 and 2015. Selected cases had distinct morphological features of mixed astrocytic and oligodendroglial component or mixed GBM and oligodendroglial component. We used a 10% cut-off for the minimum area of oligodendroglial or astrocytic component. Tumors were graded according to the 2007 WHO guidelines. The series contained 15 OAs, 14 AOAs, and 29 GBMOs (Fig. 1). Histopathologic slides were reviewed by two pathologists (S.H. Park, S.I. Kim). Immunohistochemical stainings for IDH1 (clone H09, Dianova, Hamburg, Germany) and ATRX (Sigma-Aldrich, St. Louis, MO, USA) were performed in all 58 cases. If IDH1 immunohistochemistry (IHC) was negative, direct sequencing of *IDH1*/*IDH2* was performed. Fluorescent *in situ* hybridization (FISH) using Vysis probes (Abbott, Des Plaines, IL, USA) to detect 1p/19q status was done in all 58 cases. Survival plots according to the clinical, histological, and molecular characteristics of tumors were analyzed using Kaplan-Meier (K-M) survival analysis.

Table 1. Demographic summary of the patient cohort according to the original diagnoses in this study

Parameter	OA (n=15)	AOA (n=14)	GBMO (n=29)
Age (yr)			
Mean (range)	40.8 (14–72)	41.1 (13–64)	53.5 (31–77)
Median	36	35.5	56
Sex (male:female)	11:4	5:9	22:7
Median OS (mo)	45.3	21.7	26.7
Median PFS (mo)	39.8	20.9	19.0
Tumor location	F8 T4 P1 PT1 HIPP1	F6 T5 P1 O1 TH1	F13 T10 P1 TH1 CC1 PO1 FTI1 FTP1
Treatment	Surgery only	Surgery only 13 Others 1	CCRT 21 Others 8

OA, oligoastrocytoma; AOA, anaplastic oligoastrocytoma; GBMO, glioblastoma with oligodendroglioma component; OS, overall survival; PFS, progression-free survival; F, frontal lobe; T, temporal lobe; P, parietal lobe; HIPP, hippocampus; O, occipital lobe; TH, thalamus; CC, corpus callosum; PO, parieto-occipital; FTI, frontotemporoinsular area; FTP, frontotemporoparietal lobe; CCRT, concurrent chemoradiotherapy.

With the results of our genetic studies, we reclassified tumors based on the diagram by Reuss *et al*.[13] If the ATRX IHC was negative, it was classified as astrocytic, independent of its IDH status. Tumors were then subdivided by IDH status based on IHC and direct sequencing. In contrast, all tumors with nuclear ATRX expression were divided by 1p/19q status using FISH. If 1p/19q were non-codeleted, tumors were astrocytic tumors. Then, the tumors were also subdivided by IDH status. If codeletion of 1p/19q and *IDH* mutation were present, they were defined as oligodendroglial tumors. Next, we graded the tumors according to the new 2016 WHO guidelines. Lastly, 58 cases were reclassified into seven distinct subgroups: 1) DA, IDH-mutant (DA IDH-m), 2) DA, IDH-wildtype (DA IDH-w), 3) AA, IDH-mutant (AA IDH-m), 4) AA, IDH-wildtype (AA IDH-w), 5) AO, IDH-mutant (AO IDH-m), 6) GBM, IDH-mutant (GBM IDH-m), and 7) GBM, IDH-wildtype (GBM IDH-w). We performed further classification of GBM into primary and secondary GBM. Secondary GBM was defined as cases with previous pathology-proven lower grade tumors. Then, we compared the survival plots between reclassified entities using K-M survival analysis.

This study abided by the world Medical Association Declaration of Helsinki recommendation and was approved by the Institutional Review Board of Seoul National University Hospital (IRB No. 1508-004-690). Written informed consents were obtained.

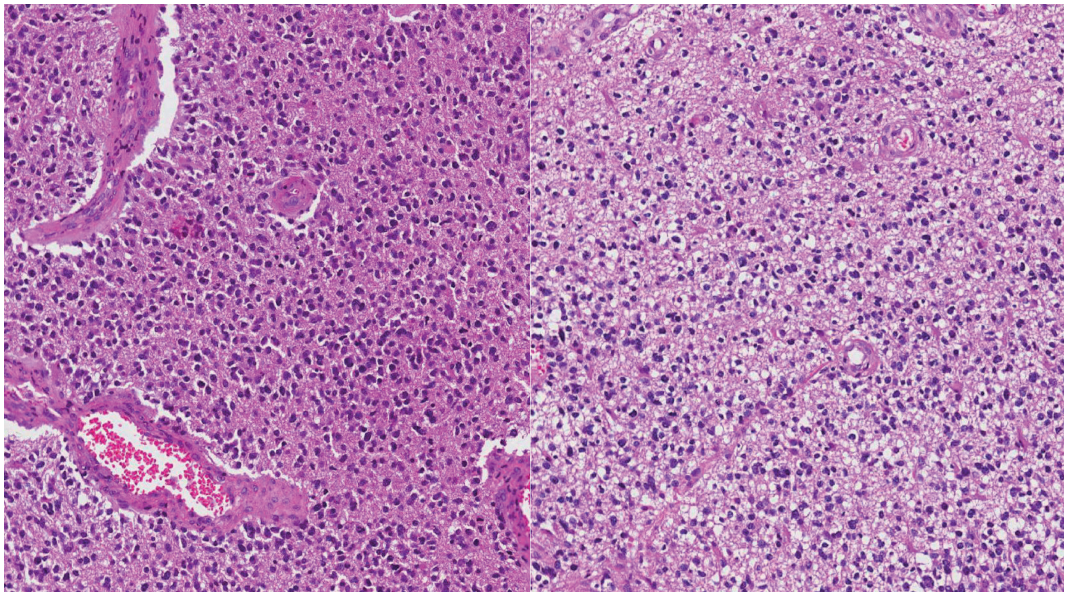

Fig. 1. Hematoxylin and eosin features of a case that was previously diagnosed as glioblastoma with oligodendroglial component. This case turned out to be glioblastoma, IDH-wildtype in new classifications.

Hematoxylin and eosin staining and IHC

FFPE (10% neutral buffered formalin, routinely processed, and paraffin-embedded) tissue sections (2–3 μm thick) were cut for hematoxylin and eosin staining and IHC. Tissue sections were stained with anti-IDH1 R132H (H09) monoclonal antibody (Dianova) using a 1:100 dilution, anti-ATRX polyclonal antibody HPA001906 (Sigma-Aldrich) using a 1:300 dilution, and anti-p53 monoclonal antibody, DO-7 code M7001 (Dako, Glostrup, Denmark) using a 1:1000 dilution. IHC staining was carried out using a standard avidin–biotin peroxidase method. Tumors were interpreted as positive for p53 expression if ≥20% of neoplastic cells showed distinct nuclear staining.

DNA extraction

Tumor areas were manually micro-dissected using 6-μm unstained tissue sections made from FFPE tissue. DNA was isolated from the micro-dissected tissue using a DNeasy Blood and Tissue Kit (Qiagen, Valencia, CA, USA) according to the manufacturer's instructions.

Polymerase chain reaction amplification and sequencing of *IDH1* and *IDH2*

Template DNA (1 μL) was added to 100 μL of polymerase chain reaction (PCR) solution (10 μL of 10× magnesium Taq High-Fidelity [HF] buffer, 10 μL deoxynucleotide triphosphate [dNTP] mixture with 2 mM magnesium, 5 μL of 10 pmol primer [2×], 1 μL of magnesium Taq-HF polymerase, and distilled water). The IDH1-Forward (F)/IDH1-Reverse (R) and IDH2-F/IDH2-R primers (Table 2) were used with the following program: 35 cycles of 95°C for 30 seconds, 55°C for 30 seconds, and 72°C for 60 seconds. The product sizes were 130-base pair (bp) (IDH1) and 293-bp (IDH2). Unincorporated PCR primers and dNTPs were removed from the PCR products using a Montage PCR Clean-up Kit (Millipore, Billerica, MA, USA).

Table 2. IDH1-F/IDH1-R and IDH2-F/IDH2-R primers

Primer	Sequence (5'→3')
IDH 1-F	ACCAAATGGCACCATACGA
IDH 1-R	GCAAAATCACATTATTGCCAAC
IDH 2-F	GCTGCAGTGGGACCACTATT
IDH 2-R	TGTGGCCTTGTACTGCAGAG

F, forward; R, reverse.

Purified products were sequenced using the same primers. Sequencing was performed using a BigDye Terminator Cycle Sequencing Kit v. 3.1 (Applied Biosystems, Foster City, CA, USA). Sequencing products were resolved on an automated DNA sequencing system, model 3730XL (Applied Biosystems).

Fluorescence *in situ* hybridization

FISH with Vysis probes was used to assess 1p/19q status. Sections (3 μm thick) were first deparaffinized in xylene, incubated with 0.3% pepsin in 10 mM HCl at 37°C for 10 minutes, and boiled with citrate buffer (pH 6.0) in a microwave. Sections were then incubated in 1 M NaSCN for 35 minutes at 80°C, immersed in the pepsin solution, and fixed in 10% neutral

https://doi.org/10.4132/jptm.2017.09.25

buffered formalin. 1p36/1q25 and 19q13/19p13 labeled locus-specific dual-color probes (Abbott Molecular) were used according to the manufacturer's protocol. We applied the probe mixture to the slides and incubated them in a humidified atmosphere with HYBrite (Abbott Molecular) at 73°C for 5 minutes for simultaneous denaturation of the probe and target DNA. Then, we cooled the samples to 37°C and incubated for 19 hours to hybridize the probe and target DNA. The slides were submerged in 0.4× SSC buffer/0.3% NP-40 for 2 minutes at room temperature, followed by incubation in 2× SSC/0.1% NP-40 for 5 minutes at 73°C.

Statistical analysis

OS and progression-free survival (PFS) were estimated using K-M survival analysis and were compared using the log-rank test. All statistical analyses were performed with SPSS ver. 22 (IBM Corp., Armonk, NY, USA); $p < .05$ was considered significant.

RESULTS

Clinicopathological information of patients is provided in Table 1. Our reclassification results are summarized in Table 3 and Fig. 2. Our reclassification analysis showed that the largest fraction of mixed OA was AA IDH-m (50%). The largest part of mixed AOA was also AA IDH-m (42.9%), followed by AA IDH-w (35.7%) and AO (21%). The largest fraction of GBMO was conventional GBM IDH-w (55.2%), followed by GBM IDH-m (37.9%) and only 6.9% AO. Except for one undetermined case of GBM IDH-w, 14 out of 16 GBM IDH-w cases (87.5%) were primary GBM and one case (6.3%) was secondary GBM. In 11 cases of GBM IDH-m, seven cases (63.6%) were primary GBM and four cases (36.4%) were secondary GBM. Therefore, the incidence of primary GBMs (21/27, 77.8%) derived from those previously diagnosed as mixed gliomas was less than the well-known incidence of primary GBM (90%–95%).

When we carried out K-M survival analysis, two cases of DA IDH-w were excluded; one patient died of suddenly developed progressive hydrocephalus of an unknown cause and the other

Table 3. Change in diagnosis after applying the genetically integrated diagnostic criteria

Original diagnosis (n=58)	Re-diagnosis (n=58)	
	Criteria	No. (%)
OA, grade II (n=14)	DA IDH-m	2 (14.3)
	DA IDH-w	2 (14.3)
	AA IDH-m	7 (50)
	AA IDH-w	2 (14.3)
	AO IDH-m and 1p/19q-codeleted	1 (7.1)
AOA, grade III (n=14)	AA IDH-m	6 (42.9)
	AA IDH-w	5 (35.7)
	AO IDH-m and 1p/19q-codeleted	3 (17.6)
GBMO, grade IV (n=29)	GBM IDH-w	16 (55.2)
	GBM IDH-m	11 (37.9)
	AO IDH-m and 1p/19q-codeleted	2 (6.9)

OA, oligoastrocytoma; AOA, anaplastic oligoastrocytoma; GBMO, glioblastoma with oligodendroglioma component; DA, diffuse astrocytoma; IDH-m, IDH-mutant; IDH-w, IDH-wildtype; AA, anaplastic astrocytoma; AO, anaplastic oligodendroglioma; GBM, glioblastoma.

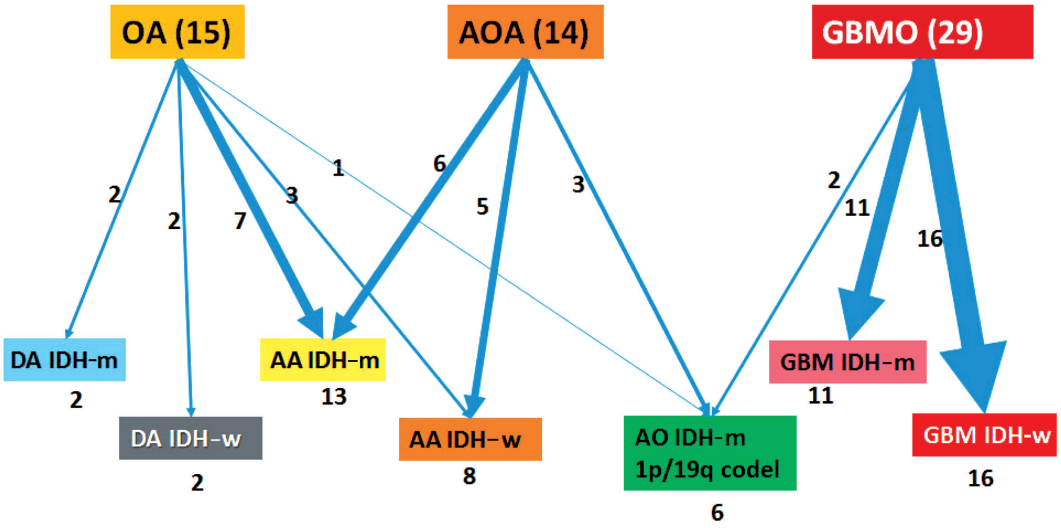

Fig. 2. Change in diagnosis after applying molecular genetics integrated diagnostic criteria. OA, oligoastrocytoma; AOA, anaplastic oligoastrocytoma; GBMO, glioblastomas with an oligodendroglial component; DA, diffuse astrocytoma; m, mutant; w, wildtype; AA, anaplastic astrocytoma; AO, anaplastic oligodendroglioma; GBM, glioblastoma.

patient didn't show up. One case of AO IDH-m was also excluded because the patient died of a worsened general condition from multiple diseases, including pulmonary thromboembolism with basal ganglia and temporal lobe infarction during hospitalization. Recent studies report a very similar incidence of stroke between cancer and non-cancer patients; therefore, it is reasonable to think that stroke was an independent variable for survival in this case, whether the tumor was a causative factor of stroke or not.[16]

OS in different clinical, histological, and molecular subgroups has been evaluated (Fig. 3). Prognosis was better in the younger (age < 45 years) (p = .010) and IDH-mutant (p = .007) subgroups. However, prognosis was worse in subgroups with microscopic necrosis (p < .001) and ATRX-positive IHC (p = .031). Similar results were drawn with PFS (Fig. 4). Other characteristics failed to show statistical significance. The subgroup with the 1p/19q co-deletion had a tendency of better prognosis in terms of OS (p = .067) and PFS (p = .077), despite the lack of statistical significance (Figs. 3F, 4F). Of those compared, all 1p/19q codeleted patients fully survived the study completion. Also, those with p53 overexpression (positive in > 20%) had a tendency for worse prognosis in terms of OS (p = .054) and PFS (p = .208) (Figs. 3E, 4E).

All these results with demographic characteristics are summarized in Table 4.

After re-classification of mixed gliomas, we compared survival plots between the reclassified entities using K-M survival analysis. In terms of OS as well as PFS, the genetically integrated diagnostic approach showed clear statistical significance (p < .001) (Fig. 5).

DISCUSSION

Mixed gliomas have been previously defined as diffusely infiltrating gliomas composed of a mixture of two distinct neoplastic cell types morphologically resembling the tumor cells in oligodendroglial or astrocytic tumors.[9] However, inter-institutional and inter-observer variations of mixed gliomas have resulted in low diagnostic reproducibility and reliability.

The ISN-Haarlem's recommendations for a genetically integrated diagnosis for the classification of diffuse gliomas suggested the removal of mixed glioma entity.[11] We reclassified mixed OA (including GBMO) into either astrocytic or oligodendroglial tumors in agreement with the emphasis by Sahm *et al*.[12]

Here, we applied the new criteria to the 58 cases that were

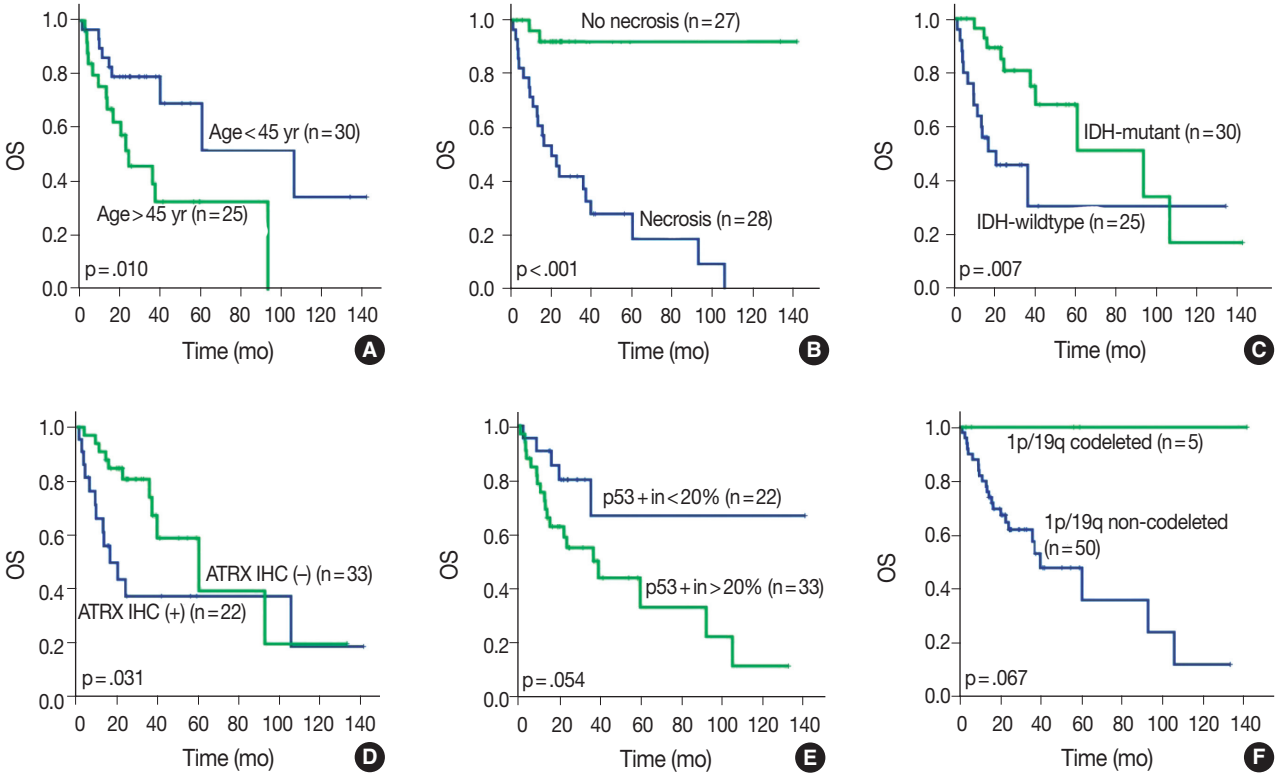

Fig. 3. Overall survival (OS) in different clinical, histological, and molecular subgroups. (A) Age over 45 years. (B) Necrosis. (C) *IDH* mutation status. (D) *ATRX* methylation status. (E) p53 positivity (more than 20% of tumor in immunohistochemistry). (F) 1p/19q-codeletion status.

https://doi.org/10.4132/jptm.2017.09.25

previously diagnosed as mixed gliomas. The purpose of our study was to determine the usefulness of genetically integrated classification, true incidence of diffuse gliomas, and prognostic value of a new classification system. Above all, we sought to find out whether there are any intermediate cases or genuine mixed gliomas.

We primarily used Reuss *et al.*'s diagnostic criteria;[13] therefore, ATRX IHC and 1p/19q FISH were used to determine whether the tumor was of astrocytic or oligodendroglial lineage.

Among DA and AA tumors, ATRX-negativity and -positivity were found in 88% and 12%, respectively. Six cases which showed 1p/19q codeletion were also ATRX-positive and *IDH1*-mutated; therefore, the diagnosis of AO was certain. Among

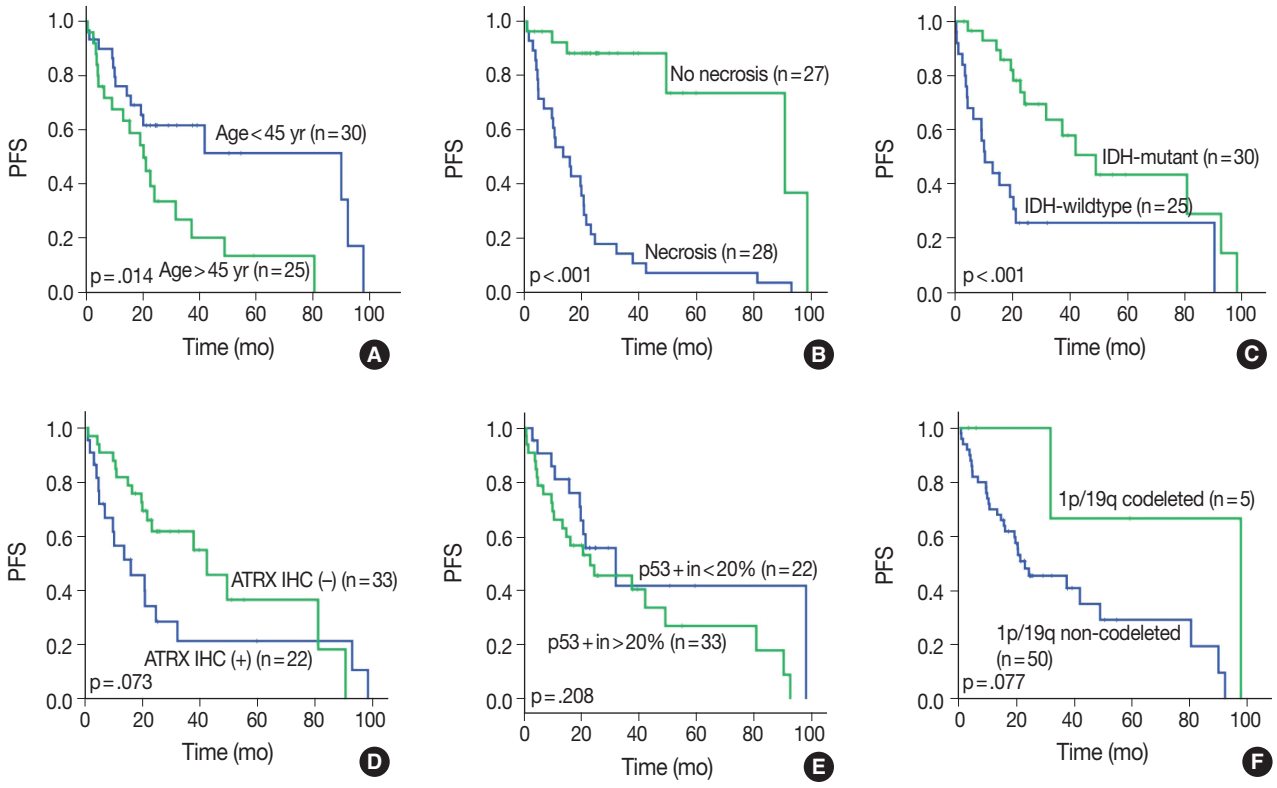

Fig. 4. Progression-free survival (PFS) in different clinical, histological, and molecular subgroups. (A) Age over 45. (B) Necrosis. (C) *IDH* mutation status. (D) *ATRX* methylation status. (E) p53 positivity (more than 20% of tumor in IHC). (F) 1p/19q-codeletion status.

Table 4. Demographic summary of our cohort according to genetics integrated reclassification

Parameter	DA IDH-m (n=2)	DA IDH-w (n=2)	AA IDH-m (n=13)	AA IDH-w (n=8)	AO (n=6)	GBM IDH-m (n=11)	GBM IDH-w (n=16)
Age, mean (range, yr)	37.5 (31–44)	49.5 (32–67)	39.3	39.9 (14–64)	52.6 (35–69)	42.3 (34–58)	58.4 (31–77)
Sex (male:female)	2:0	1:1	9:4	3:5	3:3	7:4	13:3
ATRX (–), n (%)	2 (100)	1 (50)	12 (92.3)	7 (87.5)	0	7 (63.6)	5 (31.3)
1p/19q codel	0	0	0	0	6	0	0
Primary GBM						7	14
Secondary GBM						4	1
OS (mo)	36.5	19.5	29.8	34.5	45.5	43.6	14.5
PFS (mo)	36.0	18.9	29.0	27.3	34.0	33.4	9.1
Tumor location	F1 P1	F2	F5 T6 P1 PT1	F4 T1 O1 TH1 HIPP1	F4 T2	F6 T3 FTI1 FTP1	F5 T7 P1 CC1 PO1 TH1
Treatment	Surgery only	Surgery only	Surgery only	Surgery only 7 Others 1	Surgery only 4 CCRT 1 Others 1	CCRT 10 Others 1	CCRT 11 Others 5

DA, diffuse astrocytoma; m, mutant; w, wildtype; AA, anaplastic astrocytoma; AO, anaplastic oligodendroglioma; GBM, glioblastoma; OS, overall survival; PFS, progression-free survival; F, frontal lobe; T, temporal lobe; P, parietal lobe; O, occipital lobe; TH, thalamus; HIPP, hippocampus; FTI, frontotemporoinsular area; FTP, frontotemproparietal lobe; CC, corpus callosum; PO, parieto-occipital; CCRT, concurrent chemoradiotherapy.

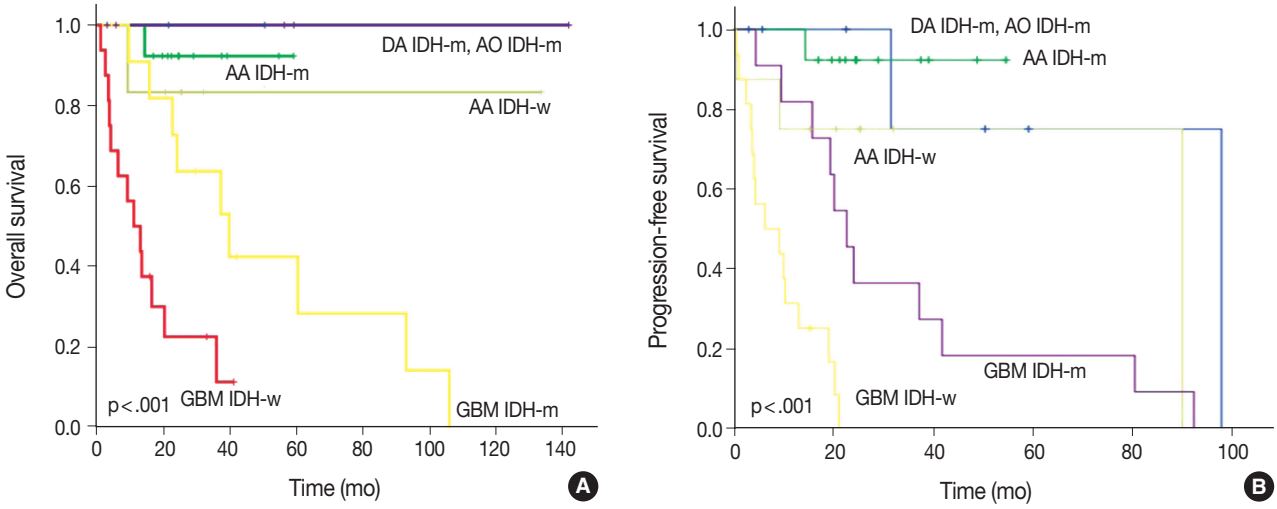

Fig. 5. Overall survival (A) and progression-free survival (B) in rediagnosed subgroups. AA, anaplastic astrocytoma; DA, diffuse astrocytoma; AO, anaplastic oligodendroglioma; GBM, glioblastoma; IDH-m, IDH-mutant; IDH-w, IDH-wildtype.

our 27 GBMs, ATRX-positive and -negative cases were 55.6% and 44.4%, respectively. Among ATRX-negative GBMs, 50% (6/12) were secondary, 41.7% (5/12) were primary, and 8.3% (1/12) were unconfirmed. Thus, half of ATRX-negative GBMs were secondary GBM, but among primary GBMs, 27.8% were ATRX-negative.

Using these criteria, our 58 cases could be classified as either astrocytic or oligodendroglial. None showed mixed genetic features of astrocytic and oligodendroglial. Our results also indicate that the codeletion status of 1p/19q is the most important criteria in the classification of diffuse gliomas into astrocytic or oligodendroglial, and could serve as a useful biomarker in the future diagnosis.

We evaluated all clinical, histological, and molecular characteristics using K-M survival analysis. OS and PFS were better in gliomas with *IDH* mutation, *ATRX* mutation, absence of microscopic necrosis, and young patient age (cut off, 45 years old). Although the impact of *ATRX* mutation on PFS had no statistical significance with log-rank test (p = .073), the Wilcoxon test and Tarone-Ware test showed statistical significance (p = .010 and p = .016, respectively). This confirms the results of previous studies on the impact of *IDH* and *ATRX* on prognosis.[17,18] Because most tumors with microscopic necrosis were diagnosed as either grade IV GBM IDH-m or GBM IDH-w, it is obvious that tumors with no necrosis showed better prognosis. Regarding the patient age, this study also confirms the results of a previous study.[1] Increase in age is associated with more high-grade glial tumors or poorer general conditions; therefore, elderly people could have a poorer prognosis.[9] Among patients with tumors of the same grade, one of the most favorable prognostic factors is young age (cut off, 45 years old).[9] Similar results can be observed in oligodendroglial tumors.[19]

In this study, 1p/19q status did not achieve statistical significance on OS or PFS. However, excluding one case, of which the cause of death was uncertain, all 1p/19q codeleted patients fully survived the follow-up period. Therefore, the lack of statistical significance might be derived from the short term follow-up period or a small number of patients.

With regard to both OS and PFS, the genetically integrated diagnostic approach showed statistically significant subgroups, which confirm the results of previous studies carried out by Reuss *et al.*[13] Our reclassification revealed that some patients should have received different treatment based on our genetically integrated diagnosis. Two patients initially diagnosed with GBMO were re-diagnosed with AO. One had primarily concurrent chemoradiation therapy and the other had primarily chemotherapy alone. However, according to our hospital protocol, the primary choice for AO is craniotomy and tumor removal with or without adjuvant therapy. Although reclassification itself might produce change in the treatment protocol of gliomas, it can also be useful in the selection of proper therapy for the patients.

ATRX negativity and p53 positivity directly indicated secondary GBM; however, among these tumors, four cases were primary GBM, which may indicate rapid progression from low grade tumors.

It is well known that astrocytic tumors have a genetic hallmark of *ATRX* and *TP53* mutation.[7,8] In the genetically integrated diagnostic flow, *ATRX* mutation proved more useful as *TP53*

https://doi.org/10.4132/jptm.2017.09.25

mutation was shown to be poorly detected by IHC.[20] In cases with intact ATRX, a 1p/19q assay should be carried out for designation of oligodendroglial tumor. Since generally extensive p53 staining is regarded as indicative of astrocytoma, p53 IHC might also be helpful in differential diagnosis of those cases. Therefore, we tried to find for a proper cutoff value of p53 positivity for astrocytic designation in our study. The cut-off value of 20% divided the subgroup stringently. However, 20% cut off of p53 had no statistical significance both in OS (p = .054) and PFS (p = .208). In our study, astrocytic tumors had p53 positivity in an average of 42.1%, with a standard deviation of 32.31%. If astrocytic tumors were entirely negative for p53 IHC, those cases should be re-verified by alternative tools, such as next generation sequencing or restriction fragment length polymorphism for detecting loss of function-mutation or methylation of p53. Further studies on staining pattern or correlation with other clinicopathological factors might be helpful.

To compare prognosis, 55 patients with previously diagnosed mixed GBMO by 2007 WHO classification were classified into six groups, and there was a statistically significant difference (p = .000); however, the number of patients was limited. Thus, if longer follow-up or more prospective studies are ensured in more patients, some prognostic factors that were not statistically significant in current studies may turn out to be statistically significant.

In conclusion, we successfully reclassified previously diagnosed mixed gliomas into either astrocytic or oligodendroglial tumors with a genetically integrated diagnostic approach. Our study suggests that genetic information, including *ATRX* and *IDH* mutation and 1p/19q co-deletion, has powerful prognostic and predictive value. In addition, this information can aid in classifying brain tumors into more distinct categories. Therefore, the integration of phenotypes and genotypes is clearly necessary in the routine practice of brain tumor diagnoses.

Conflicts of Interest

No potential conflict of interest relevant to this article was reported.

Acknowledgments

This study was supported by a grant of the Korea Health Technology R&D Project through the Korea Health Industry Development Institute (KHIDI), funded by the Ministry of Health & Welfare, Republic of Korea (grant number : HI14C1277).

REFERENCES

1. Myung JK, Cho HJ, Kim H, *et al*. Prognosis of glioblastoma with oligodendroglioma component is associated with the *IDH1* mutation and MGMT methylation status. Transl Oncol 2014; 7: 712-9.
2. Jiang H, Ren X, Cui X, *et al*. 1p/19q codeletion and *IDH1/2* mutation identified a subtype of anaplastic oligoastrocytomas with prognosis as favorable as anaplastic oligodendrogliomas. Neuro Oncol 2013; 15: 775-82.
3. Tortosa A, Viñolas N, Villà S, *et al*. Prognostic implication of clinical, radiologic, and pathologic features in patients with anaplastic gliomas. Cancer 2003; 97: 1063-71.
4. Okamoto Y, Di Patre PL, Burkhard C, *et al*. Population-based study on incidence, survival rates, and genetic alterations of low-grade diffuse astrocytomas and oligodendrogliomas. Acta Neuropathol 2004; 108: 49-56.
5. Ohgaki H. Contribution of molecular biology to the classification of low-grade diffuse glioma. In: Duffau H, ed. Diffuse low-grade gliomas in adults. London: Springer, 2013; 61-72.
6. Kros JM, Gorlia T, Kouwenhoven MC, *et al*. Panel review of anaplastic oligodendroglioma from European Organization For Research and Treatment of Cancer Trial 26951: assessment of consensus in diagnosis, influence of 1p/19q loss, and correlations with outcome. J Neuropathol Exp Neurol 2007; 66: 545-51.
7. Killela PJ, Pirozzi CJ, Reitman ZJ, *et al*. The genetic landscape of anaplastic astrocytoma. Oncotarget 2014; 5: 1452-7.
8. Liu XY, Gerges N, Korshunov A, *et al*. Frequent *ATRX* mutations and loss of expression in adult diffuse astrocytic tumors carrying *IDH1/IDH2* and *TP53* mutations. Acta Neuropathol 2012; 124: 615-25.
9. Louis DN, Ohgaki H, Wiestler OD, Cavenee WK. WHO classification of tumours of the central nervous system. 4th ed. Lyon: IARC Press, 2016.
10. Labussière M, Idbaih A, Wang XW, *et al*. All the 1p19q codeleted gliomas are mutated on *IDH1* or *IDH2*. Neurology 2010; 74: 1886-90.
11. Louis DN, Perry A, Burger P, *et al*. International Society of Neuropathology: Haarlem consensus guidelines for nervous system tumor classification and grading. Brain Pathol 2014; 24: 429-35.
12. Sahm F, Reuss D, Koelsche C, *et al*. Farewell to oligoastrocytoma: in situ molecular genetics favor classification as either oligodendroglioma or astrocytoma. Acta Neuropathol 2014; 128: 551-9.
13. Reuss DE, Sahm F, Schrimpf D, *et al*. ATRX and IDH1-R132H immunohistochemistry with subsequent copy number analysis and IDH sequencing as a basis for an "integrated" diagnostic approach for adult astrocytoma, oligodendroglioma and glioblastoma. Acta Neuropathol 2015; 129: 133-46.

14. van den Bent MJ, Brandes AA, Taphoorn MJ, *et al*. Adjuvant procarbazine, lomustine, and vincristine chemotherapy in newly diagnosed anaplastic oligodendroglioma: long-term follow-up of EORTC brain tumor group study 26951. J Clin Oncol 2013; 31: 344-50.
15. Houillier C, Wang X, Kaloshi G, *et al*. *IDH1* or *IDH2* mutations predict longer survival and response to temozolomide in low-grade gliomas. Neurology 2010; 75: 1560-6.
16. Grisold W, Oberndorfer S, Struhal W. Stroke and cancer: a review. Acta Neurol Scand 2009; 119: 1-16.
17. Yan H, Parsons DW, Jin G, *et al*. *IDH1* and *IDH2* mutations in gliomas. N Engl J Med 2009; 360: 765-73.
18. Haberler C, Wöhrer A. Clinical neuropathology practice news 2-2014: ATRX, a new candidate biomarker in gliomas. Clin Neuropathol 2014; 33: 108-11.
19. Love S, Perry A, Ironside J, Budka H. Greenfield's neuropathology. 9th ed. Boca Raton: CRC Press, 2015.
20. Louis DN, von Deimling A, Chung RY, *et al*. Comparative study of p53 gene and protein alterations in human astrocytic tumors. J Neuropathol Exp Neurol 1993; 52: 31-8.

 https://doi.org/10.4132/jptm.2017.09.25

Journal of Pathology and Translational Medicine 2018; 52: 37-44
https://doi.org/10.4132/jptm.2017.10.20

■ ORIGINAL ARTICLE ■

The Smad4/PTEN Expression Pattern Predicts Clinical Outcomes in Colorectal Adenocarcinoma

Yumin Chung · Young Chan Wi
Yeseul Kim · Seong Sik Bang
Jung-Ho Yang[1] · Kiseok Jang
Kyueng-Whan Min · Seung Sam Paik

Department of Pathology, Hanyang University College of Medicine, Seoul; [1]Department of Pathology, Kangbuk Samsung Hospital, Sungkyunkwan University School of Medicine, Seoul, Korea

Received: July 31, 2017
Revised: September 19, 2017
Accepted: October 16, 2017

Corresponding Author
Kyueng-Whan Min, MD, PhD
Department of Pathology, Hanyang University Guri Hospital, Hanyang University College of Medicine, 153 Gyeongchun-ro, Guri 11923, Korea
Tel: +82-31-560-2496
Fax: +82-31-560-2339
E-mail: kyueng@gmail.com

Seung Sam Paik, MD, PhD
Department of Pathology, Hanyang University Seoul Hospital, Hanyang University College of Medicine, 222-1 Wangsimni-ro, Seongdong-gu, Seoul 04763, Korea
Tel: +82-2-2290-8252
Fax: +82-2-2296-7502
E-mail: sspaik@hanyang.ac.kr

Background: Smad4 and PTEN are prognostic indicators for various tumor types. Smad4 regulates tumor suppression, whereas PTEN inhibits cell proliferation. We analyzed and compared the performance of Smad4 and PTEN for predicting the prognosis of patients with colorectal adenocarcinoma. **Methods:** Combined expression patterns based on Smad4+/– and PTEN+/– status were evaluated by immunostaining using a tissue microarray of colorectal adenocarcinoma. The relationships between the protein expression and clinicopathological variables were analyzed. **Results:** Smad4–/PTEN– status was most frequently observed in metastatic adenocarcinoma, followed by primary adenocarcinoma and tubular adenoma ($p < .001$). When Smad4–/PTEN– and Smad4+/PTEN+ groups were compared, Smad4–/PTEN– status was associated with high N stage ($p = .018$) and defective mismatch repair proteins ($p = .006$). Significant differences in disease-free survival and overall survival were observed among the three groups (Smad4+/PTEN+, Smad4–/PTEN+ or Smad4+/PTEN–, and Smad4–/PTEN–) (all $p < .05$). **Conclusions:** Concurrent loss of Smad4 and PTEN may lead to more aggressive disease and poor prognosis in patients with colorectal adenocarcinoma compared to the loss of Smad4 or PTEN alone.

Key Words: Smad4; PTEN; Prognosis; Colon neoplasms; Humans

Colorectal cancer (CRC) is a heterogeneous disease with diverse clinical presentations, responses to therapy, and histopathological findings at diagnosis.[1,2] The development of CRC is linked to homeostatic balance through the regulation of cellular proliferation, differentiation, and migration.[3,4] Approximately 15% of all CRCs have microsatellite instability (MSI) as a consequence of a deficient mismatch repair (MMR) system involving proteins such as MLH1, MSH2, and MSH6.[5-7] CRC with MSI is associated with various clinicopathological features, including a tendency to arise in the proximal colon, lymphatic invasion, high histological grade, and chemotherapeutic resistance.

Recent molecular studies have demonstrated several genetic and epigenetic alterations in CRC.[8-10] The four consensus molecular subtypes of CRC are CMS1 (MSI immune), CMS2 (canonical, marked WNT and MYC signaling activation), CMS3 (metabolic dysregulation), and CMS4 (mesenchymal, prominent transforming growth factor β [TGF-β] activation, stromal invasion, and angiogenesis).[11] High expression of CD133, CD44, and CD24 in cancer stem cells has been shown to be correlated with worse clinicopathological features in CRC.[12,13] Moreover, high co-expression of CD133 and CD44 has been associated with the AKT pathway and increased radiation resistance in colon cancer cells.[14,15]

Phosphatase and tensin homologue deleted on chromosome 10 (PTEN) is a phosphoinositide 3-phosphatase that can inhibit cellular proliferation, survival, growth, and differentiation in

pISSN 2383-7837
eISSN 2383-7845

several types of neoplasm such as colon, breast, and lymphoid cell neoplasms.[16-20] Smad4 (DPC4) is a tumor suppressor gene that mediates the TGF-β signaling pathway, thus suppressing epithelial cell growth.[21] Loss of Smad4 is linked to cancers arising in different organs such as the pancreas, colon, prostate, and bile duct, and it is also linked to gastric polyposis.[21-26] Ablation of Smad4 and PTEN in the pulmonary epithelium has been shown to induce metastatic adenosquamous carcinoma via the ErbB2/ELF3/AKT signaling pathway[27] and one *in vivo* study showed that coordinated deletion of the Smad4 and PTEN genes accelerated skin and stomach carcinogenesis.[25] In addition, PTEN deficiency has been shown to initiate widespread precancerous lesions triggered by Smad4 deficiency.[28]

Based on these data, we hypothesized that the loss of both Smad4 and PTEN is significantly associated with more aggressive CRC behavior than the loss of either protein individually. The purpose of this study was to investigate the expression patterns of Smad4 and PTEN in patients with CRC. We evaluated whether the combination of Smad4 and PTEN expression showed better performance for predicting patient survival than either marker alone.

MATERIALS AND METHODS

Patients and tissue specimens

This retrospective study enrolled a consecutive series of 529 patients with colorectal adenocarcinoma, 48 patients with metastatic adenocarcinoma, 14 patients with tubular adenoma, and 16 patients with normal colonic mucosae. All patients were diagnosed and treated at our institute from January 1991 to August 2001. This study included data obtained from a previously conducted research study.[15] The Reporting Recommendations for Tumor Marker Prognostic Studies (REMARK) criteria were followed throughout this study. Inclusion criteria included histopathological evidence of adenocarcinoma confirmed by a pathologist and known clinical outcome. Exclusion criteria included diagnosis of adenocarcinoma with neoadjuvant chemotherapy or inadequate clinical history. Clinicopathological findings were collected from the patients' medical records and pathological reports. Patient age ranged from 17 to 87 years (mean, 57.7 years). The tumors were located at the cecum (n = 18), ascending colon (n = 78), hepatic flexure (n = 12), transverse colon (n = 26), splenic flexure (n = 4), descending colon (n = 25), sigmoid colon (n = 113), and rectum (n = 253). Tumor size ranged from 3 to 150 mm (mean, 57 mm). A mean number of 26.7 lymph nodes (LN) were dissected for each specimen. Over a mean follow-up interval after surgery of 5.9 years, 183 patients (34.6%) died and 346 (65.4%) survived. Normal colonic mucosae, tubular adenomas, and metastatic adenocarcinoma tissues were randomly selected for evaluation of Smad4 and PTEN expression.

This study (involving human participants) was approved by the Ethics Committee of Hanyang University Hospital (No. 2016-12-030-001) and was performed in accordance with the ethical standards of the Declaration of Helsinki, as revised in 2008. The institutional review board review confirmed that informed consent was not necessary for this study.

Tissue microarray construction

A representative area was carefully selected and marked on a hematoxylin and eosin (H&E)-stained slide. Tissue microarrays (TMAs) were assembled using a tissue-array instrument (Quick-Ray Manual Tissue Microarrayer, Unitma Co. Ltd., Seoul, Korea) consisting of thin-walled stainless steel punches and stylets used to empty and transfer the needle content. Areas rich in tumor cells were identified by light microscopic examination of H&E-stained sections and selected for use in TMAs. Tissue cylinders with a diameter of 2 mm were punched from the previously marked tumor area (tumor center) of each donor block and transferred to a recipient paraffin block. All tissue cores were composed of tumor tissue in more than 70% of the core area. Considering the limitations associated with obtaining representative areas of a tumor, we used a 2-mm tissue core from each donor block.

Immunohistochemical staining and scoring of Smad4 and PTEN expression

Primary mouse monoclonal anti-Smad4 antibodies (clone B-8, Santa Cruz Biotechnology Inc, Heidelberg, Germany) were diluted 1:250 and primary mouse monoclonal anti-PTEN antibodies (clone 28H6, Novocastra Laboratories, Newcastle upon Tyne, UK) were diluted 1:200.

The Smad4 and PTEN immunohistochemical (IHC) staining results were interpreted by two pathologists (K.J. and S.S.P.) who were blinded to the clinical data. Discordant cases were reviewed on a multi-headed microscope to reach consensus. Each slide was interpreted semi-quantitatively according to the intensity of nuclear immunoreactivity (Fig. 1). The cut-off was determined by proportion rather than by intensity, because the latter was rather heterogeneous. Smad4 and PTEN expression was classified as negative (< 10% positive tumor cells out of all cancer cells) or positive (≥ 10% positive tumor cells out of all cancer cells).[29]

https://doi.org/10.4132/jptm.2017.10.20

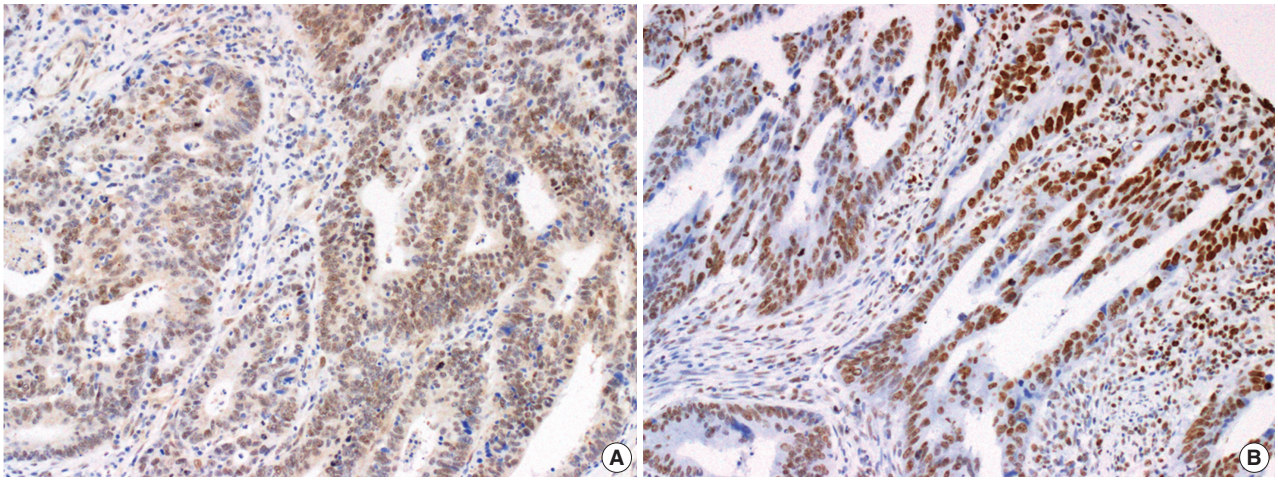

Fig. 1. Microphotographs showing immunohistochemical staining of Smad4 (A) and PTEN (B) expression in colorectal adenocarcinoma tissue.

Statistical analysis

The chi-square test was used to evaluate potential associations between Smad4 expression/PTEN expression and clinicopathologic parameters including age, gender, tumor location, tumor size, growth pattern, histological grade, of American Joint Committee on Cancer (AJCC) stage (T and N criteria), and MMR protein expression. The relationships between Smad4 and PTEN expression and normal mucosae, adenomatous polyps, adenocarcinomas, and metastatic LNs were analyzed using linear-by-linear association. Overall survival (OS) was defined as the time from curative surgery to death from any cause. Disease-free survival (DFS) was defined as the time from curative surgery to the first tumor recurrence or distant metastasis. Kaplan–Meier curves with the log-rank test were used to calculate OS and DFS. Multivariate survival analysis was used with a Cox proportional hazards regression model to evaluate independent prognostic factors. A p-value of < .05 was considered significant. Statistical analysis was performed using SPSS ver. 20.0 (IBM Corp., Armonk, NY, USA) or R packages (http://www.r-project.org/).

RESULTS

The expression patterns of Smad4 and PTEN were evaluated in normal colonic mucosae, tubular adenomas, primary adenocarcinomas, and metastatic adenocarcinomas. The loss of both Smad4 and PTEN was associated with cancer progression. Specifically, Smad4–/PTEN– status was not observed in any of the 16 normal colonic mucosa tissues; however, it was observed in one of 14 tubular adenomas (7.1%), 165 of 529 primary adenocarcinomas (31.2%), and 17 of 48 metastatic adenocarcinomas (35.4%) (p < .001) (Fig. 2).

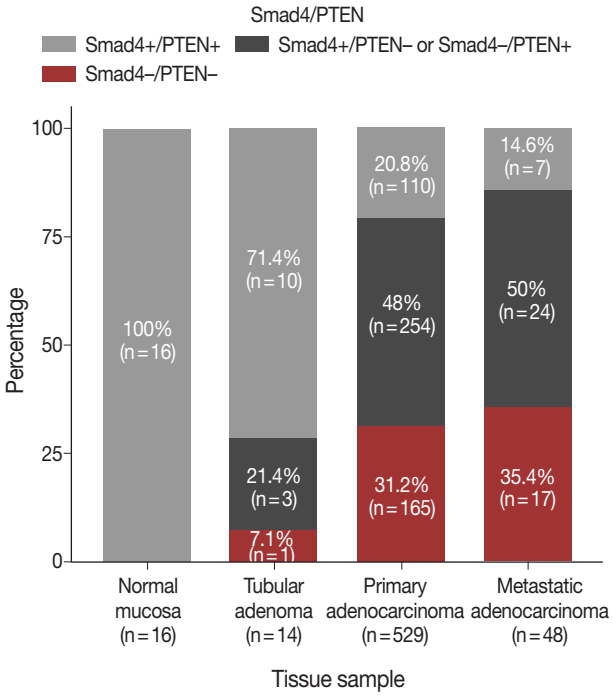

Fig. 2. Proportions of different tissues showing Smad4–/PTEN– staining: normal (0%), adenoma (7.2%), primary adenocarcinoma (31.2%), and metastatic adenocarcinoma (35.4%).

Smad4 loss was associated with higher N stage (p = .013) and showed a tendency to correlate with lymphovascular invasion (p = .081) (Supplementary Table S1). PTEN loss was correlated with defective MMR (p = .005) (Supplementary Table S2).

The distribution of Smad4 and PTEN expression status was as follows: Smad4–/PTEN–, 165 patients; Smad4–/PTEN+, 155 patients; Smad4+/PTEN–, 99 patients; and Smad4+/PTEN+, 110 patients.

Comparison of the Smad4–/PTEN– and Smad4+/PTEN+ groups showed that Smad4–/PTEN– status was associated with higher N stage (p = .018) and defective MMR (p = .006) (Table 1). In a comparative analysis between the Smad4+/PTEN+ and Smad4–/PTEN+ or Smad4+/PTEN– groups, Smad4+/PTEN+ status was correlated with lower N stage (p = .047), absence of lymphovascular invasion (p = .049), and intact MMR (p = .006) (Supplementary Table S3). Another comparative analysis between the Smad4–/PTEN+ or Smad4+/PTEN– and Smad4–/PTEN– groups showed that Smad4–/PTEN– status was correlated with defective MMR (p = .030) (Supplementary Table S4).

Survival according to Smad4/PTEN expression

Univariate and multivariate survival analyses showed that the

Table 1. Correlations between clinicopathological parameters and Smad4/PTEN in 275 patients with colon cancer

Parameter	No. (n = 275)	Smad4+/PTEN+ (n = 110)	Smad4–/PTEN– (n = 165)	p-value (chi-square test)
Age (yr)				.367
<65	189	79 (71.8)	110 (66.7)	
≥65	86	31 (28.2)	55 (33.3)	
Sex				.519
Female	121	51 (46.4)	70 (42.4)	
Male	154	59 (53.6)	95 (57.6)	
Tumor location				.413[a]
Right	63	27 (24.5)	36 (21.8)	
Transverse and left	25	12 (10.9)	13 (7.9)	
Rectosigmoid	187	71 (64.5)	116 (70.3)	
Tumor size (cm)				.472
≤4.5	98	42 (38.2)	56 (33.9)	
>4.5	177	68 (61.8)	109 (66.1)	
Growth pattern				.866
Fungating	71	29 (26.4)	42 (25.5)	
Ulcerating	204	81 (73.6)	123 (74.5)	
Histologic grade				.726[a]
1	13	3 (2.7)	10 (6.1)	
2	200	83 (75.5)	117 (70.9)	
3	62	24 (21.8)	38 (23)	
AJCC stage				.135[a]
Tis	5	1 (0.9)	4 (2.4)	
I	20	12 (10.9)	8 (4.8)	
II	101	44 (40)	57 (34.5)	
III	149	53 (48.2)	96 (58.2)	
T stage				.251[a]
Tis	5	1 (0.9)	4 (2.4)	
1	7	5 (4.5)	2 (1.2)	
2	22	12 (10.9)	10 (6.1)	
3	231	89 (80.9)	142 (86.1)	
4	10	3 (2.7)	7 (4.2)	
N stage				.018*[a]
0	126	57 (51.8)	69 (41.8)	
1	67	30 (27.3)	37 (22.4)	
2	82	26 (35.8)	59 (35.8)	
Lymphovascular invasion				.138
Absence	125	56 (50.9)	69 (41.8)	
Presence	150	54 (49.1)	96 (58.2)	
Mismatch repair protein				.006*
Intact	147	70 (63.6)	77 (46.7)	
Defective	128	40 (36.4)	88 (53.3)	

Values are presented as number (%).
AJCC, 8th edition of American Joint Committee on Cancer.
*p < .05.
[a]Linear by linear association.

https://doi.org/10.4132/jptm.2017.10.20

loss of Smad4 was associated with short DFS and OS (all $p < .05$). In univariate analyses, loss of PTEN was not associated with short DFS or OS (all $p < .05$). In multivariate analyses, no relationship was observed between DFS or OS and PTEN.

Comparison of the Smad4+/PTEN+ and Smad4–/PTEN– groups showed that Smad4–/PTEN– status was associated with short DFS and OS in both univariate and multivariate analyses (all $p < .05$). Comparison of the Smad4–/PTEN+ or Smad4+/

Table 2. Disease-free and overall survival analyses according to expression patterns of Smad4/PTEN

	Univariate significance p-value[a]	Multivariate significance p-value[b]	HR	95% CI
Disease-free survival				
T stage (1, 2 vs 3, 4)	<.001*	.018*	2.188	1.145–4.182
N stage (0 vs 1, 2)	<.001*	.269	1.386	0.777–2.474
Histological grade (1, 2 vs 3)	<.001*	.013*	1.450	1.082–1.942
Lymphovascular invasion (presence vs absence)	<.001*	.041*	1.873	1.027–3.418
MMR (intact vs defective)	.001*	.056	1.293	0.994–1.683
Smad4/PTEN				
+/+ vs –/+ or +/–	.079	.402	1.177	0.804–1.724
–/+ or +/– vs –/–	.006*	.018*	1.407	1.059–1.868
+/+ vs –/–	<.001*	.007*	1.715	1.155–2.545
Overall survival				
T stage (1, 2 vs 3, 4)	<.001*	.023	2.611	1.140–5.980
N stage (0 vs 1, 2)	<.001*	.351	1.361	0.712–2.601
Histological grade (1, 2 vs 3)	<.001*	.003*	1.635	1.185–2.257
Lymphovascular invasion (presence vs absence)	<.001*	.128	1.688	0.861–3.308
MMR (intact vs defective)	<.001*	<.001*	1.712	1.267–2.315
Smad4/PTEN				
+/+ vs –/+ or +/–	.007*	.035*	1.660	1.035–2.661
–/+ or +/– vs –/–	.011*	.048*	1.373	1.003–1.881
+/+ vs –/–	<.001*	.001*	2.238	1.379–3.630

HR, hazard ratio; CI, confidence interval; MMR, mismatch repair protein.
*$p < .05$.
[a]Log rank test; [b]Cox proportional hazard model adjusted for T and N stage, histological grade, lymphovascular invasion, MMR and Smad4/PTEN expression.

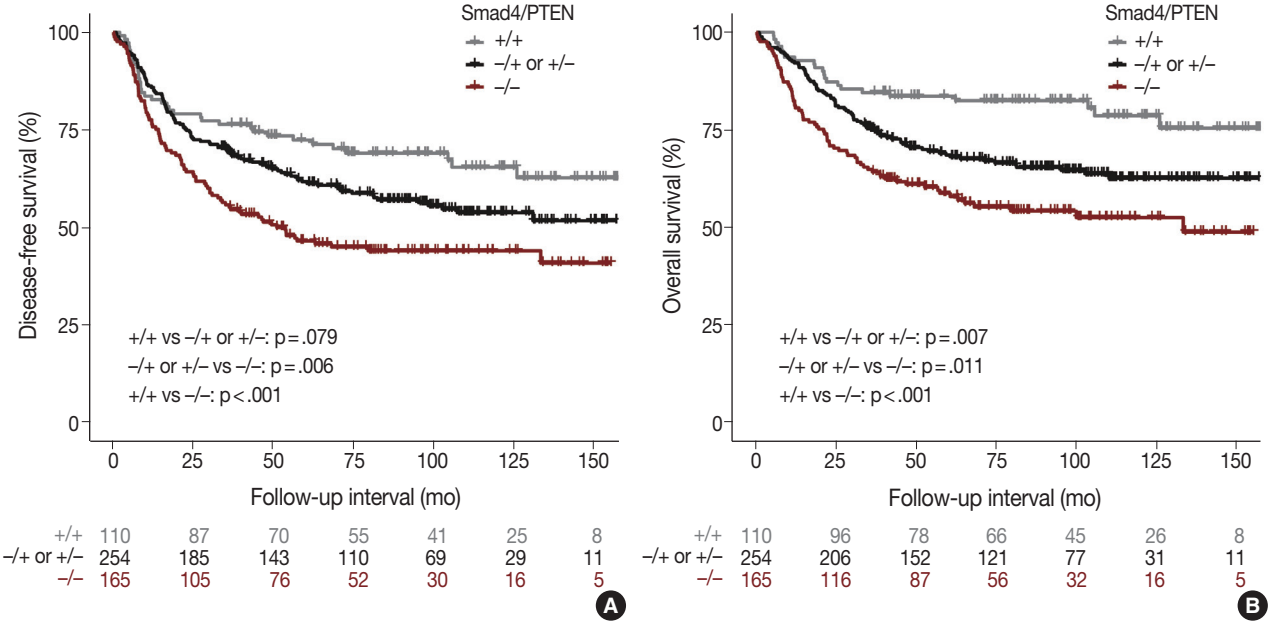

Fig. 3. Disease-free survival (A) and overall survival (B) curves derived by the Kaplan–Meier method showing the correlation of survival with Smad4/PTEN expression status.

PTEN– and Smad4–/PTEN– groups revealed significant differences in DFS and OS (all $p < .05$). Comparison of the Smad4+/PTEN+ and Smad4–/PTEN+ or Smad4+/PTEN– groups showed a significant difference in OS ($p = .035$), whereas the difference in DFS was not significant (Table 2, Fig. 3).

DISCUSSION

The aim of this study was to determine whether the Smad4/PTEN expression pattern is associated with clinical outcomes. Smad4 is part of a protein complex linked to signal transduction and interacts with DNA for cell proliferation.[30] PTEN is a negative regulator of the Akt signaling pathway and is necessary for cell proliferation and inhibition of apoptosis.[31,32] Smad4 and PTEN have been shown to be closely linked in the regulation of tumor invasion and distant metastasis. For instance, Haeger *et al*.[33] demonstrated that the loss of Smad4 could initiate lung cancer development from keratinized epithelium *in vivo*. Moreover, loss of Smad4 expression and low Smad4 expression were both shown to increase cell proliferation secondary to the loss of TGF-β–mediated growth suppression.[34] During cancer development, deletion of PTEN is common in several malignancies such as gastric, esophageal, endometrial, breast, and non-small cell lung cancers.[25,35-40] Moreover, many studies have identified PTEN mutations in HRS320 cells, a colonic cancer cell line, and shown that these mutations are significantly related to poor clinical outcomes in patients with CRC.[41,42]

The prognostic value of combinations of cancer markers for patients with CRC (which exhibits high heterogeneity) may be better than that of models using a single marker. An *in vivo* study demonstrated that loss of both Smad4 and PTEN may act synergistically to regulate cell proliferation and accelerate tumorigenesis.[25] The synergistic action of these genes is mediated by concomitant repression of PTEN transcription by Smad4 and promotion of Smad4 degradation by PTEN.[22] Liu *et al*.[27] showed that the combined loss of Smad4 and PTEN was linked to metastatic lung cancer through activation of the ErbB2/ELF3/AKT pathway. In pancreatic cancer, the absence of Smad4 and PTEN has been shown to synergistically promote ductal carcinoma.[28] Intriguingly, Smad4 deletion has been shown to drive progression of PTEN-deficient prostate cancer to highly aggressive behaviors such as tumor invasion and lymph node metastasis.[24] Thus, Smad4 deficiency can accelerate tumor cell proliferation and invasion, especially when combined with loss of PTEN expression. Although this relationship has been confirmed in an *in vitro* study, no reports have described a difference in DFS or OS in human CRC according to the loss of both Smad4 and PTEN. In the present study, we showed that Smad4+/PTEN+ status indicated good prognosis, whereas Smad4–/PTEN– status was associated with poor prognosis. These findings suggest that the loss of both Smad4 and PTEN expression is linked to worse clinical outcomes in patients with CRC. In addition, Smad4–/PTEN– status was significantly associated with higher N stage compared to Smad4+/PTEN+ status.

The precise mechanism underlying the synergistic effect between Smad4 and PTEN is not fully understood. In esophageal cancer, it has been proposed that the loss of both Smad4 and PTEN leads to the downregulation of CIP/KIP and INK4 Cdk inhibitors and subsequent suppression of cell cycle arrest.[43] Alternatively, concurrent deletion of PTEN and Smad4 has been reported to induce an oncogenic pathway including ErbB2/Akt/ELF3 and to repress tumor suppressors in lung cancer.[27] Interestingly, the lung cancer study demonstrated that the mRNA level of ELF3 (a transcriptional factor known to have oncogenic activity) was significantly higher in Smad4–/PTEN– mice compared to Smad4– mice and PTEN– mice. In pancreatic cancer, Smad4–/PTEN– status was associated with wider cancer spread and larger tumors compared with Smad4– status or PTEN– status.[28] In the present study, the Smad4–/PTEN+ and Smad4+/PTEN– groups had lower survival rates than the Smad4+/PTEN+ group, but higher survival rates than the Smad4–/PTEN– group. These biological processes, together with the concurrent loss of Smad4 and PTEN, may correlate with more aggressive clinical behavior than that seen with the loss of a single protein.

This study did have some limitations. First, in contrast to previous in vitro studies, we did not demonstrate a molecular interaction between Smad4 and PTEN, making it difficult to draw concrete conclusions from our data. Second, the cut-off value of 10% for distinguishing positive from negative expression of Smad4 and PTEN was determined by IHC evaluation. However, Smad4 and PTEN distribution may vary according to specimen type, implying that this cut-off point may not apply to other types of clinical samples or to other laboratories. Third, interactions between Smad4 and PTEN within single tumor cells could not be observed, because double staining of Smad4 and PTEN expression was not performed.

In summary, we found that the Smad4/PTEN expression pattern was statistically correlated with several clinicopathological parameters and with survival. Smad4–/PTEN– status was more frequently observed in patients who followed the multi-step carcinogenesis progression from normal colonic mucosae to tubular adenoma, primary adenocarcinoma, and metastatic adenocarci-

 https://doi.org/10.4132/jptm.2017.10.20

noma. Some differences in survival were observed among the Smad4+/PTEN+, Smad4+/PTEN– or Smad4–/PTEN+, and Smad4–/PTEN– groups. Thus, combinations of markers may be more useful for predicting the survival of patients with CRC than single markers alone. We conclude that concurrent loss of Smad4 and PTEN may accelerate cancer progression and that these two genes thus represent potential targets for cancer treatment.

Electronic Supplementary Material

Supplementary materials are available at Journal of Pathology and Translational Medicine (http://jpatholtm.org).

Conflicts of Interest

No potential conflict of interest relevant to this article was reported.

REFERENCES

1. Torre LA, Bray F, Siegel RL, Ferlay J, Lortet-Tieulent J, Jemal A. Global cancer statistics, 2012. CA Cancer J Clin 2015; 65: 87-108.
2. Cunningham D, Atkin W, Lenz HJ, *et al*. Colorectal cancer. Lancet 2010; 375: 1030-47.
3. Vogelstein B, Fearon ER, Hamilton SR, *et al*. Genetic alterations during colorectal-tumor development. N Engl J Med 1988; 319: 525-32.
4. Valcz G, Sipos F, Krenács T, *et al*. Increase of alpha-SMA(+) and CK (+) cells as an early sign of epithelial-mesenchymal transition during colorectal carcinogenesis. Pathol Oncol Res 2012; 18: 371-6.
5. Ionov Y, Peinado MA, Malkhosyan S, Shibata D, Perucho M. Ubiquitous somatic mutations in simple repeated sequences reveal a new mechanism for colonic carcinogenesis. Nature 1993; 363: 558-61.
6. Peltomäki P. Role of DNA mismatch repair defects in the pathogenesis of human cancer. J Clin Oncol 2003; 21: 1174-9.
7. Boland CR, Goel A. Microsatellite instability in colorectal cancer. Gastroenterology 2010; 138: 2073-87.e3.
8. Wood LD, Parsons DW, Jones S, *et al*. The genomic landscapes of human breast and colorectal cancers. Science 2007; 318: 1108-13.
9. Starr TK, Allaei R, Silverstein KA, *et al*. A transposon-based genetic screen in mice identifies genes altered in colorectal cancer. Science 2009; 323: 1747-50.
10. Segditsas S, Tomlinson I. Colorectal cancer and genetic alterations in the Wnt pathway. Oncogene 2006; 25: 7531-7.
11. Guinney J, Dienstmann R, Wang X, *et al*. The consensus molecular subtypes of colorectal cancer. Nat Med 2015; 21: 1350-6.
12. Choi D, Lee HW, Hur KY, *et al*. Cancer stem cell markers CD133 and CD24 correlate with invasiveness and differentiation in colorectal adenocarcinoma. World J Gastroenterol 2009; 15: 2258-64.
13. Jing F, Kim HJ, Kim CH, Kim YJ, Lee JH, Kim HR. Colon cancer stem cell markers CD44 and CD133 in patients with colorectal cancer and synchronous hepatic metastases. Int J Oncol 2015; 46: 1582-8.
14. Sahlberg SH, Spiegelberg D, Glimelius B, Stenerlöw B, Nestor M. Evaluation of cancer stem cell markers CD133, CD44, CD24: association with AKT isoforms and radiation resistance in colon cancer cells. PLoS One 2014; 9: e94621.
15. Chen KL, Pan F, Jiang H, *et al*. Highly enriched CD133(+)CD44(+) stem-like cells with CD133(+)CD44(high) metastatic subset in HCT116 colon cancer cells. Clin Exp Metastasis 2011; 28: 751-63.
16. Kechagioglou P, Papi RM, Provatopoulou X, *et al*. Tumor suppressor PTEN in breast cancer: heterozygosity, mutations and protein expression. Anticancer Res 2014; 34: 1387-400.
17. Saal LH, Gruvberger-Saal SK, Persson C, *et al*. Recurrent gross mutations of the PTEN tumor suppressor gene in breast cancers with deficient DSB repair. Nat Genet 2008; 40: 102-7.
18. Wang X, Huang H, Young KH. The PTEN tumor suppressor gene and its role in lymphoma pathogenesis. Aging (Albany NY) 2015; 7: 1032-49.
19. Zhang LL, Mu GG, Ding QS, *et al*. Phosphatase and tensin homolog (PTEN) represses colon cancer progression through inhibiting paxillin transcription via PI3K/AKT/NF-kappaB pathway. J Biol Chem 2015; 290: 15018-29.
20. Park SH, Won J, Kim SI, *et al*. Molecular testing of brain tumor. J Pathol Transl Med 2017; 51: 205-23.
21. Miyaki M, Kuroki T. Role of Smad4 (DPC4) inactivation in human cancer. Biochem Biophys Res Commun 2003; 306: 799-804.
22. Xu X, Kobayashi S, Qiao W, *et al*. Induction of intrahepatic cholangiocellular carcinoma by liver-specific disruption of Smad4 and Pten in mice. J Clin Invest 2006; 116: 1843-52.
23. Chow JY, Cabral JA, Chang J, Carethers JM. TGFbeta modulates PTEN expression independently of SMAD signaling for growth proliferation in colon cancer cells. Cancer Biol Ther 2008; 7: 1694-9.
24. Ding Z, Wu CJ, Chu GC, *et al*. SMAD4-dependent barrier constrains prostate cancer growth and metastatic progression. Nature 2011; 470: 269-73.
25. Teng Y, Sun AN, Pan XC, *et al*. Synergistic function of Smad4 and PTEN in suppressing forestomach squamous cell carcinoma in the mouse. Cancer Res 2006; 66: 6972-81.
26. Yan P, Klingbiel D, Saridaki Z, *et al*. Reduced expression of SMAD4 is associated with poor survival in colon cancer. Clin Cancer Res 2016; 22: 3037-47.
27. Liu J, Cho SN, Akkanti B, *et al*. ErbB2 pathway activation upon

Smad4 loss promotes lung tumor growth and metastasis. Cell Rep 2015; 10: 1599-613.
28. Xu X, Ehdaie B, Ohara N, Yoshino T, Deng CX. Synergistic action of Smad4 and PTEN in suppressing pancreatic ductal adenocarcinoma formation in mice. Oncogene 2010; 29: 674-86.
29. Jang KS, Song YS, Jang SH, *et al*. Clinicopathological significance of nuclear PTEN expression in colorectal adenocarcinoma. Histopathology 2010; 56: 229-39.
30. Peppercorn J, Perou CM, Carey LA. Molecular subtypes in breast cancer evaluation and management: divide and conquer. Cancer Invest 2008; 26: 1-10.
31. Stambolic V, Suzuki A, de la Pompa JL, *et al*. Negative regulation of PKB/Akt-dependent cell survival by the tumor suppressor PTEN. Cell 1998; 95: 29-39.
32. Davies MA, Koul D, Dhesi H, *et al*. Regulation of Akt/PKB activity, cellular growth, and apoptosis in prostate carcinoma cells by MMAC/PTEN. Cancer Res 1999; 59: 2551-6.
33. Haeger SM, Thompson JJ, Kalra S, *et al*. Smad4 loss promotes lung cancer formation but increases sensitivity to DNA topoisomerase inhibitors. Oncogene 2016; 35: 577-86.
34. Ahmed S, Bradshaw AD, Gera S, Dewan MZ, Xu R. The TGF-beta/Smad4 signaling pathway in pancreatic carcinogenesis and its clinical significance. J Clin Med 2017; 6: 5.
35. Tachibana M, Shibakita M, Ohno S, *et al*. Expression and prognostic significance of PTEN product protein in patients with esophageal squamous cell carcinoma. Cancer 2002; 94: 1955-60.
36. Lee HS, Lee HK, Kim HS, Yang HK, Kim WH. Tumour suppressor gene expression correlates with gastric cancer prognosis. J Pathol 2003; 200: 39-46.
37. Li J, Yen C, Liaw D, *et al*. PTEN, a putative protein tyrosine phosphatase gene mutated in human brain, breast, and prostate cancer. Science 1997; 275: 1943-7.
38. Zhao Y, Zheng R, Li J, Lin F, Liu L. Loss of phosphatase and tensin homolog expression correlates with clinicopathological features of non-small cell lung cancer patients and its impact on survival: a systematic review and meta-analysis. Thorac Cancer 2017; 8: 203-13.
39. Risinger JI, Hayes AK, Berchuck A, Barrett JC. *PTEN/MMAC1* mutations in endometrial cancers. Cancer Res 1997; 57: 4736-8.
40. Yang L, Kuang LG, Zheng HC, *et al*. *PTEN* encoding product: a marker for tumorigenesis and progression of gastric carcinoma. World J Gastroenterol 2003; 9: 35-9.
41. Dicuonzo G, Angeletti S, Garcia-Foncillas J, *et al*. Colorectal carcinomas and *PTEN/MMAC1* gene mutations. Clin Cancer Res 2001; 7: 4049-53.
42. Guanti G, Resta N, Simone C, *et al*. Involvement of *PTEN* mutations in the genetic pathways of colorectal cancerogenesis. Hum Mol Genet 2000; 9: 283-7.
43. Reynisdóttir I, Polyak K, Iavarone A, Massagué J. Kip/Cip and Ink4 Cdk inhibitors cooperate to induce cell cycle arrest in response to TGF-beta. Genes Dev 1995; 9: 1831-45.

 https://doi.org/10.4132/jptm.2017.10.20

Journal of Pathology and Translational Medicine 2018; 52: 45-50
https://doi.org/10.4132/jptm.2017.10.18

■ ORIGINAL ARTICLE ■

Importance of Individual Ghost Cells in Fine-Needle Aspiration Cytology Diagnosis of Pilomatricoma

Kanghee Han · Hwa-Jeong Ha
Joon Seog Kong · Jae Kyung Myung[1]
Sunhoo Park · Jung-Soon Kim
Myung-Soon Shin · Hye Sil Seol
Jae Soo Koh · Seung-Sook Lee[1]

Department of Pathology, Korea Cancer Center Hospital, Korea Institute of Radiological and Medical Sciences (KIRAMS), Seoul; [1]Laboratory of Radiation Pathology, Korea Institute of Radiological and Medical Sciences (KIRAMS), Seoul, Korea

Received: August 31, 2017
Revised: September 30, 2017
Accepted: October 16, 2017

Corresponding Author
Seung-Sook Lee, MD, PhD
Department of Pathology, Korea Cancer Center Hospital, Korea Institute of Radiological and Medical Sciences (KIRAMS), 75 Nowon-ro, Nowon-gu, Seoul 01812, Korea
Tel: +82-2-970-1268
Fax: +82-2-970-2430
E-mail: sslee@kirams.re.kr

Background: Although histological diagnosis of pilomatricoma is not difficult because of its unique histological features, cytological diagnosis through fine-needle aspiration cytology (FNAC) is often problematic due to misdiagnoses as malignancy. **Methods:** We reviewed the cytological features of 14 cases of histologically-proven pilomatricoma from Korea Cancer Center Hospital, with a discussion on the diagnostic pitfalls of FNAC. **Results:** Among 14 cases of pilomatricoma, 10 (71.4%) were correctly diagnosed through FNAC, and two (14.3%) were misdiagnosed as carcinoma. Cytologically, all cases had easily recognizable clusters of basaloid cells and foreign body-type multinucleated cells. Although ghost cells were also found in all cases, some were inconspicuous and hardly recognizable due to their small numbers. **Conclusions:** An accurate diagnosis of pilomatricoma in FNAC is feasible with consideration of clinical information and close examination of ghost cells.

Key Words: Pilomatricoma; Fine-needle aspiration cytology; Ghost cells

Pilomatricoma is a benign subcutaneous or dermal adnexal tumor that is usually a solitary nodule located at the head, neck, or upper limb.[1] Although it occurs in all age groups, 30%–50% of cases arise in individuals under the age of 30.[2] Histologically, pilomatricoma has conspicuous features that are well recognized, including aggregations of basaloid cells and inner eosinophilic material containing ghost cells.[2] Ghost cells are characterized by keratinized eosinophilic cells with distinctive cell borders and central unstained areas that correspond to the lost nuclei.[3] Because of these unique histological features, pilomatricoma is easy to diagnose on histologic sections. However, cytomorphological features of pilomatricoma found in aspirates are less distinctive and may mimic other benign lesions or malignant tumors.[4-7] Moreover, pilomatricoma is not infrequently mistaken for malignancies by positron emission tomography/computed tomography (PET/CT) as well as fine-needle aspiration cytology (FNAC).[8-11] Increased fluorodeoxyglucose (FDG) uptake in PET/CT generally suggests malignancy, but benign conditions such as infection/inflammation, lymphoid hyperplasia, granulomatous disease, and foreign body reactions may present as false-positive results.[12,13] Therefore, high FDG uptake of pilomatricoma in PET/CT might be attributed to a foreign body reaction in an area of keratinization.[8] Previous studies have shown diverse rates of preoperative diagnosis of pilomatricoma on FNAC, ranging from 1.1% to 81.9%.[14,15] Misdiagnosis, especially as malignancy, can lead to unnecessary treatment for patients with pilomatricoma. Here, we sought to delineate which cytomorphologic findings were useful in reliably differentiating pilomatricoma from other tumors, particularly from cancer.

pISSN 2383-7837
eISSN 2383-7845

MATERIALS AND METHODS

We identified 56 cases of pilomatricoma with a tissue diagnosis between January 1991 and December 2011 using the pathology database of the Department of Pathology at Korea Cancer Center Hospital (KCCH, Seoul, Korea). FNAC was performed in 14 out of those 56 cases prior to surgical resection.

Aspirations were performed with a 22–25-gauge needle attached to a 10 cc disposable syringe. The collected samples were smeared on slides, fixed with 95% ethyl alcohol, and stained with Papanicolaou stain.

A morphological analysis was done of the FNAC slides. The slides were reviewed by two pathologists and one cytotechnologist.

Cytomorphology focused on ghost cells, basaloid cells, nucleated squamous cells, calcium deposits, multinucleated giant cells, and the background, with scoring using a semiquantitative method (–, absent; +, small amount: occasionally observed; ++, moderate amount: easy to detect; +++, abundant: frequently detected in aggregates and/or isolated cells).

This study was approved by the Institutional Review Board of Korea Cancer Center Hospital with a waiver of informed consent (IRB No. K-1710-002008).

RESULTS

Clinicopathological findings

The present study included 14 cases of eight female and six male patients with ages ranging from 4 to 38 years (mean age, 18.4 years). All cases presented as a single mass in the head and neck region. Lesion size varied from 0.3 to 3 cm (mean, 1.3 cm). Clinical impressions were diverse; ten cases were benign and the other four cases were considered as malignancies, including metastasis from the salivary gland, thyroid, or metastasis of unknown origin. In our series, a correct diagnosis as pilomatricoma by FNAC was made in 10 cases (71.4%) and misdiagnosis was made in four cases (28.6%). The erroneous diagnoses included metastatic carcinoma (2 cases), atypical cells (1 case), and benign lymphadenopathy (1 case). Relevant clinical data and initial FNAC diagnoses are summarized in Table 1.

Histologically, all cases showed typical morphology of pilomatricoma, including two distinct populations of ghost cells and peripheral sheets of basaloid epithelial cells in varying proportions. Basaloid cells had round to oval hyperchromatic nuclei and scanty eosinophilic cytoplasm. Ghost cells had a distinct cell border and eosinophilic cytoplasm without nuclei, displaying an empty central portion.

Cytological features

The aspirates of the fourteen cases included in this study showed varying proportions of cellular components, including ghost cells, basaloid cells, nucleated squamous cells, calcium deposits, and multinucleated giant cells (Fig. 1). Importantly, basaloid cells, ghost cells and multinucleated giant cells were found in all 14 cases, and their amounts varied in each case.

Basaloid cells were usually observed as cohesive clusters and easily detected in most cases. Although they tended to form monolayer sheets of small uniform cells, hyperchromatic nuclei and conspicuous nucleoli were enough to raise the suspicion of

Table 1. Clinicopathological findings in 14 cases of pilomatricoma

Case No.	Sex	Age (yr)	Location	Tumor size (cm)	Clinical diagnosis	Initial FNAC diagnosis
1	F	36	Neck	0.6	Benign mass	Pilomatricoma
2	F	21	Preauricular	0.3	Metastatic carcinoma	Atypical cells
3	F	4	Preauricular	3	Tuberculosis	Metastatic carcinoma of salivary origin
4	F	10	Neck	0.5	Tuberculosis	Pilomatricoma
5	F	6	Mandible	1	Inclusion cyst, r/o tuberculosis, r/o carcinoma	Atypical epithelial cells, suspicious for metastatic carcinoma
6	F	38	Posterior neck	0.6	Metastatic carcinoma (history: papillary carcinoms of thyroid)	Pilomatricoma
7	M	37	Neck	1	MUO	Lymphadenitis
8	M	19	Neck	1.5	Benign mass	Pilomatricoma
9	F	16	Neck	1	Reactive hyperplasia r/o epidermal cyst	Pilomatricoma
10	F	19	Parotid gland	2.3	Pilomatricoma	Pilomatricoma
11	M	11	Preauricular	1	Epidermal cyst	Pilomatricoma
12	M	11	Postauricular	2.2	Epidermal cyst	Pilomatricoma
13	M	14	Neck	1.7	Lymphadenitis	Pilomatricoma
14	M	16	Neck	1.7	Neck mass	Pilomatricoma

FNAC, fine-needle aspiration cytology; F, female; M, male; MUO, metastasis of unknown origin; r/o, rule out.

https://doi.org/10.4132/jptm.2017.10.18

carcinoma (Fig. 1B). Nuclear pleomorphism was not found but mitosis was detected in one case. The number of basaloid cell nests was relatively small in eight cases (Table 2).

On the FNAC smears, all 14 cases displayed ghost cells. However, ten of the cases presented with only a small amount of ghost cells detected with careful observation, one case had an easily detectable moderate amount, and only three cases had abundant and frequently observed ghost cells (Table 2, Fig. 2). It was easy to notice in the four cases with sheet-forming ghost cells that they were characteristic ghost cells derived from pilomatricoma, in contrast with the five cases where ghost cells only constituted a very small number of individual cells. The relative appearance rates of basaloid cells and ghost cells also varied. As shown in Table 2, five cases showed a relative abun-

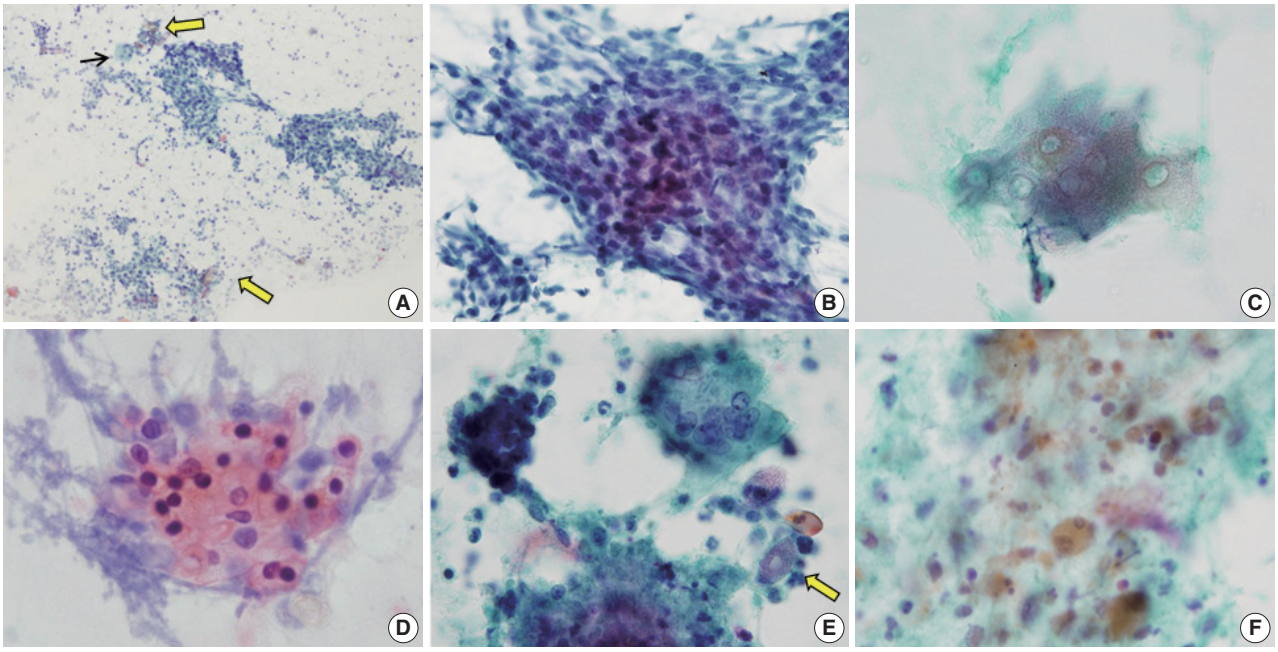

Fig. 1. Cytological features of pilomatricoma. (A) Low power view exhibiting large clusters of basaloid cells, ghost cells (thick arrows), and a multinucleated giant cell (thin arrow) in an inflammatory background. (B) Large clusters of basaloid cells mimicking carcinoma. (C) Ghost cells. (D) Nucleated squamous cells. (E) Foreign body-type multinucleated giant cell (right upper), small cluster of basaloid cells (left upper), calcific debris (lower), isolated ghost cell (arrow), and inflammatory cells. (F) Cellular debris (Papanicolaou stain).

Table 2. Cytological features in 14 cases of pilomatricoma

Case No.	Initial FNAC diagnosis	Cytological feature					
		Ghost cells	Basaloid cells	Nucleated squamous cells	Calcium deposits	Giant cells	Background
1	Pilomatricoma	+	++	++	++	+	Debris, inflammatory
2	Atypical cells	+	+	–	–	+	Bloody
3	Metastatic carcinoma of salivary origin	+	++	+	–	++	Bloody
4	Pilomatricoma	+++	+	+	–	+	Debris
5	Atypical epithelial cells, suspicious for metastatic carcinoma	+	+++	+	+	+	Debris
6	Pilomatricoma	+	+++	–	+	+	Debris
7	Lymphadenitis	+	+	–	+	+	Inflammatory
8	Pilomatricoma	+	+	+	+	+	Clear
9	Pilomatricoma	+++	+	-	-	+	Clear
10	Pilomatricoma	+++	+++	+	-	+	Debris
11	Pilomatricoma	+	+	-	-	+	Clear
12	Pilomatricoma	+	++	++	+	+	Debris, mitosis
13	Pilomatricoma	++	+	+	+	++	Cystic
14	Pilomatricoma	+	+	–	+	+	Inflammatory

FNAC, fine-needle aspiration cytology; –, absent; +, mild; ++, moderate; +++, abundant.

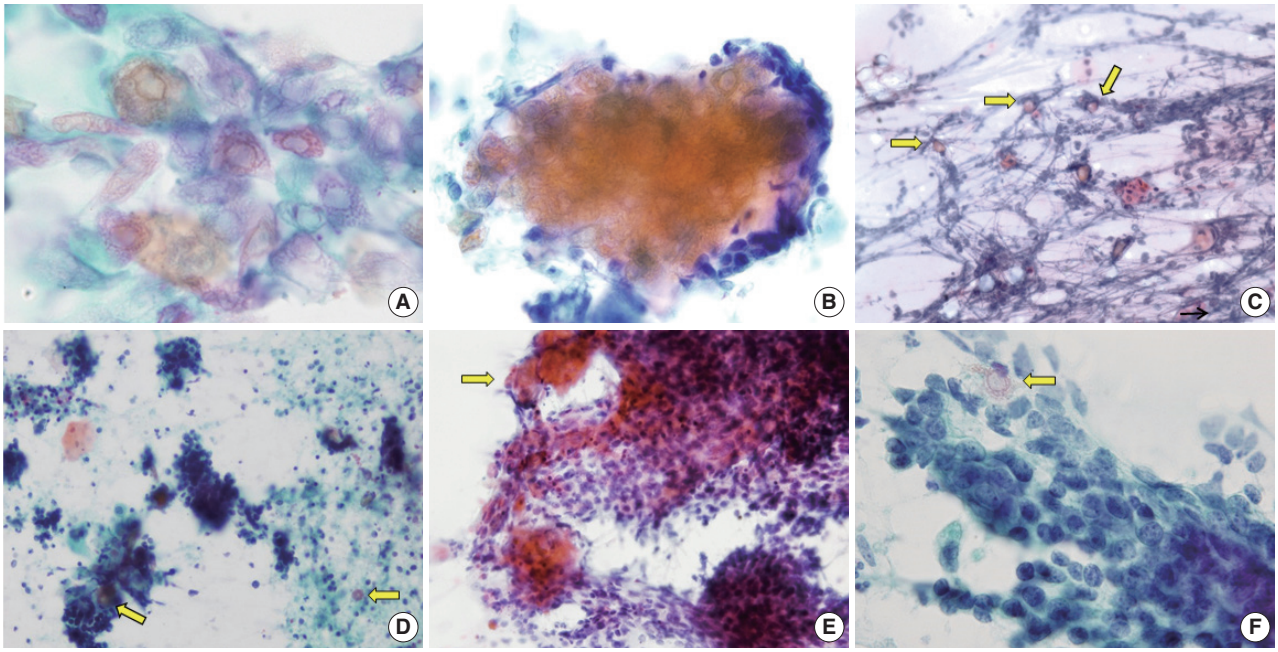

Fig. 2. Variable features of ghost cells in aspirates of pilomatricoma. (A) Ghost cell sheet showing abundant cytoplasm with distinct cell borders and central unstained area. (B) Clusters of ghost cells with peripheral basaloid cells. (C) Isolated ghost cells (arrows) and a small cluster of nucleated squamous cells in an inflammatory background. (D) Predominance of basaloid cell clusters and a few ghost cells (arrows). (E) Ghost cell nests (arrow) at the periphery of a large cluster of basaloid cells. (F) A single ghost cell (arrow) can be overlooked due to a basaloid cell cluster.

dance of basaloid cells compared to ghost cells (cases 1, 3, 5, 6, and 12). Among the five cases, two were misdiagnosed as malignancy or suspicious malignancy, but the other three were correctly diagnosed as pilomatricoma. On the other hand, the FNAC diagnosis was correct in the three cases where ghost cells were abundant or moderate but basaloid cells were present in small amounts (cases 4, 9, and 13). In addition, the case with both abundant basaloid cells and ghost cells (case 10) was correctly diagnosed on FNAC.

Foreign body-type giant cells were also present in all the cases in varied amounts, and were most frequent in two cases (cases 3 and 13). Nucleated squamous cells presented in eight cases. Calcium deposits were found in eight cases. The background showed keratin, cellular debris, blood, and inflammatory cells. These findings are summarized in Table 2 and shown in Fig. 1. As for the four misdiagnosed cases, ghost cells were present, even though they were not easily detected due to their small amounts. In the two cases that were initially either mistaken for metastatic carcinoma (case 3) or suspicious for metastatic carcinoma (case 5), basaloid cells overwhelmed ghost cells (Fig. 2D, F). In both cases, multinucleated giant cells and inflammatory cells were accompanied in the background by blood (case 3) or necrotic debris (case 5). In case 2, which was initially over-diagnosed as atypical cells, both basaloid cells and ghost cells appeared in small numbers, although the basaloid cells looked atypical due to the high nuclear/cytoplasmic ratio. Finally, case 7, which was erroneously diagnosed as lymphadenitis, showed mainly inflammatory cells, some calcium deposits, and giant cells with a few scattered basaloid cells and ghost cells.

DISCUSSION

Pilomatricoma is a benign skin adnexal tumor that commonly occurs in the head and neck of young adults or children.[11] It is not infrequent for pilomatricoma to be misdiagnosed as a malignant tumor in FNAC, which is problematic because the patient is then over-treated. From our observations, we suggest that it is important to recognize that ghost cells can appear in a wide variety of forms (Fig. 2). The presence of ghost cells is of value in the diagnosis of pilomatricoma, but the small amount of individual ghost cells may be overlooked in aspirates. Accordingly, detection of ghost cells, even a few by careful observation appears to be the most important way to reach a correct diagnosis of pilomatricoma in conjunction with clinical information.

In previous studies of 179 cases of pilomatricoma by Lan *et al.*,[14] only two cases were correctly diagnosed as pilomatricoma

https://doi.org/10.4132/jptm.2017.10.18

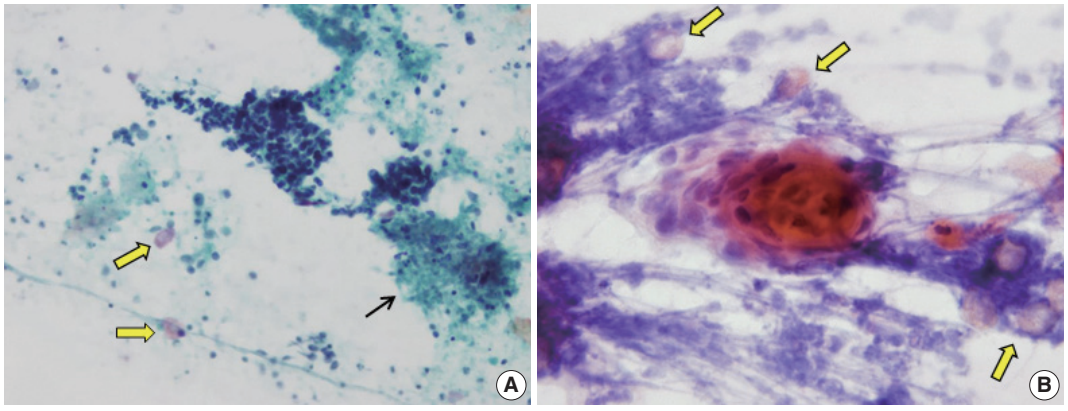

Fig. 3. Fine-needle aspiration cytology smear from pilomatricoma mimicking carcinoma. (A) Tight clusters of basaloid cells and necrotic debris (thin arrow) simulate carcinoma. However, a few scattered ghost cells are noted (thick arrows). (B) A nest of nucleated keratinizing squamous cells (center) may raise the suspicion of carcinoma. Nevertheless, if ghost cells are noted (arrows), a correct diagnosis of pilomatricoma can be made.

in preoperative examination. The other cases were mostly misdiagnosed as benign skin lesions such as epidermoid cysts.[16] In our series, a correct diagnosis of pilomatricoma by preoperative FNAC was made in 10 cases (71.4%). All of those cases had ghost cells, basaloid cells, and giant cells. The presence of nucleated squamous cells, calcium deposits, and background varied. Pilomatricoma is often confused with malignant tumors such as small round cell tumor,[17,18] rhabdomyosarcoma,[6] Merkel cell carcinoma,[7] or metastatic small cell carcinoma of the lung[19] due to the aggregation of basaloid cells with small nuclei and scanty cytoplasm. In addition, because of the unusual location, incorrect diagnosis has been made as metastatic adenocarcinoma in the abdominal wall[5] and breast cancer.[20]

In the current study, two cases mistaken for carcinomas showed numerous small and large clusters of hyperchromatic epithelial cells. Background cellular debris mimicking tumor necrosis (Fig. 3A) and small clusters of keratinizing cells may have led to a false positive diagnosis (Fig. 3B). Moreover, the ghost cells were not easily detected on the smears, especially in the hypercellular cases, because they were present individually or obscured by inflammatory cells, blood cells, or necrotic debris.

Given the causes of misdiagnosis as malignancy in this study, we have two observations. One is that clinical information, especially patient age, was neglected, and the other is that a few ghost cells were overlooked due to the overwhelming number of basaloid cells. It was careless to suggest metastatic carcinoma in children. Even if malignancy is suspected by cytologic findings, patient age is an important consideration in careful diagnosis.

The current study is limited by the small number of cases. During the same period, 56 cases were diagnosed as pilomatricoma by surgical excision and only 14 cases underwent preoperative FNAC (25%) in this study. This is similar to other studies in the literature. Compared to the number of surgically resected tissue specimens, the number with FNAC is relatively small, ranging from 26% to 53.6%.[7,14,21,22] Few reports are available on the cytological features of pilomatricoma, and the largest series in the literature includes 22 cases.[7] This deficit might be due to surgical excision without a preoperative cytologic examination depending on the clinical impression of a benign-looking mass.

In conclusion, consideration of clinical manifestation in patient age, location, consistency, and skin mobility is very important to avoid over-diagnosis in interpreting preoperative FNAC smears of pilomatricoma. It is also important to try to identify the coexistence of basaloid cells and ghost cells, and to avoid focusing too much on a predominance of basaloid cells.

Conflicts of Interest

No potential conflict of interest relevant to this article was reported.

Acknowledgments

This study was supported by a grant from the Korea Institute of Radiological and Medical Science (KIRAMS), funded by the Ministry of Science, ICT and Future planning, republic of Korea (1711045543;1711045540/50476-2017).

REFERENCES

1. Fletcher CD. Diagnostic histopathology of tumors. 4th ed. Philadelphia: Elsevier Saunders, 2013; 1707.
2. LeBoit PE, Burg G, Weeden D, Sarasain A. World Health Organiza-

tion classification of tumours: pathology and genetics of skin tumours. Lyon: IARC Press, 2006; 153-5.
3. Domanski HA, Domanski AM. Cytology of pilomatrixoma (calcifying epithelioma of Malherbe) in fine needle aspirates. Acta Cytol 1997; 41: 771-7.
4. Agrawal L, Kaur P, Singh J, Singh N. Pilomatrixoma misdiagnosed as round cell tumor on fine-needle aspiration cytology. Indian J Cancer 2010; 47: 483-5.
5. Sharma D, Agarwal S, Jain LS, Kamal V. Pilomatrixoma masquerading as metastatic adenocarcinoma: a diagnostic pitfall on cytology. J Clin Diagn Res 2014; 8: FD13-4.
6. Singh S, Gupta R, Mandal AK. Pilomatrixoma: a potential diagnostic pitfall in aspiration cytology. Cytopathology 2007; 18: 260-2.
7. Wang J, Cobb CJ, Martin SE, Venegas R, Wu N, Greaves TS. Pilomatrixoma: clinicopathologic study of 51 cases with emphasis on cytologic features. Diagn Cytopathol 2002; 27: 167-72.
8. Bhatt MK, Sommerville R, Ravi Kumar AS. FDG PET/CT appearance of benign pilomatricoma. Clin Nucl Med 2012; 37: 684-6.
9. Tay JK, Nga ME, Loh KS. Pilomatricoma of the cheek: a benign tumor mimicking metastatic squamous cell carcinoma on FDG PET/CT. Am J Otolaryngol 2014; 35: 452-5.
10. Szturz P, Rehák Z, Koukalová R, Adam Z, Mayer J. FDG-PET positive pilomatrixoma: reconsidering multicentricity in Langerhans cell histiocytosis. Nucl Med Rev Cent East Eur 2014; 17: 94-6.
11. Jung YS, Kang JG, Park WS, Ryu J. Pilomatricoma: diagnostic pitfalls in PET/CT and fine-needle aspiration biopsy. Otolaryngol Head Neck Surg 2007; 137: 845-6.
12. Pirouzmanesh A, Reinisch JF, Gonzalez-Gomez I, Smith EM, Meara JG. Pilomatrixoma: a review of 346 cases. Plast Reconstr Surg 2003; 112: 1784-9.
13. Rosenbaum SJ, Lind T, Antoch G, Bockisch A. False-positive FDG PET uptake: the role of PET/CT. Eur Radiol 2006; 16: 1054-65.
14. Lan MY, Lan MC, Ho CY, Li WY, Lin CZ. Pilomatricoma of the head and neck: a retrospective review of 179 cases. Arch Otolaryngol Head Neck Surg 2003; 129: 1327-30.
15. Cigliano B, Baltogiannis N, De Marco M, *et al*. Pilomatricoma in childhood: a retrospective study from three European paediatric centres. Eur J Pediatr 2005; 164: 673-7.
16. Al-Khateeb TH, Hamasha AA. Pilomatricoma of the maxillofacial area in the northern regional Jordanian population: report of 31 cases. J Oral Maxillofac Surg 2007; 65: 261-6.
17. Gupta M, Bansal R, Tiwari G, Sharma S. Aggressive pilomatrixoma: a diagnostic dilemma on fine-needle aspiration cytology with review of literature. Diagn Cytopathol 2014; 42: 906-11.
18. Ieni A, Todaro P, Bonanno AM, Catalano F, Catalano A, Tuccari G. Limits of fine-needle aspiration cytology in diagnosing pilomatrixoma: a series of 25 cases with clinico-pathologic correlations. Indian J Dermatol 2012; 57: 152-5.
19. Lemos MM, Kindblom LG, Meis-Kindblom JM, Ryd W, Willén H. Fine-needle aspiration features of pilomatrixoma. Cancer 2001; 93: 252-6.
20. Nori J, Abdulcadir D, Giannotti E, Calabrese M. Pilomatrixoma of the breast, a rare lesion simulating breast cancer: a case report. J Radiol Case Rep 2013; 7: 43-50.
21. Bansal C, Handa U, Mohan H. Fine needle aspiration cytology of pilomatrixoma. J Cytol 2011; 28: 1-6.
22. Kumaran N, Azmy A, Carachi R, Raine PA, Macfarlane JH, Howatson AG. Pilomatrixoma--accuracy of clinical diagnosis. J Pediatr Surg 2006; 41: 1755-8.

 https://doi.org/10.4132/jptm.2017.10.18

Journal of Pathology and Translational Medicine 2018; 52: 51-55
https://doi.org/10.4132/jptm.2017.01.23

■ CASE STUDY ■

An Autopsy Case of Epstein-Barr Virus–Associated Diffuse Large B-Cell Lymphoma of the Central Nervous System in an Immunocompromised Host

Sun-Young Park · Seong Ik Kim
Hannah Kim · Yoojin Lee
Sung-Hye Park

Department of Pathology, Seoul National University Hospital, Seoul National University College of Medicine, Seoul, Korea

Received: September 15, 2016
Revised: January 19, 2017
Accepted: January 23, 2017

Corresponding Author
Sung-Hye Park, MD
Department of Pathology, Seoul National University Hospital, Seoul National University College of Medicine, 103 Daehak-ro, Jongno-gu, Seoul 03080, Korea
Tel: +82-2-740-8278
Fax: +82-2-765-5600
E-mail: shparknp@snu.ac.kr

Lymphomas arising in the central nervous system (CNS) of immunocompromised hosts are most commonly non-Hodgkin's lymphomas and are highly associated with Epstein-Barr virus (EBV). Here we report an autopsy case of EBV-associated CNS diffuse large B-cell lymphoma (DLBCL) in a host suffering from systemic lupus erythematosus who underwent immunosuppressive therapy. After autopsy, EBV-associated CNS DLBCL as well as pulmonary mixed aspergillosis and *Pneumocystis jirovecii* pneumonia were added to the cause of clinical manifestations of complicated pneumonia and cerebral hemorrhage in this immunocompromised patient. In conclusion, complex disease processes were revealed by autopsy in this case, indicating that the clinicopathological correlations observed through autopsy can improve our understanding of disease progression and contribute to the management of similar patients in the future.

Key Words: Autopsy; Central nervous system; Lymphoma; Epstein-Barr virus; Immunocompromised host

Lymphomas arising in an immunocompromised host are most commonly non-Hodgkin's lymphoma, which is associated with Epstein-Barr virus (EBV) and can appear in the central nervous system (CNS).[1,2] However, even when lymphoma is localized to the CNS, if the host is immunodeficient patients this does not represent primary CNS lymphoma (PCNSL), because the 2008 World Health Organization (WHO) classification of hematopoietic and lymphoid tissues limits PCNSL to diffuse large B-cell lymphoma (DLBCL) in immunocompetent patients.[3] Therefore, PCNSL cannot be diagnosed in the patients with a history of underlying autoimmune diseases, organ transplantation, or immunosuppressive therapy. In addition, primary T-cell, NK-T cell or intravascular large B-cell lymphomas occurring in the CNS are not PCNSL, because they are not DLBCL. While PCNSL accounts for 2.4%–3.0% of all CNS tumors and comprises more than 95% of CNS lymphomas, EBV-associated CNS lymphoma (CNSL) is extremely rare.[4] The majority of PCNSLs are sporadic and non-EBV–associated, and the incidence increases with age. Few CNSLs are related to immunocompromised states such as human immunodeficiency virus infection and iatrogenic immunosuppression following organ transplantation.[5] In the latter cases, EBV infection is the most common cause of CNSL.[6]

We report a case of an immunocompromised patient diagnosed with EBV-associated CNSL after autopsy, focusing on the clinicopatholgical features of CNSL in immunocompromised patients. This case report followed the principles of the World Medical Association Declaration of Helsinki and it was approved by the Institutional Review Board of SNUH (H-1305-625-491 and IRB No. H-1506-080-681) with a waiver of informed consent.

CASE REPORT

The patient is a 60-year-old woman with a 2-year history of systemic lupus erythematosus (SLE) treated with prednisolone. Twelve years ago, she donated her left kidney to her daughter, who suffered from SLE for 12 years. She also had history of splenectomy due to idiopathic thrombocytopenic purpura (ITP) 8 years ago. One year ago, she underwent segmental resection of the small bowel due to cytomegalovirus (CMV) enteritis with perforation possibly related to steroid medication for SLE. Five months

pISSN 2383-7837
eISSN 2383-7845

prior, she presented with left-side weakness and seizure. Magnetic resonance imaging (MRI) of the brain revealed multiple acute and subacute infarct-like lesions with hemorrhagic transformation of the left frontal and fronto-parietal lobe lesions (Figs. 1, 2). Two months before death, she experienced fever relapses; at that time, chest imaging (chest posteroanterior) revealed patchy ground glass opacities of the bilateral upper lobes, indicating aggravated diffuse pneumonia (Fig. 3). On last admission, liver function test revealed abnormalities: aspartate aminotransferase, 125 IU/L (normal, 0 to 40 IU/L); alanine aminotransferase, 57 IU/L (normal, 0 to 40 IU/L); and total bilirubin, 1.1 mg/dL (normal, 0.2 to 1.2 mg/dL). The patient's general condition worsened and she died in December, 2012. A limited autopsy was performed confined to the brain, right lung and liver.

On autopsy, the whole brain was removed, which weighed 1,230 g in a fresh state. Both cerebral hemispheres were symmetric and dura and meninges were unremarkable. There was a 2.0×1.7×1.2-cm-sized hemorrhagic lesion on the left frontoparietal area of the coronal section (Fig. 1). Right pneumonectomy was carried out (960 g in the fresh state). There were adhesions between the chest wall and parietal pleura. Patchy consolidations were found in the right upper lobe and a hemorrhagic lesion was found in the right lower lobe. Wedge resection of bilateral lobes of the liver revealed a clear external surface and a diffusely greenish bile-tinged cut surface. Cirrhosis was absent.

Microscopically, the frontal lobe had a small infarct, but the larger lesion on the left frontoparietal lobe of the brain was DLBCL, showing robust CD20 positivity and 100% EBV positivity of lymphoma cells on EBV-encoded small RNA *in situ* hybridization (Fig. 2). The margin of the lymphoma was relatively well demarcated, but the cells were also infiltrating blood vessels up to 2 mm from the main tumor margin (Fig. 2). There were tiny clusters of lymphoma cells in the right frontal, upper midbrain and lower medulla oblongata. The right upper lobe of the lung showed invasive aspergillosis and *Pneumocystis jirovecii* pneumonia (Fig. 3). There was alveolar hemorrhage in the right lower lobe. The liver had bile plugs in the interlobular bile ducts with bile ductular proliferation consistent with intrahepatic cholestasis,

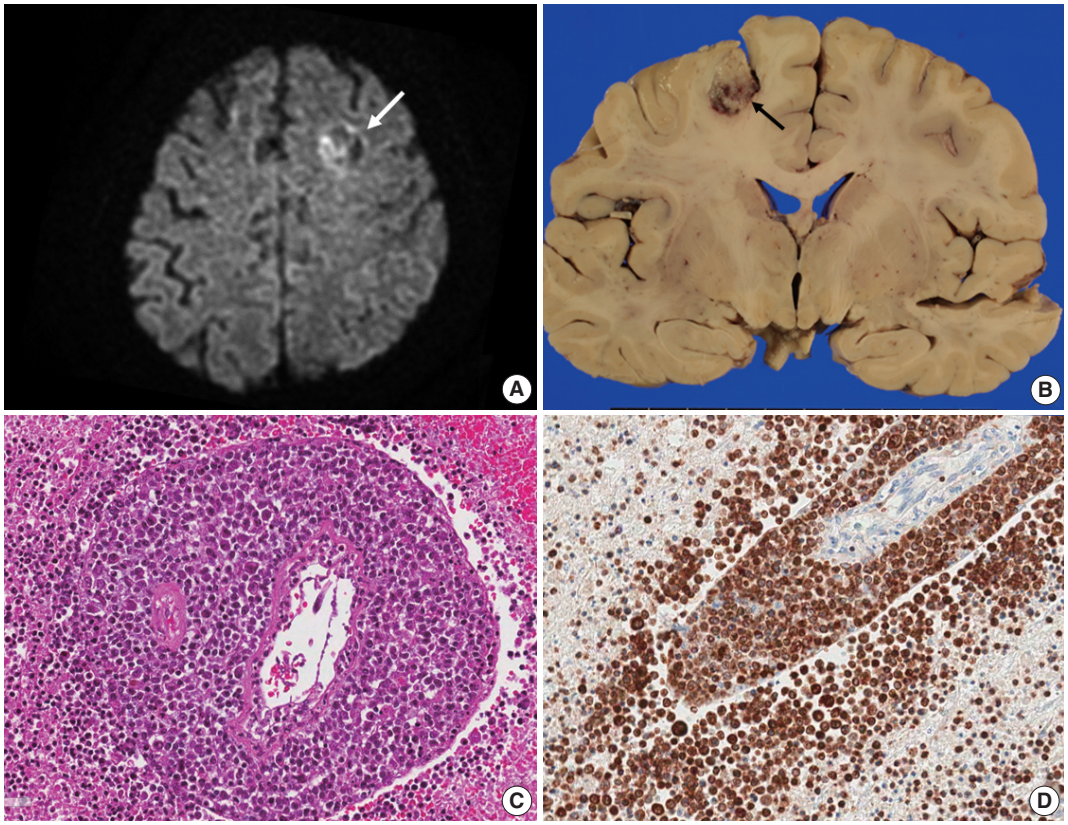

Fig. 1. (A) Brain computed tomography shows a round enhanced lesion (arrow) in the left frontal area. (B) The cut surface of the brain shows a relatively well-demarcated friable lesion with hemorrhage and necrosis (arrow) in the left frontal cortex and white matter. (C) On light microscopy the tumor is composed of sheets of large atypical lymphocytes with angiocentricity. (D) CD20 immunostaining reveals that neoplastic lymphocytes are robustly positive.

https://doi.org/10.4132/jptm.2017.01.23

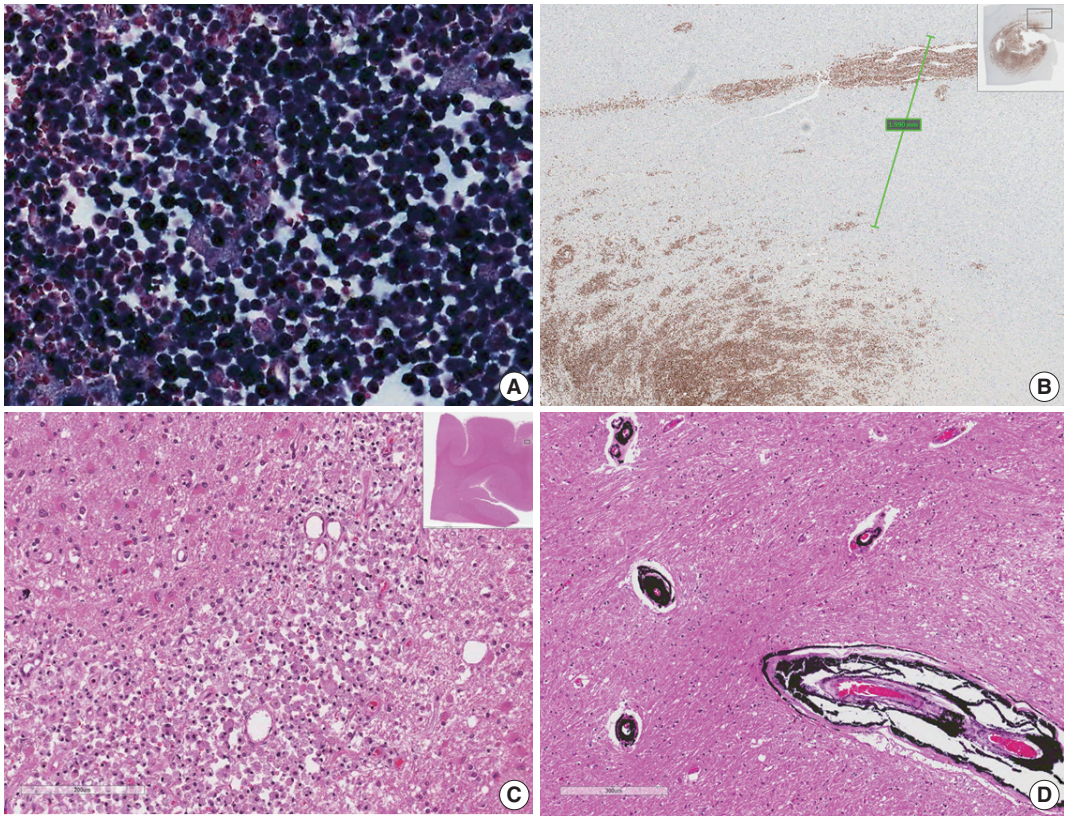

Fig. 2. (A) Epstein-Barr virus (EBV)-encoded small RNA *in situ* hybridization shows that nearly 100% of tumor cells are positive for EBV. (B) CD20 immunostaining delineates individual infiltrating tumor cells and perivascular spread of tumor cells along blood vessels. The largest distance from the margin of the main mass is approximately 3 mm. (C) An infarct was found in the right frontal lobe, demonstrating rarefied brain with vascular proliferation, foamy macrophage infiltration and perilesional gemistocytic reactive gliosis. (D) The internal capsule exhibits thick perivascular calcifications.

but neither inflammatory cell infiltration nor any fungal or viral organism was present.

DISCUSSION

There are two kinds of CNS DLBCL; one appears in immunocompetent patients and the other in immunodeficient patients. Primary CNS DLBCL in immunocompetent hosts are designated as PCNSLs by the WHO classification of tumors of hematopoietic and lymphoid tissue in 2008.[3] Primary CNS DLBCL exhibits specific gene expression and genomic profiles that differ from extra-CNS DLBCL, and the patients are managed with different protocols.[7] The most significantly upregulated gene is extracellular matrix (ECM)-related osteopontin (secreted phosphoprotein 1, *SPP1*). This ECM- and adhesion-related pathways may be related to the biologic characteristic of PCNSL, such as CNS tropism.[7]

Immunodeficiency-related lymphoma of the CNS differs from PCNSL of immunocompetent people based on its EBV positivity and tendency toward multifocality.[5,8] In general, CNS is one of the common site of EBV-associated DLBCLs in immunocompromised patients.[9] There are two kinds of EBV-associated CNS DLBCL: age-related CNS DLBCL occurring in immunocompetent elderly patients (≥65 years old) and immunodeficiency-associated CNS DLBCL.[1] According to one study, the incidence of age-related EBV-associated CNSL without congenital or acquired immunodeficiency was reported to be about 4% (5/134). Primary CNS EBV-associated DLBCL in the elderly was higher in Asian countries than in Western countries.[2]

The prognosis of CNSL is very poor in both immunocompetent and immunocompromised hosts.[10] Accumulated clinical experience over the past decade has proven that first-line treatment of PCNSL patients should avoid whole brain radiation. One approach includes combined induction immunotherapy with methotrexate, temozolomide, and rituximab followed by consolidative infusional etoposide plus high-dose cytarabine administered during the first complete remission.[11]

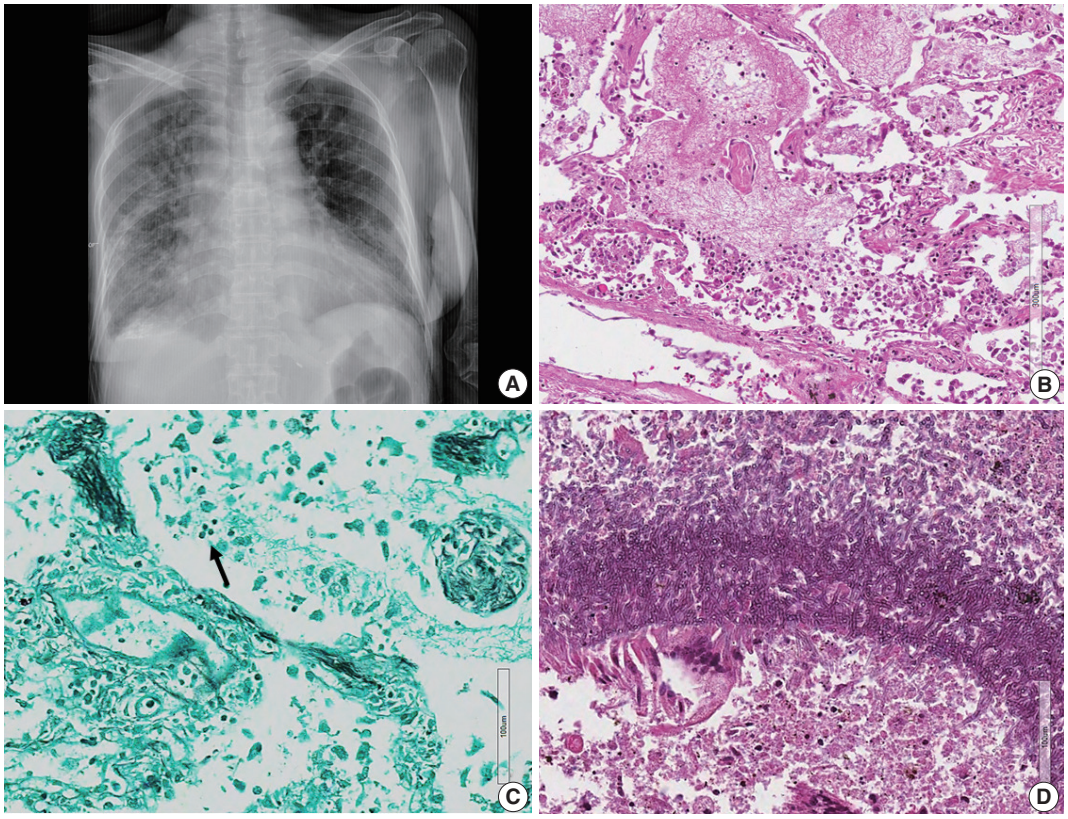

Fig. 3. (A) Chest posteroanterior view shows diffuse haziness of both lungs with marked interstitial and right pleural effusion. (B) Microscopically, the lung shows diffuse alveolar damage, frothy intra-alveolar spaces, detached alveolar lining cells and many macrophages. (C) Gomori methenamine silver staining reveals tiny black oval-to-round *Pneumocystis jirovecii* organisms (arrow) in the intra-alveolar space. (D) Lung tissue shows a cavitary lesion with a fungus ball of aspergillosis (Periodic acid–Schiff staining).

Here, we report a case of autopsy-proven EBV-associated CNSL arising in an immunocompromised host. The pre-autopsy clinical diagnosis was underlying SLE and immunosuppressive therapy-related intestinal CMV enteritis, and intrahepatic cholestasis as well as suspected brain infarcts in the right frontal and frontoparietal lobes. In addition to preautopsy clinical diagnosis, EBV-associated CNS DLBCL and pulmonary aspergillus and *P. jirovecii* pneumonia were found on autopsy.

The pathology of the liver suggests extrahepatic occlusion because bile plugs and bile duct proliferation were found. The patient had a CMV enteritis with perforation in the small bowel. CMV usually does not affect healthy people, but does symptomatically infect immunocompromised hosts. In this case, the patient had been taking prednisolone for a couple of years because of SLE and ITP; therefore, she is presumed to have had steroid-induced immunosuppression. Invasive aspergillosis and *P. jirovecii* pneumonia are also infectious diseases related to immunocompromised status.

Diagnosis of CNSL can be difficult because MRI features overlap with other pathologies.[12] In our case, the radiologic report from brain MRI suggested embolic infarctions. Since the majority of CNS lymphomas are diagnosed via stereotactic biopsy or, less commonly, by flow cytometric analysis of cerebrospinal fluid lymphocytes, the detailed pathology and appearance of infiltrations remain unclear. Therefore, our case is important because we were able to examine the lesions in detail. In this autopsy case, the gross margins of the main CNSL mass were relatively well demarcated, but tumors had spread to other areas as tiny clusters of lymphoma cells.

The tumor cells were robustly positive for CD20 and Bcl-2; however, they were negative for CD3, Bcl-6, CD10, MUM-1, and CMV. Bcl-6 and CD10 are usually positive in germinal center type DLBCL and Bcl-6 can be considered as a good prognostic marker, but our case was negative for these two markers.[13] MUM-1 is usually positive in activated B-cell type of DLBCL,[14] but it was also negative in our case.

Radiologically, differential diagnosis of primary CNS DLBCL may include CNS embryonal tumors (previously called primitive

 https://doi.org/10.4132/jptm.2017.01.23

neuroectodermal tumors) and high-grade gliomas, because both show high cellularity and necrosis. Pathological diagnosis is not difficult with the help of immunohistochemistry.[1]

In conclusion, we report an autopsy case of EBV-associated CNS-DLBCL in an immunocompromised host. The patient suffered from SLE for 2 years and had a history of splenectomy due to ITP, small bowel resection due to CMV enteritis and complications of bowel perforation, and complex pneumonia, which was associated with long-term steroid therapy for SLE. Pre-mortem MRI findings of CNS lesions were suspicious of infarcts, but the lesions were found to be EBV-associated DLBCL on pathology. The patient's pulmonary lesions represented aspergillosis and *P. jirovecii* pneumonia. Therefore, the major pathology of this complicated case involving an immunocompromised host was correctly diagnosed on autopsy. Despite advances in diagnostic options and technology, autopsy remains an essential tool for determining cause of death and obtaining important pathologic information.

Conflicts of Interest

No potential conflict of interest relevant to this article was reported.

REFERENCES

1. Sugita Y, Muta H, Ohshima K, *et al*. Primary central nervous system lymphomas and related diseases: pathological characteristics and discussion of the differential diagnosis. Neuropathology 2016; 36: 313-24.
2. Jamal SE, Li S, Bajaj R, *et al*. Primary central nervous system Epstein-Barr virus-positive diffuse large B-cell lymphoma of the elderly: a clinicopathologic study of five cases. Brain Tumor Pathol 2014; 31: 265-73.
3. Sabattini E, Bacci F, Sagramoso C, Pileri SA. WHO classification of tumours of haematopoietic and lymphoid tissues in 2008: an overview. Pathologica 2010; 102: 83-7.
4. Doucet S, Kumthekar P, Raizer J. Primary central nervous system lymphoma. Curr Treat Options Oncol 2013; 14: 185-97.
5. Bayraktar S, Bayraktar UD, Ramos JC, Stefanovic A, Lossos IS. Primary CNS lymphoma in HIV positive and negative patients: comparison of clinical characteristics, outcome and prognostic factors. J Neurooncol 2011; 101: 257-65.
6. Bibas M, Antinori A. EBV and HIV-related lymphoma. Mediterr J Hematol Infect Dis 2009; 1: e2009032.
7. Tun HW, Personett D, Baskerville KA, *et al*. Pathway analysis of primary central nervous system lymphoma. Blood 2008; 111: 3200-10.
8. Roschewski M, Wilson WH. EBV-associated lymphomas in adults. Best Pract Res Clin Haematol 2012; 25: 75-89.
9. Romero M, González-Fontal GR, Saavedra C, *et al*. Primary CNS plasmablastic lymphoma in an HIV/EBV negative patient: a case report. Diagn Cytopathol 2016; 44: 61-5.
10. Campo E, Swerdlow SH, Harris NL, Pileri S, Stein H, Jaffe ES. The 2008 WHO classification of lymphoid neoplasms and beyond: evolving concepts and practical applications. Blood 2011; 117: 5019-32.
11. Fraser E, Gruenberg K, Rubenstein JL. New approaches in primary central nervous system lymphoma. Chin Clin Oncol 2015; 4: 11.
12. Phillips EH, Fox CP, Cwynarski K. Primary CNS lymphoma. Curr Hematol Malig Rep 2014; 9: 243-53.
13. Mahmoud HM, El-Sakhawy YN. Significance of Bcl-2 and Bcl-6 immunostaining in B-Non Hodgkin's lymphoma. Hematol Rep 2011; 3: e26.
14. Hunt KE, Reichard KK. Diffuse large B-cell lymphoma. Arch Pathol Lab Med 2008; 132: 118-24.

Journal of Pathology and Translational Medicine 2018; 52: 56-60
https://doi.org/10.4132/jptm.2017.04.08

■ CASE STUDY ■

Colloid Carcinoma of the Uterine Cervix and Its Immunohistochemical Analysis: A Case Report

Nermin Koc · Sevcan Arzu Arinkan[1]
Nurver Ozel Ozbay[2] · Selcuk Selcuk[1]

Departments of Pathology and [1]Obstetrics and Gynecology, Zeynep Kamil Maternity and Pediatric Research and Training Hospital, Istanbul; [2]Department of Pathology, Fatih Sultan Mehmet Research and Training Hospital, Istanbul, Turkey

Received: September 29, 2016
Revised: March 27, 2017
Accepted: April 8, 2017

Corresponding Author
Sevcan Arzu Arinkan, MD
Department of Obstetrics and Gynecology, Zeynep Kamil Maternity and Pediatric Research and Training Hospital, Istanbul 34660, Turkey
Tel: +90-505-683-7557
Fax: +90-216-391-0680
E-mail: pataraa96@gmail.com

Colloid carcinoma, which is a very rare tumor of the uterine cervix, is composed of an excessive amount of mucus and a relative paucity of tumoral glandular cells within them. Herein, we report a rare case of colloid carcinoma of the cervix with adenocarcinoma *in situ* (AIS), intestinal and usual types, and endocervical adenocarcinoma (usual type) components. We also discuss the morphological and immunohistochemical characteristics of this tumor. A 51-year-old woman was referred to our outpatient clinic with the symptom of genital bleeding lasting for 5 months. She had a cervix surrounded by an irregular tumor with a diameter of 5 cm. The colloid carcinoma cells were positive for MUC2, MUC5AC, and cytokeratin (CK) 7, focal positive for CDX2, and negative for MUC6 and CK20. Also, the intestinal type AIS showed a similar staining pattern. Colloid carcinoma cells producing mucin showed an intestinal phenotype and AIS. The intestinal type can be considered as a precursor lesion of colloid carcinoma.

Key Words: Colloid carcinoma; Cervix uteri; Neoplasms

Colloid carcinoma is a very rare tumor of the uterine cervix. Presence of a large amount of extracellular mucin resulting in the formation of mucous lakes with a relative paucity of neoplastic cells within them is called colloid (gelatinous) carcinoma.[1-4] The classification and prognosis of colloid carcinoma is controversial.[1-4]

In the literature, only two colloid carcinoma cases with immunohistochemical features have been reported.[1,2] One of the cases was reported as pure colloid carcinoma,[2] while the second case was reported as colloid carcinoma with endocervical type adenocarcinoma *in situ* component.[2]

In this case report, we present the histopathologic and immunohistochemical features of the tumor.

CASE REPORT

A 51-year-old female was admitted for examination of anemia. She complained of easy fatigability and uterine bleeding for 5 months. She has been in menopause for 2 years and has no past medical history. Her laboratory test results were within normal range except for hemoglobin levels (9.8 mg/dL). There was no palpable mass upon gynecologic examination. Chest X-ray and gastroscopic evaluation were normal. Endometrial and endocervical samplings were performed. Fragments of adenocarcinoma were identified in the assessment of the materials obtained from endocervical curettage. In imaging studies, the cervix was surrounded by a lesion with a diameter of 5 cm, flattening the cervix wall. In detailed imaging studies, there was no additional lesion in gastrointestinal tract or in any other location. Cervical adenocarcinoma was prediagnosed according to the results of frozen section. Total abdominal hysterectomy with bilateral oophorectomy and pelvic and para-aortic lymph node dissection was performed. The cervix was grossly surrounded by an irregular tumor with a diameter of 5 cm, and the cervix wall was flattened. The cross-sectional area was gelatinous and some parts were covered with mucinous layer (Fig. 1). In addition, endo-

pISSN 2383-7837
eISSN 2383-7845

metrial lesion and a 3-cm-sized cyst in left ovary were detected. The remaining parts of the specimen were grossly unremarkable.

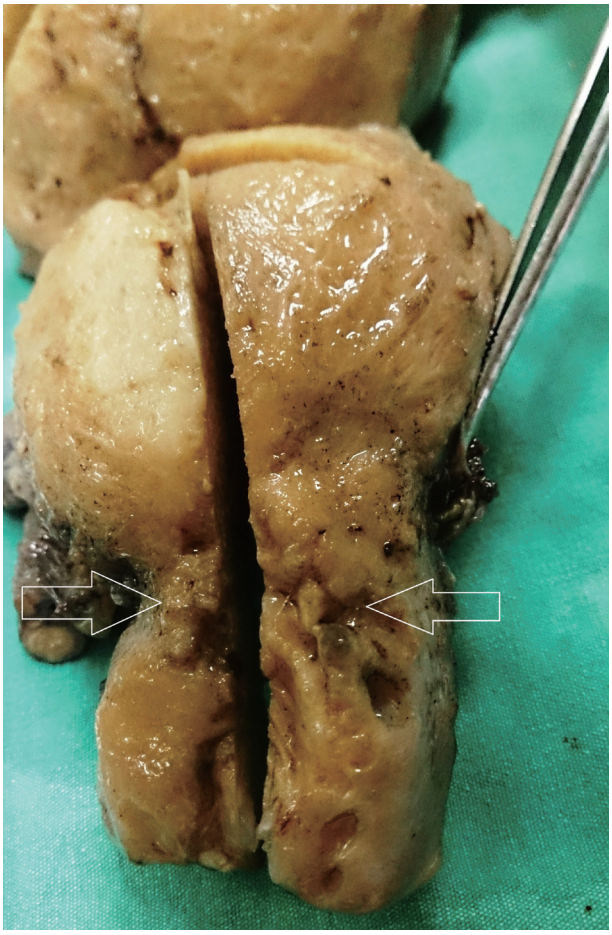

Fig. 1. Gross appearance of the tumor. The cervix is surrounded by an irregular tumor (arrows), with erosion in the mucosal surface covered by mucinous layer.

Formalin-fixed paraffin embedded tissue blocks of the surgical specimens were cut, deparaffinized and rehydrated. Sections were stained with hematoxylin and eosin. Immunohistochemistry was performed using manual polymer detection system with citrate buffer heat induced epitope retrieval. The following prediluted ready to use primary antibodies were used: MUC2 (M53, mouse monoclonal antibody, Thermo Fisher Scientific, Waltham, MA, USA), MUC5AC (USM1, mouse monoclonal antibody, Thermo Fisher Scientific), MUC6 (CLH 5, mouse monoclonal antibody, Thermo Fisher Scientific), cytokeratin (CK) 20 (Ks 20.8, mouse monoclonal antibody), carcinoembryonic antigen (rabbit polyclonal antibody, Thermo Fisher Scientific), CD10 (S6C6, mouse monoclonal antibody, Thermo Fisher Scientific), p16 (INK4, BioGenex, San Ramon, CA, USA). Periodic acid-Schiff (PAS) and alcian blue (AB) stains were performed.

On histopathological examination, the tumor deeply invaded the cervical wall (Fig. 2A). Also, adenocarcinoma *in situ* (AIS) of intestinal and usual types were detected in superficial areas. In these areas, the surface and glands were lined by tall columnar cells with pseudostratified nuclei containing coarse chromatin, and goblet cells were observed in some areas. In deeper regions, numerous variably sized mucous lakes were present. Cuboidal or low columnar neoplastic cells forming tubular or cribriform structures floated within the mucous lakes or were lining the inner surface. Some of the mucous lakes did not contain any cellular component. Neoplastic cells had enlarged oval nuclei without conspicuous nucleoli and large apical cytoplasm containing basophilic mucus. They resembled goblet cells. Since they were inside the mucous lakes, they were flattened because of the pressure. Mitotic figures were rarely observed. Lymphovascular invasion was not shown. Approximately 80% of the invasive

Table 1. Immunohistochemical and histochemical findings

	Colloid carcinoma cells	Mucous lakes	Adenocarcinoma *in situ* cells		Adenocarcinoma (usual)
			Intestinal	Usual	
MUC2	+	–	+	–	–
MUC5AC	+	+	+	+	+
MUC6	–	–	Weak+	–	–
CDX2	Focally+	–	Focally+	Focally+	Focally+
CK7	+	–	+	+	+
CK20	–	–	–	–	–
CEA	+	Focally+	+	–	–
p16	+	–	+	+	+
PAS	+	+	+	–	–
Alcian-blue	+	+	+	–	–
Mucicarmine	+	+	+	Focally+	Focally+

CK, cytokeratin; CEA, carcinoembryonicantigen; PAS, periodicacid-Schiff.

component was composed of the colloid carcinoma, and other invasive component was formed by the usual type of endocervical adenocarcinoma. The latter component consisted of glands or cribriform structures lined by tumor cells with pseudostratified large nuclei containing coarse chromatin. Intracellular mucin was reduced, and mitosis was increased. The tumor was invading the endometrial surface. Invasion of the cystic tumor tissue consisting of mucinous component was found in the left ovary and tumor infiltration was found in the serosa of the right fimbrial end. The peritoneal washing was positive for tumor cells and the pelvic lymph node was also positive.

The results of histochemical and immunohistochemical studies are presented in Table 1. Mucous lakes and tumor cells of both colloid carcinoma and AIS intestinal type were positive for MUC5AC and negative for MUC6, and the tumor cells were positive for MUC2 but mucous lakes were negative for MUC2 (Fig. 2B–D). Mucous lakes and tumor cells of both colloid carcinoma and AIS intestinal type were positive for PAS, AB, and mucicarmine stains.

The patient was treated with chemotherapy and radiotherapy. She had generalised tumor recurrence 1.5 years after the surgery.

Written informed consent was obtained and this manuscript was written in accordance with the principles of the Declaration of Helsinki.

DISCUSSION

Colloid adenocarcinoma of the cervix is a very rare tumor and its histopathologic classification is not clear. In the literature, only two cases were reported as colloid carcinoma of the cervix.[1,2] It is a unique subtype due to the phenotype of contained mucus, and its prognosis is controversial. Mucinous adenocarcinoma is

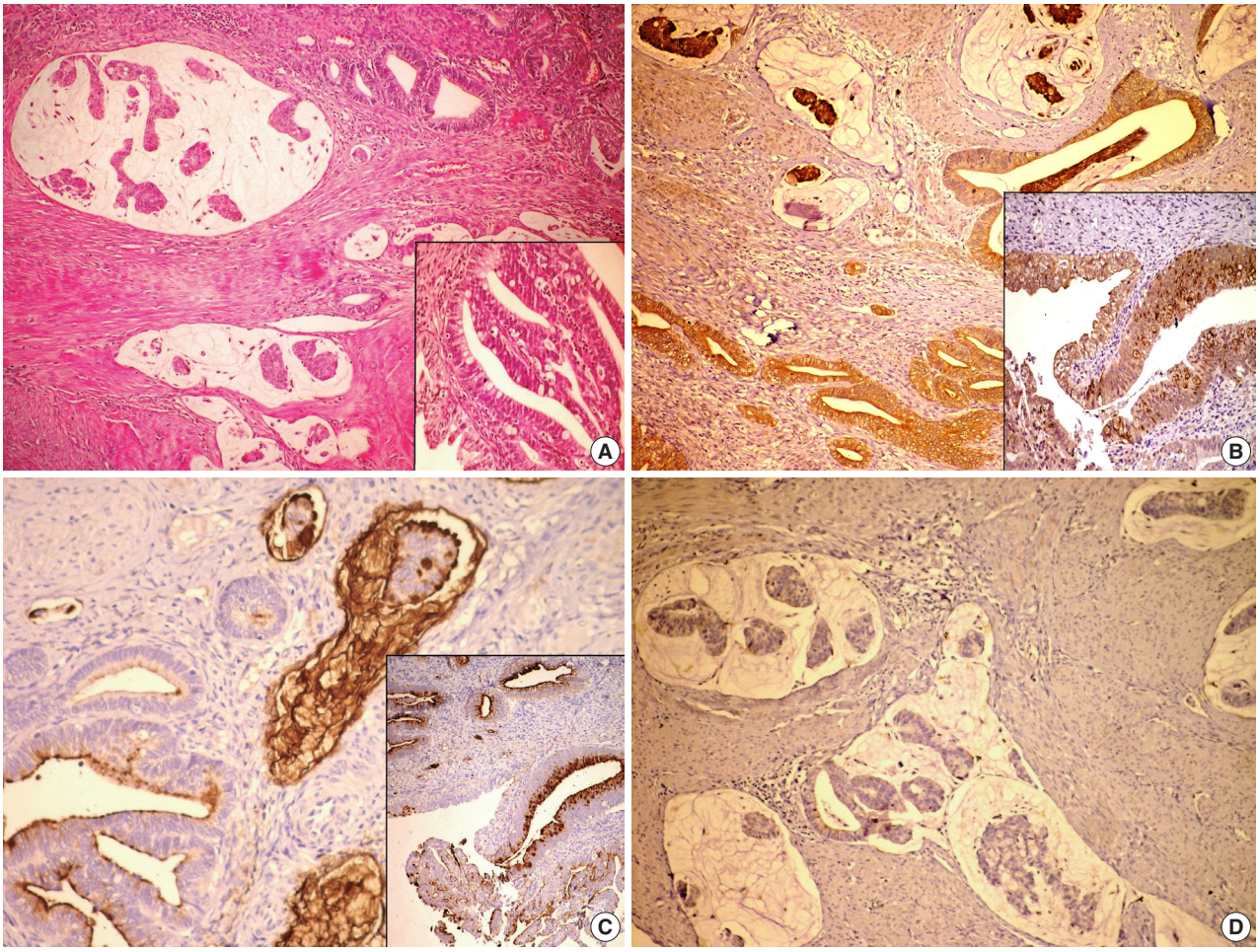

Fig. 2. Colloid carcinoma component is present in the deep area. Adenocarcinoma *in situ* (AIS), usual and intestinal types (inset), and endocervical adenocarcinoma (usual type) components are present in the superficial area (A). Colloid carcinoma cells and AIS intestinal type cells (inset) are positive for MUC2(B) and MUC5AC (C) and negative for MUC6 (D).

https://doi.org/10.4132/jptm.2017.04.08

classified into not otherwise indicated, gastric, intestinal, and signet-ring cell types according to the World Health Organization classification,[5] but the classification of colloid carcinoma is controversial. It has been reported that large pools of mucin may occasionally be present within the stroma in endocervical adenocarcinoma usual type, and colloid carcinoma is treated and managed as a variant of the endocervical type.[1] According to Young and Clement,[6] mucinous adenocarcinoma consists of, in addition to the endocervical (usual type) adenocarcinoma, two variants: minimal deviation adenocarcinoma and intestinal type adenocarcinoma. Colloid carcinoma is a subgroup of the intestinal type.[1,6] On the other hand, colloid tumor is also considered as a heterogeneous group of tumors which might have intestinal and endocervical phenotypes.[1,2]

The expression of *MUC* genes is relatively tissue-specific. MUC5AC is a gastric foveolar epithelial type of mucin. MUC6 is a pyloric gland type of mucin and both types were expressed by endocervical cells while MUC2 is an intestinal type of mucin and not expressed by endocervical cells.[1,2,7-9] When an epithelium undergoes malignant transformation, the mucin genes can undergo aberrant expression causing reduced production of an expected mucin and/or production of a structurally different and unexpected mucin within the transformed epithelium.[8] Immunohistochemical analyses on different types of mucins have been conducted in pancreatic, gastrointestinal and endocervical tumors. While MUC2 is not expressed in normal endocervical epithelial cells, it is expressed in endocervical adenocarcinomas.[2,8] It is observed that *de novo* MUC2 is expressed in neoplastic endocervical glands and postulated that MUC2 expression may accompany neoplastic transformation of endocervical glands.[7] MUC2 staining pattern in our case is compatible with the staining of endocervical adenocarcinomas in the literature.[7,8] Similar to our case, Shintaku *et al*.[1] reported that while colloid cells stained with MUC2, mucin lakes did not. On the other hand, Ishida *et al*.[2] did not refer to any staining. The difference in the staining pattern may be attributed to the mucin production during the malignant transformation and laboratory techniques. In our case, MUC5AC staining was positive, which is compatible with the staining pattern of classical endocervical adenocarcinomas described in the literature.[7,8] While Ishida *et al*.[2] reported MUC5AC staining, Shintaku *et al*.[1] did not refer to any staining.

In additon to the cervix, mucin expression in mucinous carcinomas of other organs is also discussed.[9] In cases of colon carcinoma, MUC5AC and MUC2 stainings in mucinous and signet-ring cell carcinomas are detected at higher levels than in classical colon carcinomas. Also, it is considered that transformation process of the mucinous and signet ring cell carcinomas might be different from the traditional adenoma-carcinoma sequence of the colorectal carcinomas.[9]

CDX2 is a transcription factor expressed by the entire intestinal type of cervical adenocarcinomas and some conventional cervical adenocarcinomas. The importance of CDX2 lies in its essential role in the differentiation of the intestinal mucosal epithelium.[10,11]

In previously reported case of colloid carcinoma of the cervix, Shintaku *et al*.[1] demonstrated that tumor cells were positive for MUC2 and CDX2, but negative for MUC5AC and MUC6. The authors concluded that the mucin-producing tumor cells were intestinal phenotype.[1] In other case report of colloid carcinoma of the cervix, Ishida *et al*.[2] found that MUC5AC and MUC6 were positive and MUC2 and CDX2 were negative in colloid carcinoma cells, and MUC5AC was positive and MUC2 and CDX2 were negative in endocervical type AIS component. In light of these evidences, the authors concluded that the mucin-producing neoplastic cells were endocervical phenotype, and that the endocervical type AIS can be a precursor lesion of colloid carcinoma.[2]

In present case, the colloid carcinoma cells were positive for MUC5AC and MUC2, focal positive for CDX2, and negative for MUC6. Besides, in other parts of the tumor, AIS intestinal type revealed a similar staining pattern. We concluded that mucin-producing neoplastic cells were intestinal phenotype and intestinal type AIS might be a precursor lesion of colloid carcinoma.

Metastatic colloid adenocarcinoma from the gastrointestinal tract is an important tumor type in differential diagnosis of the colloid carcinoma of the cervix. In differential diagnosis, however, immunohistochemical staining alone is inadequate because the immunophenotyping of metastatic colloid adenocarcinoma from the gastrointestinal tract can be similar: positive for MUC2, MUC6, and CK7 and positive/negative for CDX2 and CK20.[2]

In our case, immunohistochemical staining was not effective in the differential diagnosis of colloid carcinoma of the cervix from metastatic colloid adenocarcinoma arising from the gastrointestinal tract. Because there was no other tumor detected in the systemic examination of the patient, the presence of AIS was considered as an evidence for the primary cervical tumor.

In conclusion, since colloid carcinomas of the cervix are rare, detailed assessments with more samples are necessary to determine whether they are heterogeneous or homogeneous group depending on the type(s) of mucin and to describe the status of colloid carcinoma of the cervix in the classification of adenocarcinoma.

Conflicts of Interest

No potential conflict of interest relevant to this article was reported.

REFERENCES

1. Shintaku M, Kushima R, Abiko K. Colloid carcinoma of the intestinal type in the uterine cervix: mucin immunohistochemistry. Pathol Int 2010; 60: 119-24.
2. Ishida M, Iwai M, Kagotani A, Yoshida K, Okabe H. Colloid carcinoma of the uterine cervix: a case report with respect to immunohistochemical analyses. Int J Gynecol Pathol 2014; 33: 248-52.
3. Walker AN, Mills SE. Unusual variants of uterine cervical carcinoma. Pathol Annu 1987; 22 Pt 1: 277-310.
4. Hurt WG, Silverberg SG, Frable WJ, Belgrad R, Crooks LD. Adenocarcinoma of the cervix: histopathologic and clinical features. Am J Obstet Gynecol 1977; 129: 304-15.
5. Kurman RJ, Carcangiu ML, Herrington CS, Young RH. WHO classification of tumors of female reproductive organs. Lyon: International Agency for Research on Cancer, 2014.
6. Young RH, Clement PB. Endocervical adenocarcinoma and its variants: their morphology and differential diagnosis. Histopathology 2002; 41: 185-207.
7. Riethdorf L, O'Connell JT, Riethdorf S, Cviko A, Crum CP. Differential expression of MUC2 and MUC5AC in benign and malignant glandular lesions of the cervix uteri. Virchows Arch 2000; 437: 365-71.
8. Baker AC, Eltoum I, Curry RO, *et al*. Mucinous expression in benign and neoplastic glandular lesions of the uterine cervix. Arch Pathol Lab Med 2006; 130: 1510-5.
9. Bu XD, Li N, Tian XQ, *et al*. Altered expression of MUC2 and MUC5AC in progression of colorectal carcinoma. World J Gastroenterol 2010; 16: 4089-94.
10. McCluggage WG, Shah R, Connolly LE, McBride HA. Intestinal-type cervical adenocarcinoma in situ and adenocarcinoma exhibit a partial enteric immunophenotype with consistent expression of CDX2. Int J Gynecol Pathol 2008; 27: 92-100.
11. Sullivan LM, Smolkin ME, Frierson HF Jr, Galgano MT. Comprehensive evaluation of CDX2 in invasive cervical adenocarcinomas: immunopositivity in the absence of overt colorectal morphology. Am J Surg Pathol 2008; 32: 1608-12.

Journal of Pathology and Translational Medicine 2018; 52: 61-63
https://doi.org/10.4132/jptm.2017.06.13

Liquid-Based Cytology of the Cerebrospinal Fluid in a Case of Cryptococcal Meningitis

Jiwoon Choi · Se Hoon Kim[1]

Department of Pathology, Yonsei University Wonju College of Medicine, Wonju; [1]Department of Pathology, Yonsei University College of Medicine, Seoul, Korea

Received: April 30, 2017
Revised: June 11, 2017
Accepted: June 13, 2017

Corresponding Author
Se Hoon Kim, MD, PhD, FIAC, EFN
Department of Pathology, Yonsei University College of Medicine, 50-1 Yonsei-ro, Seodaemun-gu, Seoul 03722, Korea
Tel: +82-2-2228-1769
Fax: +82-2-362-0860
E-mail: paxco@yuhs.ac

Cryptococcus neoformans is the most common microorganism found in cerebrospinal fluid (CSF) cytology and causes life-threatening infections in immunocompromised hosts. Although its cytomorphologic features in conventional smear cytology have been well described, those in liquid-based cytology have rarely been. A 73-year-old woman with diffuse large B-cell lymphoma presented with mental confusion and a spiking fever. To rule out infectious conditions, CSF examination was performed. A cytology slide that was prepared using the ThinPrep method showed numerous spherical yeast-form organisms with diameters of 4–11 μm and thick capsules. Occasional asymmetrical, narrow-based budding but no true hyphae or pseudohyphae were observed. Gomori methenamine silver staining was positive. Cryptococcosis was confirmed in blood and CSF through the cryptococcal antigen test and culture. Liquid-based cytology allows for a clean background and additional slides for ancillary testing, facilitating the detection of microorganisms in CSF specimens, particularly when the number of organisms is small.

Key Words: *Cryptococcus neoformans*; Cerebrospinal fluid; Liquid-based cytology

Cryptococcus neoformans is the most common microorganism found in cerebrospinal fluid (CSF) cytology.[1] Detecting *C. neoformans* in CSF specimens is crucial for cytopathologists as the organism causes life-threatening infections in immunocompromised hosts. Although the cytomorphologic features of *C. neoformans* in conventional smear cytology have been well described, those in liquid-based cytology have rarely been. Recently, a case in sputum cytology sample has been reported.[2] Here, we report the findings of a liquid-based cytologic preparation of a CSF specimen in a case of culture-proven cryptococcal meningitis.

CASE REPORT

A 73-year-old woman visited the hospital with complaints of myalgia, night sweats, and anorexia for 1 week. Her past medical history was unremarkable. On physical examination, a palpable mass was discovered in the right neck, and abdominopelvic computed tomography showed generalized lymphadenopathy. Excisional biopsy of the cervical mass revealed diffuse large B-cell lymphoma, and she received chemotherapy treatment. After completing 1 cycle of chemotherapy, she presented with a spiking fever (up to 38.3°C) and mental confusion. Laboratory tests revealed leukocytosis (white blood cell count, $11.01 \times 10^3/\mu L$) and increased C-reactive protein levels (207.3 mg/L) in peripheral blood. Therefore, CSF examination by lumbar puncture was performed to rule out infectious meningitis.

The CSF specimen submitted for cytologic examination was clear and colorless. It was processed onto a ThinPrep slide and stained with the Papanicolaou stain. Microscopic examination revealed many round to oval structures with thick halos (Fig. 1). They stained pale blue and ranged in size from 4 to 11 μm. The initial impression was a contaminant, such as glove powder, because the structures were numerous while the background was almost acellular (Fig. 1A). However, when viewed carefully, the structures contained a brownish dot-like internal structure that was suspected as being a nucleus, with occasional tear drop-shaped budding (Fig. 1B, C). When an additional slide was stained with the Gomori methenamine silver method, they stained black (Fig. 1D). Based on positive cryptococcal antigen detection and India ink tests of the CSF specimen prior to the initial cytologic diagnosis, the presence of *C. neoformans* was reported. Subsequently, CSF and blood cultures confirmed cryptococcosis. Although treatment with amphotericin B was started and the organisms were not seen in a repeat CSF examination, the patient died approximately 3

pISSN 2383-7837
eISSN 2383-7845

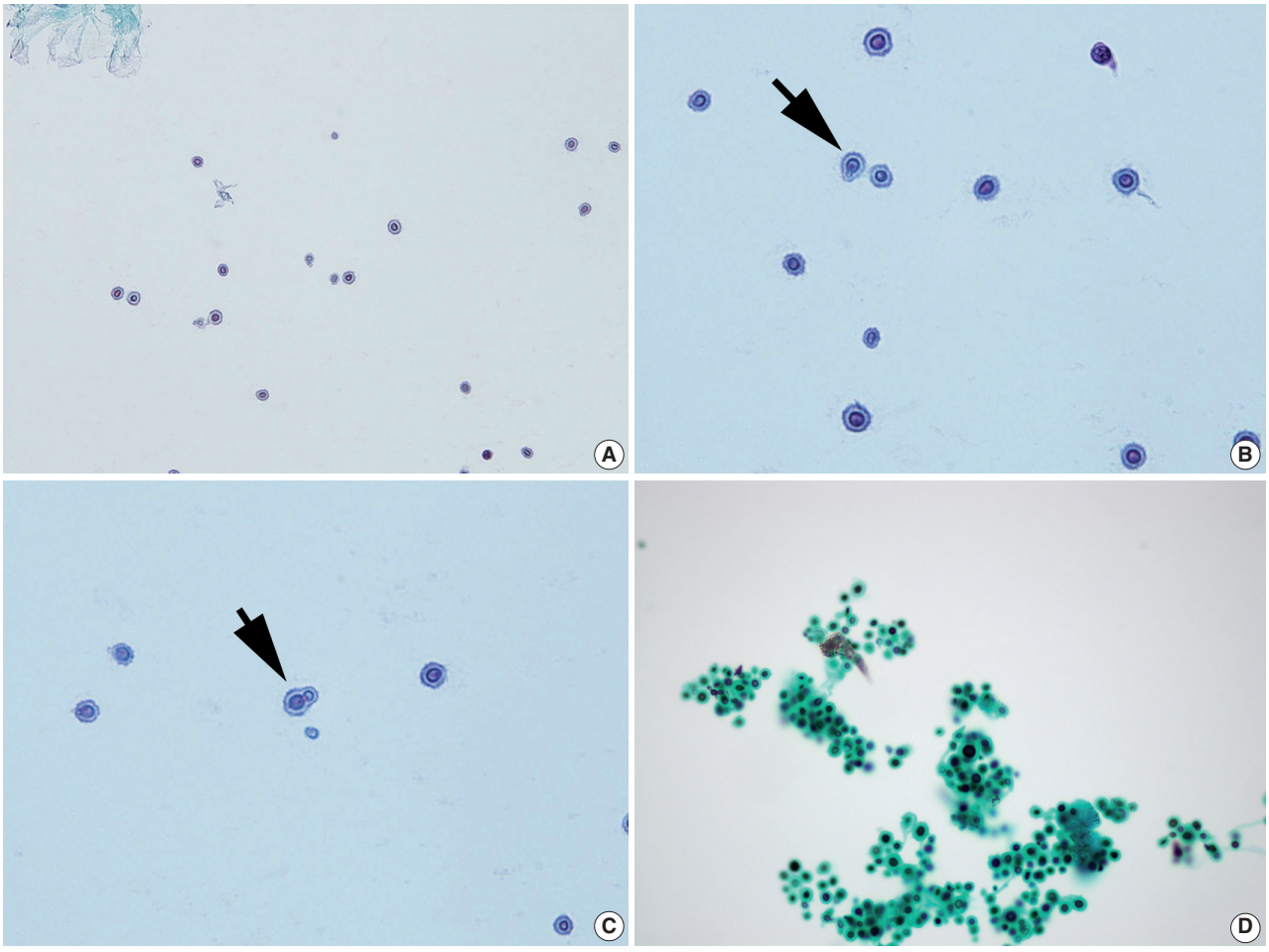

Fig. 1. Representative images of ThinPrep slide preparations of the cerebrospinal fluid. (A) Liquid-based cytology shows numerous spherical yeast cells against a clean background (Papanicolau stain). (B, C) The cells have varying sizes, clear halos, and show occasional narrow-based single budding (arrows) (Papanicolau stain). (D) Black staining is observed with the Gomori methenamine silver stain.

months later owing to worsening of her general condition and recurrence of cryptococcal meningitis.

The authors comply with the guidelines for human studies. The patient died approximately 3 months later owing to worsening of her general condition and recurrence of cryptococcal meningitis. Therefore, the authors could not receive the patient's informed consent for this manuscript. This was notified to the Institutional Review Board (IRB), who waived the IRB protocol approval (4-2017-0814).

DISCUSSION

C. neoformans is a ubiquitous encapsulated yeast that causes infections ranging from asymptomatic pulmonary colonization to life-threatening meningoencephalitis.[3] *C. neoformans* enters the body by inhalation through the respiratory tract and spreads hematogenously to the central nervous system. It has long been recognized that while *C. neoformans* may cause meningoencephalitis in otherwise healthy people, it more frequently presents as an opportunistic infection in immunocompromised individuals with acquired immunodeficiency syndrome, neoplastic conditions, or those undergoing corticosteroid therapy; it is fatal without treatment. Therefore, rapid recognition and diagnosis are required to decrease mortality rates.

The cytomorphology of *C. neoformans* in conventional smear cytology has been well described.[4,5] *Cryptococcus* has yeast but not pseudohyphal or hyphal forms with rare exceptions. With the routine Papanicolaou stain, yeast cells can be seen as pale, brownish-pink, slightly refractile spheres surrounded by clear halos. In Diff-Quik-stained preparations, purple yeast cells with accentuated clear halos against a dark purple background give the smear a punched-out appearance. Cells generally range from

 https://doi.org/10.4132/jptm.2017.06.13

5 to 10 μm in diameter, but this can vary from 2 to 20 μm. A useful cytologic feature is the appearance of the asymmetric, narrow-based budding. Special stains, such as mucicarmine, periodic acid-Schiff and alcian blue, can aid the diagnosis as *Cryptococcus* has a characteristic thick mucopolysaccharide capsule. In patients with cryptococcal meningitis, the inflammatory response shows variable degrees depending on the immunocompetence of the hosts.[6] While CSF smears from immunocompetent patients typically manifest as CSF pleocytosis, smears from immunocompromised patients often show large numbers of yeast cells without an inflammatory response, as shown in our case.

Recently, *Cryptococcus gatti*, which is closely related to *C. neoformans*, has emerged in North America and has been responsible for a large disease epidemic in a population of generally healthy individuals including immunocompromised hosts.[7] Unfortunately, it is difficult to differentiate *C. gatti* from *C. neoformans* by morphology alone. Further differentiation of cryptococcal species can be accomplished on L-canavanine-glycine-bromthymol blue agar; *C. gattii* colours the medium blue while *C. neoformans* does not (the medium remains yellow).[8]

In the cytologic examination of non-gynecological body fluids, including CSF, the liquid-based preparation method has not been used as widely as the conventional method. Moreover, the literature describing the morphologic features of cryptococci in liquid-based cytology is scarce.[9] In this report, we observed that the most important cytomorphologic features of cryptococci, such as the thick capsule and tear-drop shaped budding, are well maintained in liquid-based cytology. Moreover, liquid-based cytology provided a clean background that facilitated the detection of the microorganisms and allowed for the preparation of additional slides for special staining to confirm the diagnosis.

In patients with cryptococcal meningitis, cytologic examination of the CSF has been shown to have a low diagnostic yield as the yeast cells can be easily overlooked, particularly when few in number, and can be confused with erythrocytes or artifacts (e.g., surgical glove powder, dust, or glass powder).[4] Moreover, cryptococci sometimes show unusual cytomorphology that can cause diagnostic difficulty, such as chains of budding yeasts, pseudohyphae, or capsule-deficient forms.[10,11] Our experience in this case suggests that liquid-based cytology may improve the sensitivity of the detection of microorganisms and thus diagnostic accuracy by providing opportunities for ancillary testing. In addition, for CSF examinations, liquid-based cytology might be superior to conventional cytology for clear morphology, as cellular components can be deformed in the latter during cytospin preparations.

Conflicts of Interest

No potential conflict of interest relevant to this article was reported.

REFERENCES

1. Prayson RA, Fischler DF. Cerebrospinal fluid cytology: an 11-year experience with 5951 specimens. Arch Pathol Lab Med 1998; 122: 47-51.
2. Sharma S, Gupta N, Behera D, Rajwanshi A. Detection of cryptococcosis in liquid-based sputum cytology. Cytopathology 2017; 28: 177-8.
3. Levitz SM. The ecology of *Cryptococcus neoformans* and the epidemiology of cryptococcosis. Rev Infect Dis 1991; 13: 1163-9.
4. Saigo P, Rosen PP, Kaplan MH, Solan G, Melamed MR. Identification of *Cryptococcus neoformans* in cytologic preparations of cerebrospinal fluid. Am J Clin Pathol 1977; 67: 141-5.
5. Powers CN. Diagnosis of infectious diseases: a cytopathologist's perspective. Clin Microbiol Rev 1998; 11: 341-65.
6. Walts AE. Cerebrospinal fluid cytology: selected issues. Diagn Cytopathol 1992; 8: 394-408.
7. Dixit A, Carroll SF, Qureshi ST. *Cryptococcus gattii*: an emerging cause of fungal disease in North America. Interdiscip Perspect Infect Dis 2009; 2009: 840452.
8. Kwon-Chung KJ, Polacheck I, Bennett JE. Improved diagnostic medium for separation of *Cryptococcus neoformans* var. *neoformans* (serotypes A and D) and *Cryptococcus neoformans* var. *gattii* (serotypes B and C). J Clin Microbiol 1982; 15: 535-7.
9. Kobayashi TK, Ueda M, Nishino T, Moritani S, Higaki T, Bamba M. Cytologic detection of cryptococcosis coexisting with herpes simplex virus infection in sputum: use of liquid-based, thin-layer preparations. Acta Cytol 2003; 47: 103-6.
10. Williamson JD, Silverman JF, Mallak CT, Christie JD. Atypical cytomorphologic appearance of *Cryptococcus neoformans*: a report of five cases. Acta Cytol 1996; 40: 363-70.
11. Kanazawa M, Ishii M, Sato Y, Kitamura K, Oshiro H, Inayama Y. Capsule-deficient meningeal cryptococcosis. Acta Cytol 2008; 52: 266-8.

Journal of Pathology and Translational Medicine 2018; 52: 64-66
https://doi.org/10.4132/jptm.2016.11.04

■ BRIEF CASE REPORT ■

Hyalinizing Cholecystitis and Associated Carcinoma: A Case Report

Youngjin Kang · Yang-Seok Chae · Chul Hwan Kim · Youngseok Lee · Dong-Sik Kim[1] · Young-Dong Yu[1] · Joo Young Kim

Departments of Pathology and [1]Surgery, Korea University Anam Hospital, Korea University College of Medicine, Seoul, Korea

Hyalinizing cholecystitis (HC) is a recently described rare variant of chronic cholecystitis that is characterized by replacement of the normal structures of the entire gallbladder wall with diffuse and dense hyaline sclerosis.[1] Some cases of cholecystitis are associated with variable degrees of calcification. Porcelain gallbladder (PG) is an extensively calcific example that is a vaguely and radiologically defined entity whose pathologic correlation has not been identified.[2-4] PG is subclassified into "complete porcelain," showing extensive dystrophic calcifications that form an intramural continuous band involving more than 80% of the gallbladder wall, and "incomplete porcelain," which lacks these findings.[2,5-7] Although HC is rare and found in only approximately 1.6% of cholecystectomy specimens, it is more commonly accompanied by carcinomas with more aggressive clinical behavior compared to usual gallbladder carcinomas.[1] However, preoperative diagnosis of HC-related carcinoma is challenging, because the wall is thinner than that of typical chronic cholecystitis or usual carcinomas, and discrete masses are not formed. There has been only one case report of HC, which was accompanied by immunoglobulin G4–related disease,[8] since Patel *et al*.[1] first described the entity in a retrospective case series. We present a case of HC and associated carcinoma masquerading as primary biliary cancer.

CASE REPORT

A 54-year-old man visited the hospital due to fatigue, pruritus, and diarrhea. Laboratory findings revealed elevations in aspartate aminotransferase (98 IU/L; reference range, 3 to 45 IU/L), alanine transaminase (232 IU/L; reference range, 3 to 45 IU/L), alkaline phosphatase (320 IU/L; reference range, 30 to 120 IU/L), and gamma-glutamyl transpeptidase (619 IU/L; reference range, 9 to 64 IU/L). Biliary computed tomography scan and magnetic resonance cholangiography revealed enhancing wall thickening of the cystic duct and common hepatic duct and multiple calcified gallstones as well as sludge in the gallbladder with mild wall thickening (Fig. 1A). Radiologically, carcinoma of the primary bile duct or cystic duct and associated chronic calculous cholecystitis was suspected, and bile duct resection with cholecystectomy was performed.

An 8.0×5.5×5.5 cm gallbladder was submitted for intraoperative frozen diagnosis. Grossly, the gallbladder wall was diffusely fibrotic, and the mucosal surface was covered by yellowish necrotic material with a gallstone (2.0×1.2×1.0 cm). There were no mass-like lesions (Fig. 1B). Two random frozen sections were examined microscopically, and an inflammatory lesion without malignancy was suggested. After the operation, we also received the segmentally resected common hepatic duct (1.7 cm in length, 0.6 cm in diameter) and the attached cystic duct (1.7 cm in length, 0.4 cm in diameter). The bile duct wall was diffusely thickened; however, the mucosa of the ducts was smooth and did not form mass-like lesions. The entire permanent sections of the gallbladder and bile ducts were examined microscopically. The gallbladder wall was nearly completely replaced by dense lamellated eosinophilic hyaline material, with multifocal neutrophilic and lymphoplasmacytic infiltration. Focal intramural calcifications were identified (Fig. 2A, B). Multifocal invasive glands with irregular borders were sparsely scattered in the hyalinized gallbladder wall in a longitudinal arrangement (Fig. 2C). The mucosal surface of the gallbladder showed extensive denudation of the epithelium, but some foci of high-grade biliary intraepithelial neoplasia were noted (Fig. 2D). There

Corresponding Author
Joo Young Kim, MD, PhD
Department of Pathology, Korea University Anam Hospital, Korea University College of Medicine, 73 Inchon-ro, Seongbuk-gu, Seoul 02841, Korea
Tel: +82-2-920-6268, Fax: +82-2-920-6576, E-mail: lepetit80@hanmail.net

Received: September 2, 2016 **Revised:** October 31, 2016
Accepted: November 3, 2016

pISSN 2383-7837
eISSN 2383-7845

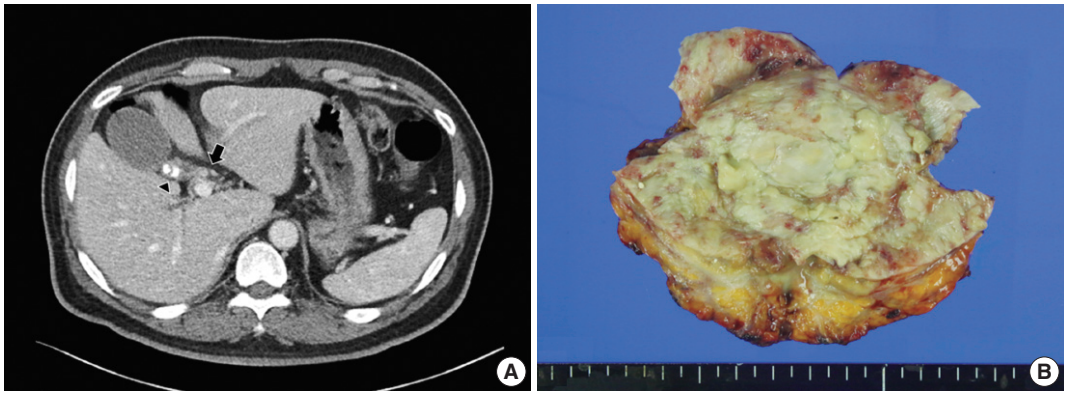

Fig. 1. Computed tomography and gross findings of hyalinizing cholecystitis and associated carcinoma. (A) Biliary computed tomography scan reveals subtle enhancement of wall thickening at the confluence of the cystic duct and the common hepatic duct (arrow). There is mild wall thickening of the gallbladder with multiple calcified gallstones in the neck portion (arrowhead). (B) Grossly, the gallbladder wall shows diffuse fibrosis and is covered by yellowish necrotic materials, without mass-like lesions.

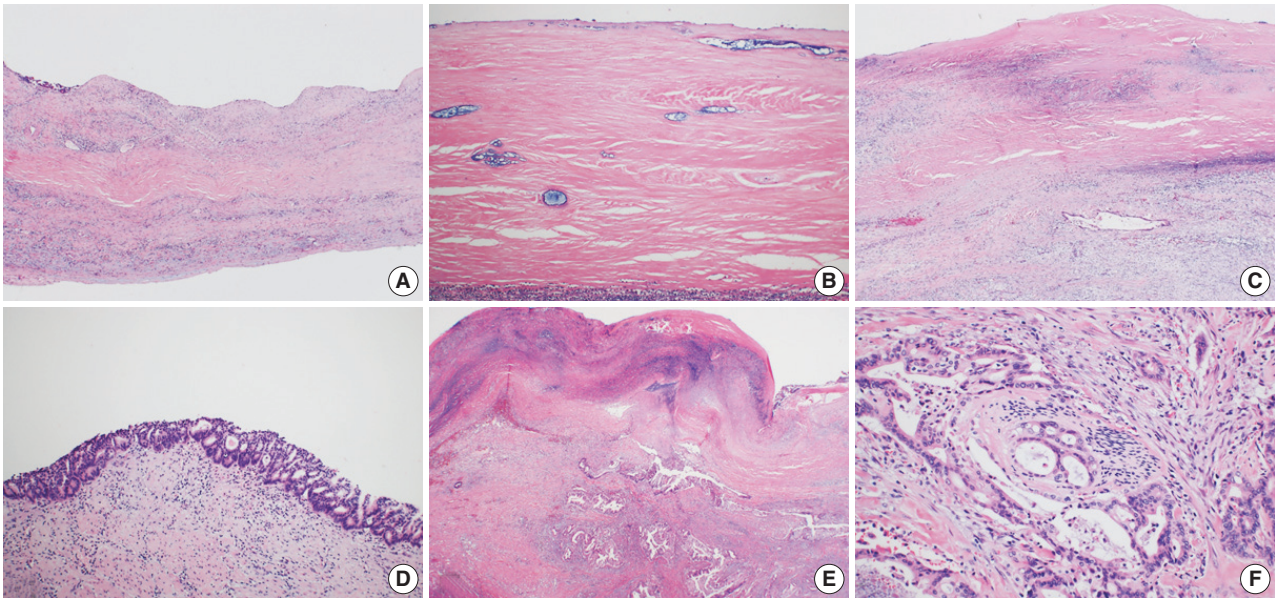

Fig. 2. Microscopic findings of hyalinizing cholecystitis and associated carcinoma. (A, B) The gallbladder wall is replaced by dense lamellated eosinophilic hyaline material. Inflammatory cells are also seen. (C) A few invasive glands are longitudinally arranged in the hyalinized gallbladder wall with a denuded epithelium. (D) Multifocal carcinoma *in situ* lesions are found on the surface. (E) Focal clusters of invasive glands are identified in the hyalinized wall. (F) Invasive glands have irregular borders and cytologic atypia with perineural invasion.

were focal areas composed of clusters of invasive glands in the gallbladder wall (Fig. 2E). The invasive glands were composed of stratified depolarized atypical cells with enlarged hyperchromatic nuclei containing coarse chromatin and occasionally prominent nucleoli. Some glands also showed perineural invasion (Fig. 2F). Diffuse involvement of the walls of the common hepatic duct and cystic duct by adenocarcinoma was observed (Fig. 3A, B); however, the mucosa was relatively spared, with no intraepithelial lesions (Fig. 3C). Considering all of these findings, we made the diagnosis of HC and associated adenocarcinoma, with direct invasion of the cystic duct and common hepatic duct.

This study was approved by the Institutional Review Board of Korea University Anam Hospital (ED17246), and informed consent was waived.

DISCUSSION

HC is a recently described, distinctive entity, comprising 1.6% of cholecystectomy specimens.[1] HC is characterized by diffuse and dense hyalinization of the gallbladder wall with

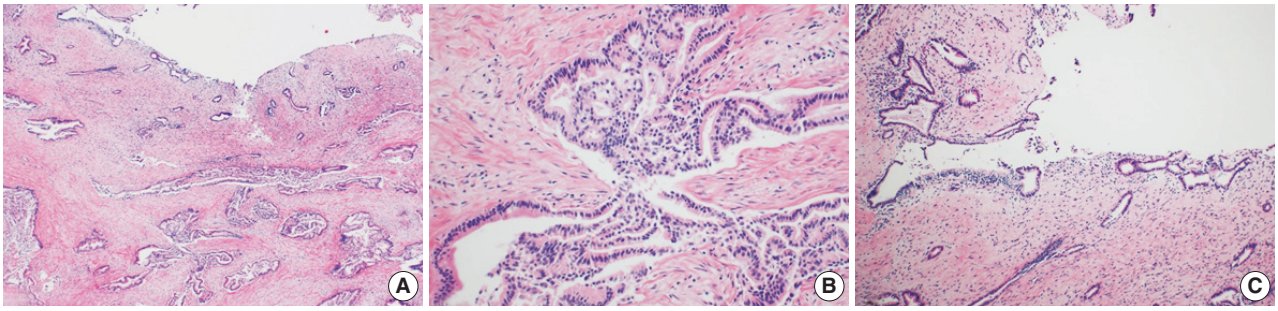

Fig. 3. Microscopic findings of the common hepatic and cystic ducts. (A, B) Invasive glands infiltrate the common hepatic and cystic ducts beneath the surface epithelium. (C) The surface epithelium is relatively spared, with no intraepithelial lesion.

complete effacement of normal histologic components. Focal to extensive calcification may also be seen. HC is more often associated with carcinoma; the frequency of carcinoma was 15% compared to 4% of all cholecystectomy specimens in a South American cohort.[1] However, to identify the carcinoma component is diagnostically challenging because it does not form distinct mass lesions or induce significant thickening of the gallbladder wall.[1] Furthermore, the malignant glands are not easily found due to the paucity and sparse distribution of tumor glands within an abundant hyalinizing sclerotic background. In our case, there were no mass-like lesions, and the entire gallbladder wall was diffusely fibrotic with no significant wall thickening. The carcinoma component was not found in two randomly submitted frozen sections; however, it was identified after extensive sampling of permanent sections. Therefore, careful examination with extensive or entire sampling of the gallbladder is crucial in HC to identify associated carcinoma.

Preoperative diagnosis of HC-related carcinoma is also highly challenging. Patel *et al*.[1] reported that about 70% of malignancies had been diagnosed as benign preoperatively. This might be because HC-associated carcinomas typically do not form a mass or result in thickening of the gallbladder. Subsequently, surgical resection can be delayed until progression of the malignancy. In our case, the malignancy was identified radiologically after the tumor directly extended to the extrahepatic bile duct, and the preoperative diagnosis was primary bile duct cancer with chronic calculous cholecystitis. The final pathologic stage was T3 (direct invasion of the extrahepatic bile ducts). The late discovery of carcinoma is associated with advanced stage at diagnosis and poor prognosis of HC-related carcinomas. The median survival for HC-associated carcinoma is shorter than that of usual carcinomas.[1]

In conclusion, HC is a rare variant of chronic cholecystitis and is often associated with carcinoma with aggressive behavior. Suspicion of the possibility of HC and identification of HC as an unusual variant of chronic cholecystitis are important in gross examination of cholecystectomy specimens. After the identification of HC, extensive sampling and meticulous microscopic examination are essential to determine the possibility of associated carcinoma. In addition, close follow-up is recommended because carcinoma associated with HC can have more aggressive behavior than typical gallbladder cancer.

Conflicts of Interest

No potential conflict of interest relevant to this article was reported.

REFERENCES

1. Patel S, Roa JC, Tapia O, *et al*. Hyalinizing cholecystitis and associated carcinomas: clinicopathologic analysis of a distinctive variant of cholecystitis with porcelain-like features and accompanying diagnostically challenging carcinomas. Am J Surg Pathol 2011; 35: 1104-13.
2. Kane RA, Jacobs R, Katz J, Costello P. Porcelain gallbladder: ultrasound and CT appearance. Radiology 1984; 152: 137-41.
3. Ochsner SF, Carrera GM. Calcification of the gallbladder ("porcelain gallbladder"). Am J Roentgenol Radium Ther Nucl Med 1963; 89: 847-53.
4. Weiner PL, Lawson TL. The radiology corner: porcelain gallbladder. Am J Gastroenterol 1975; 64: 224-7.
5. Shimizu M, Miura J, Tanaka T, Itoh H, Saitoh Y. Porcelain gallbladder: relation between its type by ultrasound and incidence of cancer. J Clin Gastroenterol 1989; 11: 471-6.
6. Stephen AE, Berger DL. Carcinoma in the porcelain gallbladder: a relationship revisited. Surgery 2001; 129: 699-703.
7. Towfigh S, McFadden DW, Cortina GR, *et al*. Porcelain gallbladder is not associated with gallbladder carcinoma. Am Surg 2001; 67: 7-10.
8. Gupta RK, Patton KT. Hyalinizing cholecystitis with features of immunoglobulin G4-related disease-coincidence or an unrecognized association? A case report. Hum Pathol 2015; 46: 625-8.

Journal of Pathology and Translational Medicine 2018; 52: 67-70
https://doi.org/10.4132/jptm.2017.11.09

■ BRIEF CASE REPORT ■

An Extremely Rare Case of Back and Hip Pain due to the Metastasis of Late Recurrent Myxopapillary Ependymoma to the Inguinal Lymph Node

Suheyla Ekemen · Ozlem Yapicier[1] · Hatice Deniz Boler[2] · Umit Ince[1]

Laboratory of Acibadem Pathology, Departments of [1]Pathology and [2]General Surgery, Acibadem University Medical Faculty, Istanbul, Turkey

Myxopapillary ependymomas (ME) are rare and slowly growing gliomas usually with spinal cord localization originating from the ectopic ependymal residues. They are commonly located in the conus medullaris, cauda equina and filum terminale. ME is known to be more aggressive in childhood, but has a good prognosis in adults with a very low metastasis risk.[1,2] If successfully excised, ME are usually cured completely. However, in adults, ME at the sacrococcygeal region metastasizing to organs outside central nervous system has rarely been reported so far.[3-5] Herein, we report an extremely rare case of an inguinal lymph node metastasis developed 19 years after removal of primary ME at the sacrococcygeal region, which presented with unusually severe back and hip pain. Because the metastasis of ME to the lymph node after such a long time is rare, our case may contribute to improving the differential diagnosis of extremely rare metastatic ME cases and identifying their unexpected role in the pain of unknown origin.

CASE REPORT

A 36-year-old woman presented to our surgical clinic with severe back and hip pain that had been present for a year. She was otherwise healthy except for histories of initially named "cyst" operation at the sacrococcygeal region at 17 years of age and cesarean section delivery at 32 years of age. Left inguinal lymphadenopathy (around 3 cm in diameter) was noted. Magnetic resonance image (MRI) scanning of the spinal cord showed minimal fibrotic changes and edema in the posterior subcutaneous soft tissue at the distal tip of the coccyx, just to the right of the midline. These findings suggested that the lymphadenopathy might have developed as secondary to the previous sacrococcygeal cystic mass operation at 17 years of age. The inguinal lymph node was totally excised.

The macroscopic cut-section of the lymph node showed a near-total effacement of the normal structure with soft and grayish gelatinous appearance. Hematoxylin and eosin (H&E) staining revealed a metastatic tumor (Fig. 1A) showing cystic and papillary structures with a single-row cuboidal-columnar epithelium in the myxoid and vascularized stroma and mucinous material within the lumens (Fig. 1A–C). In addition, periodic acid-Schiff–Alcian blue (PAS-AB) histochemical staining confirmed the presence of acidic mucin (Fig. 2A).

A wide range of immunohistochemical (IHC) staining panel was applied to cover epithelial and mesenchymal tumors, germ cell neoplasms and malignant mesothelioma. While the tumor was positively stained with vimentin, glial fibrillary acidic protein (GFAP), epidermal growth factor receptor (EGFR), and S100 (Fig. 2B–D and data not shown, respectively), there was no staining for pan-cytokeratin (5/6/8/18), CDX2, cytokeratin (CK) 20, CK7, α-fetoprotein, SALL4, epithelial membrane antigen, CD31, CD34, WT1, calretinin, CD117, CD10, OLİG2, p63, and MOC31. The Ki-67 labeling index was very low with only 1%–2%. The results of IHC stainings together with the history of the patient were evaluated, and we concluded that the case was compatible with inguinal lymph node metastasis of ME. Unfortunately, the original radiology and pathology materials were not available for review.

Corresponding Author
Suheyla Ekemen, MD
Laboratory of Acibadem Pathology, Acibadem University Medical Faculty, Kayısdagi Street, No. 32, B block, 8F, Atasehir, Istanbul TR-34752, Turkey
Tel: +90-216-500-4874, Fax: +90-216-340-7708
E-mail: suheylaekemen@gmail.com

Received: August 31, 2017 **Revised:** November 6, 2017
Accepted: November 9, 2017

pISSN 2383-7837
eISSN 2383-7845

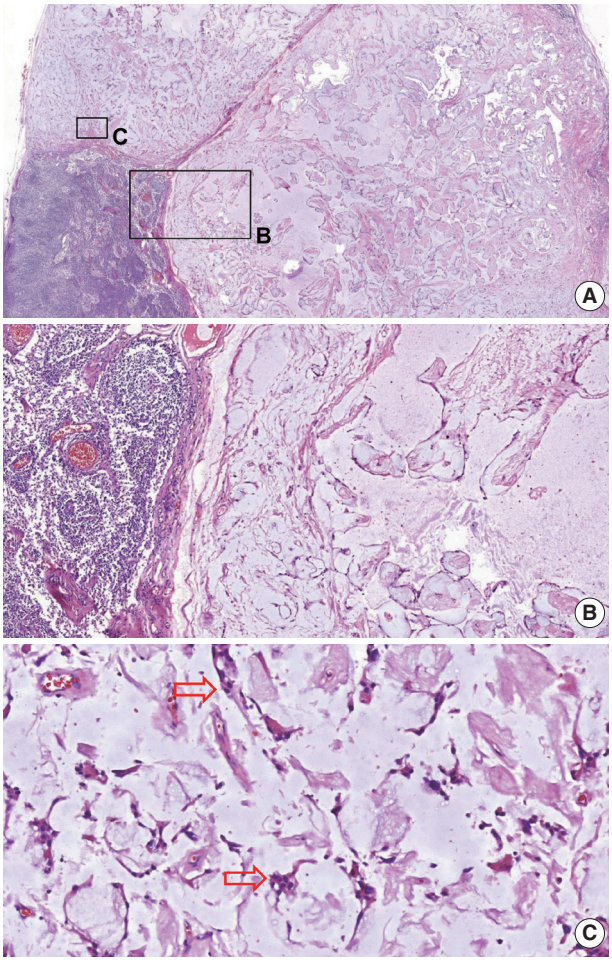

Fig. 1. Metastatic tumor in the lymph node. (A) In the lower-left corner is a normal lymph node structure; in the remaining areais the metastasis. (B, C) Higher magnification view of the metastasis-cystic and papillary structures (B) with a single-row cuboidal-columnar epithelium in the myxoid and vascularized stroma (arrows) (C). Lumens contain mucinous material.

The institutional review board (IRB) approval has been waived, but informed consent was obtained from the patient (2016-12/05).

DISCUSSION

Myxopapillary ependymoma is most commonly seen in conus medullaris, cauda equina, and filum terminale. The subcutaneous, sacrococcygeal, or presacral-situated extramedullary MEs are considered as a prominent subgroup originating from the ectopic ependymal residue. Long-term leg pain is a typical clinical symptom of ME. Depending on its settlement location, a total removal of the tumor can be difficult, which may cause recurrence after years. It is very rarely found that ME may progress

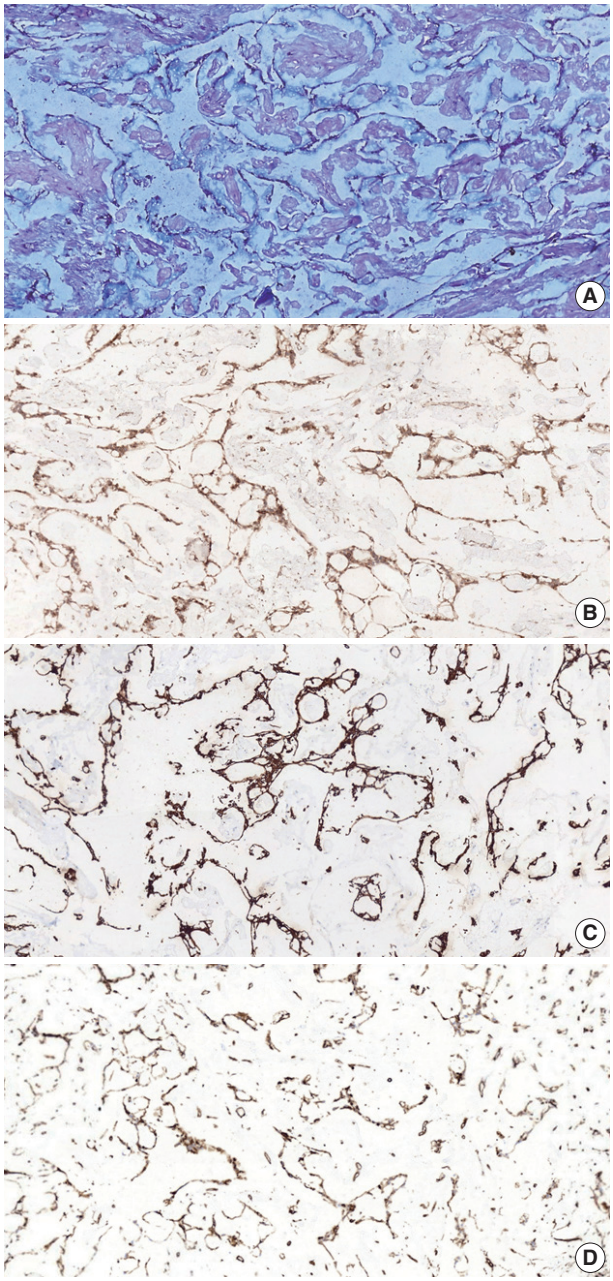

Fig. 2. Histopathological findings suggest that the tumor is originated from the central nervous system, consistent with myxopapillary ependymoma metastasis. (A) Periodic acid-Shiff–Alcian blue histochemical stain shows the presence of acidic mucin. (B) Epidermal growth factor receptor positivity of the tumor cells by immunohistochemistry (IHC). (C) Glial fibrillary acidic protein positivity of the tumor cells by IHC. (D) Vimentin positivity of the tumor cells by IHC.

along the spinal nerves during its repetition and thus may cause multiple lesions in the spinal canal via cerebrospinal fluid.[4]

ME is known to be more aggressive in childhood, but has a good prognosis in adults with a very low risk of metastasis.[1,2]

https://doi.org/10.4132/jptm.2017.11.09

Table 1. Studies reporting metastases of myxopapillary ependymomas into lymph node at adult age

Reference	Age (first diagnosis)/ Sex	Origin/ Histololgy	Metastasis (yr)	Metastasis
Wight *et al.* (1973)[7]	20/M	CE/ME	32	Aortic lymph node, lung, pleura, rib, pelvis, humerus
Helwig and Stern (1984)[8]	Case series 1–47/M, F	SC/ME	7–30	One with inguinal lymph node metastasis
Kramer *et al.* (1988)[5]	15/M	SC/ME	20	Inguinal lymph node, pelvis
Bardales *et al.* (1994)[9]	19/M	SC/ME	16	Inguinal lymph nodes, abdomen
Vega-Orozco *et al.* (2011)[10]	22/M	CE/ME	16	Inguinal lymph node
This study	17/F	SC/ME	19	Inguinal lymph node

M, male; CE, Cauda equina; ME, myxopapillary ependymoma; F, female; SC, sacrococcygeal.

According to the World Health Organization report in 2015, metastasis was detected in only 17 cases out of 183 cases, 11 of which involved brain metastasis.[1] All of these previously reported cases of young patients. In adults, sacrococcygeal placement of ME metastasis has been reported to be extremely rare and is often presented as soft tissue or bone metastasis.[5,6]

In our case, the patient had a history of previous operation at the sacrococcygeal region 19 years prior with an initial coccygeal cyst. MRI findings of the left inguinal lymphadenopathy and minimal fibrotic changes and edema of the posterior subcutaneous soft tissue at the coccyx suggested ME metastasis. H&E sections of the lymph node confirmed the metastasis of myxoid and vascularized stroma showing cystic and papillary structures with single rowed cuboidal columnar epithelium and mucinous material within the lumen. Positive IHC staining for vimentin, GFAP, S100, and EGFR was observed. Negativity for cytokeratin markers and specific positivity for GFAP, vimentin, and S100 are especially noted in ME.[2] The presence of acidic mucin in myxoid matrices shown by PAS-AB histochemical staining is typical of ME,[2] and we found similar positive staining with PAS-AB stain. In addition, Ki-67 proliferation index was very low (1%–2%) in our case, supporting the earlier literature.[2,4] Recent studies have also focused on EGFR positivity because EGFR positivity is an indicator of aggressive tumor progression.[2] These morphologic and IHC findings of our case are consistent with ME metastasis, even though the initial pathology of the primary tumor is not available. A recurrence of ME within 12–15 years has been reported. However, metastasis to the lymph nodes is very rare and only a few cases with late metastasis have been reported (Table 1).[5,7-10]

In conclusion, to the best of our knowledge, the current case is an extremely rare case of ME occurring at an adult age with lymph node metastasis after a long time. Thus, this case has multiple implications for future pathological diagnosis. First, in cases of lymph node metastasis presenting as innocuous myxopapillary tumor morphology, myxopapillary ependymoma should be additionally considered. In such cases, origin of the primary tumor such as conus medullaris, cauda equina and filum terminale should be investigated. Second, the rarity of our case sheds light on the fact that these tumors may metastasize after many years. The role of MRI in the diagnosis of ME is important but may not be conclusive by itself in cases like ours presenting as a lymph node metastasis. Therefore, examination of all past surgical records and pathology reports can aid in diagnosis. Lastly, our case may contribute to the understanding of the unexpected role of rare and late ME metastasis in the differential diagnosis of pain of unknown origin.

Conflicts of Interest

No potential conflict of interest relevant to this article was reported.

REFERENCES

1. Weber DC, Wang Y, Miller R, *et al*. Long-term outcome of patients with spinal myxopapillary ependymoma: treatment results from the MD Anderson Cancer Center and institutions from the Rare Cancer Network. Neuro Oncol 2015; 17: 588-95.
2. Wang H, Zhang S, Rehman SK, *et al*. Clinicopathological features of myxopapillary ependymoma. J Clin Neurosci 2014; 21: 569-73.
3. Satti M, Firoze M, Malaker K, Hussain M, Maniyar I. Mediastinal myxopapillary ependymoma primary or late metastases of paracoccygeal ependymoma: a case report. Ann Diagn Pathol 2005; 9: 215-8.
4. Fujimori T, Iwasaki M, Nagamoto Y, Kashii M, Sakaura H, Yoshikawa H. Extraneural metastasis of ependymoma in the cauda equina. Global Spine J 2013; 3: 33-40.
5. Kramer GW, Rutten E, Sloof J. Subcutaneous sacrococcygeal ependymoma with inguinal lymph node metastasis: case report. J Neurosurg 1988; 68: 474-7.
6. Lee KJ, Min BW, Seo HJ, Cho CH. Subcutaneous sacrococcygeal

myxopapillary ependymoma in asian female:a case report. J Clin Med Res 2012; 4: 61-3.
7. Wight DG, Holley KJ, Finbow JA. Metastasizing ependymoma of the cauda equina. J Clin Pathol 1973; 26: 929-35.
8. Helwig EB, Stern JB. Subcutaneous sacrococcygeal myxopapillary ependymoma: a clinicopathologic study of 32 cases. Am J Clin Pathol 1984; 81: 156-61.
9. Bardales RH, Porter MC, Sawyer JR, Mrak RE, Stanley MW. Metastatic myxopapillary ependymoma: report of a case with fine-needle aspiration findings. Diagn Cytopathol 1994; 10: 47-53.
10. Vega-Orozco R, Rembao-Bojórquez D, Salmerón-Mercado M, García-Marquez A, Tena-Suck ML. Inguinal lymph nodal metastasis of myxopapillary ependymoma confirmed by fine-needle aspiration cytology, biopsy, and immunohistochemistry: case report. Diagn Cytopathol 2011; 39: 689-93.

 https://doi.org/10.4132/jptm.2017.11.09


JPTM
Journal of Pathology and
Translational Medicine